SU-SEL-70-036

The Effect of Polarization Rotation on the Amplitude of Ionospherically Propagated Sea Backscatter

by

J. R. Barnum

JUNE 1970

TECHNICAL REPORT NO. 157

Prepared under
Office of Naval Research Contract
Nonr-225(64), NR 088 019, and
Advanced Research Projects Agency ARPA Order 196

RADIOSCIENCE LABORATORY

STANFORD ELECTRONICS LABORATORIES

STANFORD UNIVERSITY • STANFORD, CALIFORNIA

SU-SEL-70-036

THE EFFECT OF POLARIZATION ROTATION ON THE AMPLITUDE OF IONOSPHERICALLY PROPAGATED SEA BACKSCATTER

by

J. R. Barnum

June 1970

Technical Report No. 157

Prepared Under

Office of Naval Research Contract Nonr-225(64), NR 088-019, and Advanced Research Projects Agency ARPA Order No. 196

Radioscience Laboratory
Stanford Electronics Laboratories
Stanford University · Stanford, California

ABSTRACT

Previous experiments have shown that an ocean surface represents a strong source of high-frequency (HF) backscatter. The author has used a 2.5 km receiving antenna array--the world's largest--to study such backscatter both from the Gulf of Mexico and the Pacific Ocean. The narrow beamwidth of this antenna (1/3 deg average), together with SFCW sounding, confer unusually good azimuth and time-delay (range) resolution. The resulting detail and clarity has made possible more precise quantitative studies of sea backscatter. A particular goal of these studies is to develop a method of locating storms, or areas of unusual calm.

During routine sweep-frequency recordings, it was found that the high-resolution data revealed a new type of amplitude variation--periodic in both time-delay and radio frequency--which roughly resembled large thumbprints on the time-delay-versus-frequency plots. This was clearly a new phenomenon, seen only during the fall and winter months. It was hypothesized that magnetoionic splitting in the ionosphere produced a polarization-rotation modulation on the received backscatter signals and that the continuity of the sea cross-section polarization dependence was responsible for making the lines visible only in backscatter from the sea.

Theoretical development of this hypothesis led to simple trigonometric expressions which describe the received voltage. Using an approximate computer raytracing technique, and representative ionospheric models, synthetic backscatter records were constructed which agree very well with the "thumbprint" line-families observed experimentally. The computer-aided predictions also showed that the inability to detect "polarization modulation" during the summer is due to the more sensitive dependence of

polarization rotation upon frequency, time delay, and azimuth during that season.

Conclusive proof of the theory came when the transmitted polarization was changed while successive frequency sweeps were recorded. When the transmitter polarization is switched from vertical to approximately circular, the "thumbprint" lines in the time-delay-vs-frequency data are usually blurred. When "fixed"-frequency, amplitude-vs-time-delay data were recorded, and when the polarization at the transmitter is switched from vertical to horizontal, the shift in the positions of the enhancements in slant range correlated very well with the theory.

When the equivalent beamwidth of the 2.5 km array is broadened from 1/2 to 4 deg the polarization modulation is usually undetectable. Examination of azimuth-scanned, fixed-frequency measurements and their theoretically-synthesized counterparts explained this beamwidth dependence very well. It was found that a beamwidth as small as 2 deg is not likely to be sufficient to resolve polarization m dulation on an east-west backscatter path, which probably explains why the effect was not positively identified in data taken before the use of the 2.5 km array. These conclusions do not necessarily apply to north-south backscatter paths, however.

The measurements showed that the variation in backscatter amplitude can easily be as much as 10 dB, and this also was predicted theoretically. Therefore, any measurement of changes in sea roughness versus distance made with high sounder resolution must account for "polarization modulation," since it tends to alter the otherwise smoothly-varying amplitude of the backscatter with slant range, azimuth, and frequency. It was shown, however, that the effect of this new modulation can be controlled by suitably modifying the polarization of the transmitting antenna.

CONTENTS (Continued)

CONTENTS (Continued)

CONTENTS (Continued)

CONTENTS (Concluded)

ILLUSTRATIONS

ILLUSTRATIONS (Continued)

ILLUSTRATIONS (Continued)

ILLUSTRATIONS (Concluded)

TABLES

ACKNOWLEDGMENT

The author wishes to thank Professor O. G. Villard, Jr. for his guidance and encouragement throughout this work. Professors R. A. Helliwell and L. A. Manning also made useful suggestions regarding this manuscript, and Mabel Rockwell helped a great deal to prepare it for publication. Lewis Wetzel (Naval Research Laboratory, Washington, D.C.) and Donald Barrick (Battelle Memorial Institute, Columbus, Ohio), provided stimulating discussions on the theory of HF sea backscatter and ocean wave spectra. The people in the Ionospheric Dynamics Group contributed toward this work by helping in the experiments, data reduction and display, or by typing and re-typing the early drafts of the manuscript. I am very grateful for all this help.

The work was funded by the Advanced Research Projects Agency, with the Office of Naval Research, contract Nonr-225(64). The author appreciates this support.

I. INTRODUCTION

A. PURPOSE

High-frequency (HF) radio waves which propagate to or across the earth's surface are found to scatter from rough areas thereon. In particular, it is known that an irregular ocean surface provides an excellent backscatter reflector. Thus, obliquely-incident HF radio waves can reflect from sea waves and then return to the vicinity of the transmitter. The purpose of the research described in this report was to investigate a new type of "modulation" on sea-backscatter echoes. This type of modulation causes the amplitude of the backscatter to pass through successive peaks and nulls in the dimensions of range (time delay), azimuth, and radio frequency. The new modulation was first portrayed by families of lines of signal enhancement resembling thumbprints on swept-frequency sea-backscatter records. This remarkable phenomenon was revealed when a linear receiving antenna array 2.5 km long was put into operation in central California by Stanford University.

A specific purpose of the investigation was to verify a hypothesis that the newly-discovered modulation is caused by the rotation of the polarization of ionospherically-propagated radio waves which illuminate and scatter from a given area of the sea. Additionally, it was desired to study the limitations imposed by antenna beamwidth on ability to detect the new sea-backscatter modulation. An aim of the work was to afford means for identifying the "polarization modulation," and thereby to make possible better control of sea-backscatter amplitude, and to aid in the interpretation of ionospherically propagated sea backscatter using high azimuthal resolution.

B. BACKGROUND

1. Ionospherically Propagated Backscatter

The term "high-frequency backscatter" is used to describe the following process: A pulse of radio-wave energy is sent out from a transmitter. After a delay on the order of 0 to 50 msec some of that energy is received while the transmitter is off. This implies that the energy has returned after reflection from a distant object. The description of this process centers upon the comparison of the received energy with the transmitted energy wave form, together with the delay before the received energy is recorded. At high frequencies (between 3 and 30 MHz), the energy can propagate via line of sight (ground wave) or via one or more ionospheric reflections. Because of the latter, one may observe backscatter from irregularities on the earth's surface (such as mountains or sea waves) out to distances far beyond the visual horizon--on the order of 3,000 miles and more. It is also possible that "blobs" of enhanced ionization will act as reflectors. Figure 1 illustrates this process schematically. The present work concerns the ionospheric mode of backscatter propagation from the sea surface.

Measurements of HF backscatter date back to the late 1920's, when investigators first recorded pulse echo returns with unusually long time delays. In 1926, Breit and Tuve [Ref. 1] proved that a "conducting layer" existed in the atmosphere, and it was proposed in the same year by R. A. Watson-Watt that this layer be called the "ionosphere" [Ref. 2]. In 1927 Ekersley [Ref. 3] recorded pulse returns from longer ranges than were typical from the ionosphere. In 1928-29, Taylor and Young [Refs. 4, 5] observed the same phenomena and decided that the echoes probably came from the earth's surface via an ionospheric reflection. They also reported that backscatter from the direction of the sea was unusually strong.

A great deal of debate then ensued in the literature, as to whether or not the returns actually came from the earth, rather than from

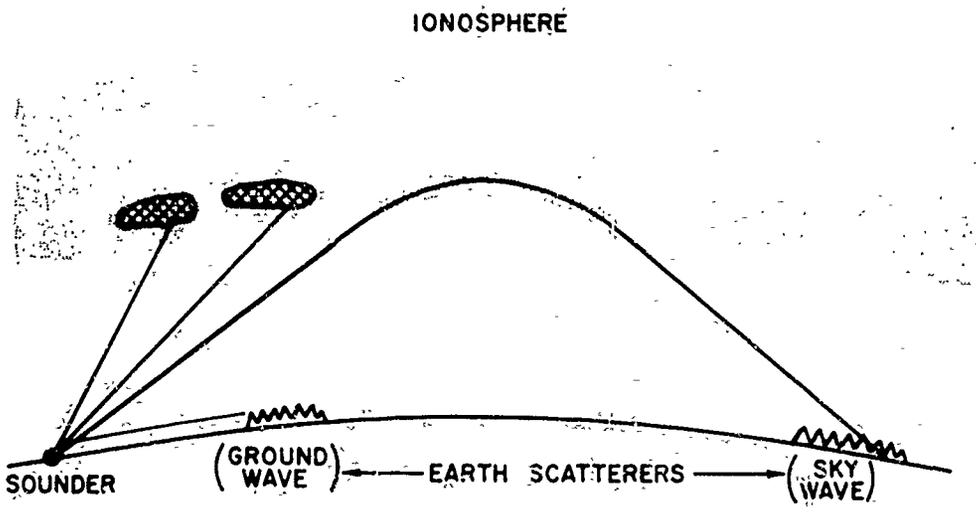

Figure 1. Forms of backscatter.

irregularities in the ionosphere. (Wilkins and Sherman, [Ref. 6, 1957], give a history of these developments.) The arguments were finally resolved in 1951, when Peterson [Ref. 7] and Dieminger [Ref. 8] almost concurrently proved that what was termed "2 X F" scatter (that seen most often) was due to backscatter from irregularities on the earth's surface. In the same year, Abel and Edwards [Ref. 9] used a beacon transponder to return signals from 700 to 2,000 miles distant, and by this means showed that the backscatter originated from the earth and traveled via the ionosphere. There is still evidence that some backscatter comes directly from ionospheric irregularities, both in the E and F regions. The latter type of scattering is rare and has no bearing on the present work. It is also true that electron-density irregularities ("blobs") in the ionosphere will disturb the propagation of radio waves between the sounder and the earth's surface, and hence will affect the amplitude of the earth backscatter. The latter effect will be discussed in Chapter IV.

2. Comparison of Land and Sea Backscatter

Early comparisons of land and sea backscatter by Villard and Peterson [Refs. 10, 11, 1952] revealed essentially no difference between the two. In 1956, McCue [Ref. 12] observed that land was probably the better scatterer, but his sounder illuminated a rather rough, hilly terrain, from which he identified a mountain echo, and his results below 30 deg elevation angle are difficult to interpret. In contrast, Ranzi [Refs. 13, 14, 1959-62] reported that sea backscatter propagated by the F_2 layer was much stronger than that from land with smooth terrain. During this same period of time, Hagn [Ref. 15], using an airplane, measured backscatter directly from several earth sources and found that, at elevation angles above 10 deg, the "scattering cross section" per unit

area, σ_o,* was on the average about a hundred times stronger for the sea than for the land. Hagn used a 1 μsec pulse length, which is much shorter than is normally realized in ionospheric sounding.

In 1965, Steele [Refs. 16, 17] reported the results of a well calibrated experiment in which he measured the difference between land and sea backscatter. Using a comparatively broad-beamed antenna and long (600 μsec) pulses, he determined that $\sigma_o(\text{sea}) \approx 10\ \sigma_o(\text{land})$ for elevation angles higher than 10 deg. These results agree roughly with those obtained by Ranzi and Hagn, and for elevation angles above 10 deg they represent probably the most reliable measurement of the average difference between sea and land backscatter yet reported. There is still need of accurate measurements of σ_o(sea) vs σ_o(land) below 10 deg elevation angle.

Washburn [Refs. 18, 19] has obtained absolute numbers of σ_o(land) using the same apparatus as the author of the present work. Washburn has conjectured that the average scattering cross section per unit area from land is of the order of 10^{-5} to 10^{-4}, with discrete excursions in σ_o rising to 10^{-1} near mountains.

3. Sea Backscatter

To date in the open literature, values of sea backscattering cross section per unit area at HF have been measured to be 10^{-4} by Ingalls and Stone [Ref. 20] and 10^{-5} to 10^{-4} by Hagn [Ref. 15]. The author [Ref. 21] used a new method for calibrating the σ_o of the sea, and obtained a value close to 10^{-3} in the Gulf of Mexico. It is clear

---

* A very useful parameter for defining the reflecting magnitude of a scatterer is its "scattering cross section" per unit area, σ_o, which is defined as σ/A_o, where σ is the total scattering cross section and A_o is the illuminated area. σ is defined as the power reflected from the scatterer, divided by the incident power density, and is usually expressed in square meters.

that more such measurements are needed; however, it is already apparent that the sea surface represents a much more continuous scatterer at HF than does the land.

The "doppler dependence" of the sea echo--i.e., the way in which the traveling sea waves shift the frequency of the backscattered radio waves--was observed and explained by Crombie [Ref. 22] in 1955. The same type of doppler dependence was observed in 1956 by Anderson [Ref. 23], in 1957 by Dowden [Ref. 24], in 1961 by Ranzi [Ref. 25], and by many others. All observations agree with Crombie's, and point out that the sea-backscatter doppler spectrum is usually confined to just two frequency components located by equal amounts above and below the illuminating radio frequency. These components are directly related to the value of the radio frequency, so that they may be predicted with good confidence. (see Chapter II). A dramatic utilization of the sea's doppler was shown by Blair et al. [Ref. 26] in 1969. The backscatter from the land was separated from that from the sea in both time delay and azimuth by virtue of the difference in doppler, so that a map of Florida could be visualized. With regard to the correlation between the doppler spectrum and sea state, it was shown by Tveten [Ref. 27] and Ward [Ref. 28] that ionospherically-propagated sea-backscatter spectra manifested second-order doppler components which seem to increase in size with sea state. Crombie (private communication) is also studying this property by measuring ground-wave-propagated sea backscatter.

Very little experimental data have been accumulated to show the polarization dependence of σ_o(sea) at high frequencies. Ranzi [Refs. 13, 14] concluded in 1961 that the sea's reflection was 26 dB stronger for vertical as compared with horizontal polarization. In 1965, Steele [Refs. 16, 17] reported a "knee" effect in the backscatter from the sea as the lower elevation angles were approached, which he associated with the pseudo-Brewster angle of the sea's reflection for vertical polarization.

Steele's results may be interpreted by assuming that the sea backscatter at HF is primarily vertically polarized at the lower elevation angle. Further measurements of the polarization dependence of σ_o(sea) are greatly needed, however, as is a determination of its relation to sea state and to the radio frequency. Chapter II will discuss a theory which has been found to agree with measurements of σ_o(sea), and which includes terms for the polarization dependence of the sea echo.

C. APPROACH

The author has had the privilege of being the first to use the world's largest HF receiving antenna (to be described later), with which backscatter from the sea has been recorded. Because of the high azimuthal resolution afforded by this antenna, greater detail and clarity in backscatter data can now be realized than were previously possible. It has therefore become of major interest to determine whether the state of the sea can be estimated by studying its backscatter characteristics through use of the large antenna. Such information would provide distant warning of storm activity at sea; or one might also be able to locate areas of unusual calm. In this regard, current effort is directed toward the measurement of the sea's backscattering cross section per unit area and its polarization dependence at HF. Future work should include the study of the sea's second-order doppler backscatter, which (on the basis of previous research) should yield a more sensitive indicator of sea state.

A second topic of great scientific interest has been the study of the general differences between land and sea backscatter that are revealed by high azimuthal resolution.

During the course of these studies, a new type of modulation on the sea backscatter echoes was discovered. This modulation was found to be unique to backscatter from the sea, and appears only when a very large sounding antenna is utilized. The appearance of this modulation initiated

a thorough study of its source, which is shown to be the rotation of the polarization of received backscattered radio waves.

The present report will proceed first to establish a reasonable model for the sea's backscattering cross section per unit area at HF. Next the experimental equipment, system parameters, and antennas used to verify this model will be described; after which, data will be shown which display the new type of modulation. A fairly rigorous theory will be set down to explain the way in which polarization rotation can cause the modulation, and an approximate computer raytracing method will be used to synthesize the effect on model backscatter data. The last chapter of the report will give conclusive experimental proof that the newly observed modulation is caused by polarization rotation.

II. A MODEL FOR SEA BACKSCATTER

It was noted in Chapter I that not enough experimental measurement of HF σ_o(sea) characteristics has been made. Most notably, the polarization dependence of sea backscatter has not been measured to good accuracy. Fortunately, a very good mathematical model for the sea has been derived by others. It is now intended to review this theory in order to supplement our experimental knowledge. A model for sea backscatter will then be summarized.

A. BACKGROUND

1. The "Resonant" Character of Sea Backscatter

Early attempts to derive a theory for sea backscatter, such as Hoffman's [Ref. 30, 1955], were helpful, but did not solve the problem in general. In particular, it became known--first by Crombie [Ref. 22]--that the sea's backscatter-doppler spectrum contained well-defined frequency components whose values were dependent upon the radio frequency. Crombie said that any wind-driven sea would manifest a continuous spectrum of sea wave lengths, L (up to a maximum)--each of which would travel at a different velocity (see below and Kinsman's excellent book [Ref. 31] for details on this). Therefore, Crombie postulated that the sea acted as a diffraction grating, whereby the waves spaced by multiples of half the radio wavelength λ (i.e. $L = n\,\lambda/2$, where $n = 1, 2, 3, \ldots$), did most of the scattering, and hence determined the value of the discrete doppler shifts induced onto the sea echoes. Physically, this meant that the backscatter from adjacent waves would add up in phase, whereas that from waves with other periods would not.

Mathematically, Crombie observed the following: the velocity, v, of a sea gravity wave whose crests are spaced by L meters is given by

$$v = \left(\frac{g}{2\pi} L\right)^{\frac{1}{2}} ,$$

where g is the gravitational acceleration. Then the doppler shift (frequency shift) δf produced by such a sea wave on a radio wave of wavelength λ which is reflected by this wave is given by

$$\delta f = \pm \frac{2v}{\lambda} = \pm \left(\frac{g}{\pi} \frac{n}{\lambda}\right)^{\frac{1}{2}} ,$$

where $L = n\lambda/2$, $n = 1, 2, 3, \ldots$, and the (+) sign denotes waves traveling toward the sounder, and (-) away.* Crombie's data agreed well with this theory. The strongest component in the backscatter (by far) was that for $n = 1$ (or $L = \lambda/2$), which will be denoted "first-order scattering." Data taken by other investigators agree with this, but as mentioned above, the scatter for $n = 2, 3, \ldots$ is also being seen. It is hoped to correlate the amplitude of these "second-order" doppler shifts with storm areas.

---

* The equation for δf must be modified by obliquity factors when a bistatic sounder is used, and when elevation angles are not low. This correction amounts to calculating the effective sea wavelength, L, viewed by the sounder; but this operation is straightforward and consistent with the above mechanism.

2. The Ocean-Wave Energy Spectrum

The sketch in Fig. 2* is included to help visualize Crombie's observation of the "resonant" character of sea gravity waves when they backscatter. Here, the approximate behavior of the sea's energy (proportional to the square of the wave height) is plotted as a function of the inverse sea wavelength (1/L), assuming various wind speeds. The region of 1/L which satisfies $L = \lambda/2$ over the HF band ("first-order scattering") is shown. The energy spectrum shown in Fig. 2 assumes that for a given curve, its corresponding wind speed has been sustained for a long enough period of time and has blown over a sufficiently large area (the "fetch"), to achieve stable conditions. The spectrum is somewhat idealized in this regard, since it assumes that large sea wave "swells" are not present except at extremely strong wind speeds. In fact, however, storms at sea can generate these large "swell" wave trains which can propagate for hundreds of miles into an area which would otherwise be calm. One must then add the energy in the swells to the appropriate curve in Fig. 2, at the correct inverse wavelength of the swell. Backscatter effects due to the presence of high-energy swells appear not to be common; but Muldrew [Ref. 32] believes that he recorded backscatter from such swells in the Atlantic Ocean, and Chapter IV discusses this further. For the present we may disregard their effect entirely.

Therefore, referring again to Fig. 2, we note that for wind speeds greater than about 10 to 15 knots, the wave heights which contribute to the first-order HF scattering ($L = \lambda/2$) increase very slowly. When this

---

* This sketch is very similar to one shown by Wetzel (Naval Research Lab., Washington, D.C.) in an unpublished paper entitled "HF Sea Scatter and Ocean Wave Spectra". The author of the present report benefited greatly by reading this work and discussing it with its author.

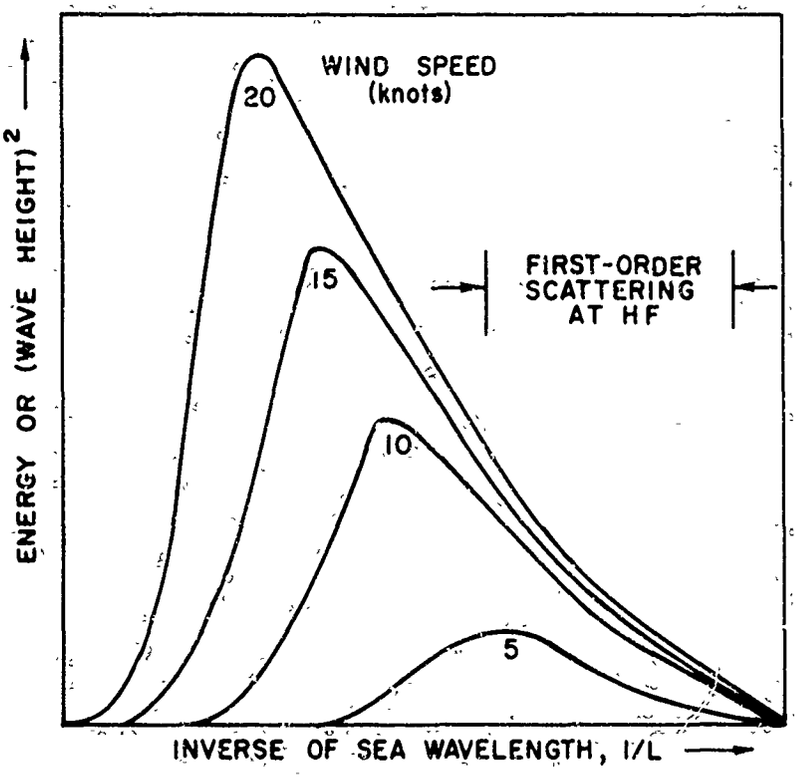

Figure 2. Energy spectrum of sea waves.

condition is reached, the sea is said to be "saturated." It is then clear from this model that for winds greater than 15 knots the $L = \lambda/2$ waves will present a nearly constant surface to the incident radio waves which backscatter from them. This will usually not be true for the $L = \lambda, 3\lambda/2, 2\lambda, \ldots$ waves, however, so that for the higher wind speeds the "second-order" doppler components in the sea echoes can increase--which is observed experimentally.

It is also known that the spectrum of a given patch of wind-driven sea is directional. Its energy is maximum in the direction the wind blows, and zero in the opposite direction. To first order this directionality can be modeled by multiplying the energy spectrum by a directionality factor such as $\cos^2\beta$ for $|\beta| \leq \pi/2$, where β is the angle between the direction of wind propagation and the direction of interest, and the energy is zero for all other β. (See Ref. 31 for more details). It will usually be true, however, that an average patch of ocean will contain waves coming from many different directions, so that a directional spectrum would be difficult to measure, especially when the wave components have reached saturation.

B. THE GENERAL THEORY FOR SEA BACKSCATTER

In view of the discussion above, the consideration of how the sea scatters radio waves at HF is greatly simplified. Specifically, the sea exhibits a "resonance" characteristic, whereby the wavelengths $L = \lambda/2$ are usually found to produce most of the scattering. This is consistent with the mechanics of ocean waves, and one may conclude that for HF backscattering the sea surface roughness does not appear to be random, but rather, it is smooth and periodic.

In 1965, Wetzel (private communication) used the "Kirchoff approximation" in rough-surface scatter theory, and with the Neuman spectrum

he showed that the sea should scatter primarily at the predicted $\lambda/2$ wave spacings, with an average cross section per unit area, σ_o, of $3(10^{-3})$ at saturation, along or opposite to the wind's direction. This value changes little over the HF band. He showed that when the radio waves illuminated the sea wave train in the direction of the latter's energy propagation, the doppler was minus. Likewise when viewing the waves "head on," the doppler is plus. All this agrees with experiment and intuition; but this approach does not account for the polarization dependence of the sea backscatter (although Wetzel thought that there should be such a dependence).

A theory utilizing the "Rayleigh-Rice perturbation method" has been developed, however, which does yield the polarization dependence of the sea backscattering cross section per unit area. There is a long and detailed history underlying this approach, and many have used it. The author is inclined to employ the results of Barrick and Peake [Refs. 33, 34], who seem to have used the theory a great deal. The theory is valid for small roughness scales relative to a radio wavelength. By examining the wave height (energy) spectrum for a saturated sea, one can show that for backscatter at HF from gravity waves and at microwave frequencies from capillary waves, it is true that this roughness criterion is usually satisfied. (Barrick, private communication.)

After some inspection, it is seen that Barrick and Peake's results are almost equivalent to Wetzel's, when one multiplies the latter by a function which accounts for polarization dependence. From Ref. 34, this function is $\sin^4\psi|\alpha_{\eta_\epsilon}|^2$, where ψ is the angle of elevation, and α_{η_ϵ} is given in the paper referred to. For a perfect conductor, $|\alpha_{\eta_\epsilon}|^2$ is equal to $(1 + \cos^2\psi)^2/\sin^4\psi$ for vertically polarized incident waves, and 1.0 for horizontally polarized waves. Thus the ratio of $|\alpha_{\eta_\epsilon}|^2$ for vertical over horizontal polarization becomes very large at lower elevation angles. Using realistic values for sea conductivity (4 mhos/m) and relative dielectric constant (80), the relative polarization dependence,

σ_v (vertical polarization)/σ_h (horizontal polarization), is plotted in Fig. 3 using Barrick and Peake's equations for α_{η_ϵ}. According to this theory, it is clear that for elevation angles normally encountered in HF backscatter ($\psi \leq 30$ deg), the sea should represent an almost vertically-polarized reflector.

C. VERIFICATION OF THE THEORY

It should be noted that the theoretical work just described neglects the effect of shadowing by adjacent waves, which appears difficult to take into account. Also, the development is strictly valid only for wave heights $\ll$ radio wavelengths. A first-order verification of the theory has been published by Munk and Nierinberg [Ref. 35], however, in which they used Barrick and Peake's results to show that for a saturated sea, $\sigma_o \approx 5(10)^{-3}$ at low elevation angles. Munk and Nierinberg used the "Philips saturation spectrum" to get this value, but note that it also agrees with Wetzel's prediction, $3(10)^{-3}$, using the "Neuman spectrum". Both these values agree roughly with experimental measurements of σ_o(sea) [Ref. 21].

It also appears that the results in Fig. 3 agree with the small amount of experimental evidence that the sea as a reflector of HF radio waves is primarily vertically polarized. However, probably the best verification of the theory's prediction of the σ_o(sea) polarization dependence has come from its application to backscatter measurements at microwave frequencies. The history of such measurements dates back to World War II, when radar sea "clutter" became a nuisance. The most up-to-date comparison between theory and experimental sea backscatter at these frequencies was given by Guinard and Daley [Ref. 36]. For our present purpose it will be sufficient to note the results given by Wright [Refs. 37, 38], who generated water waves in a wave tank with wave

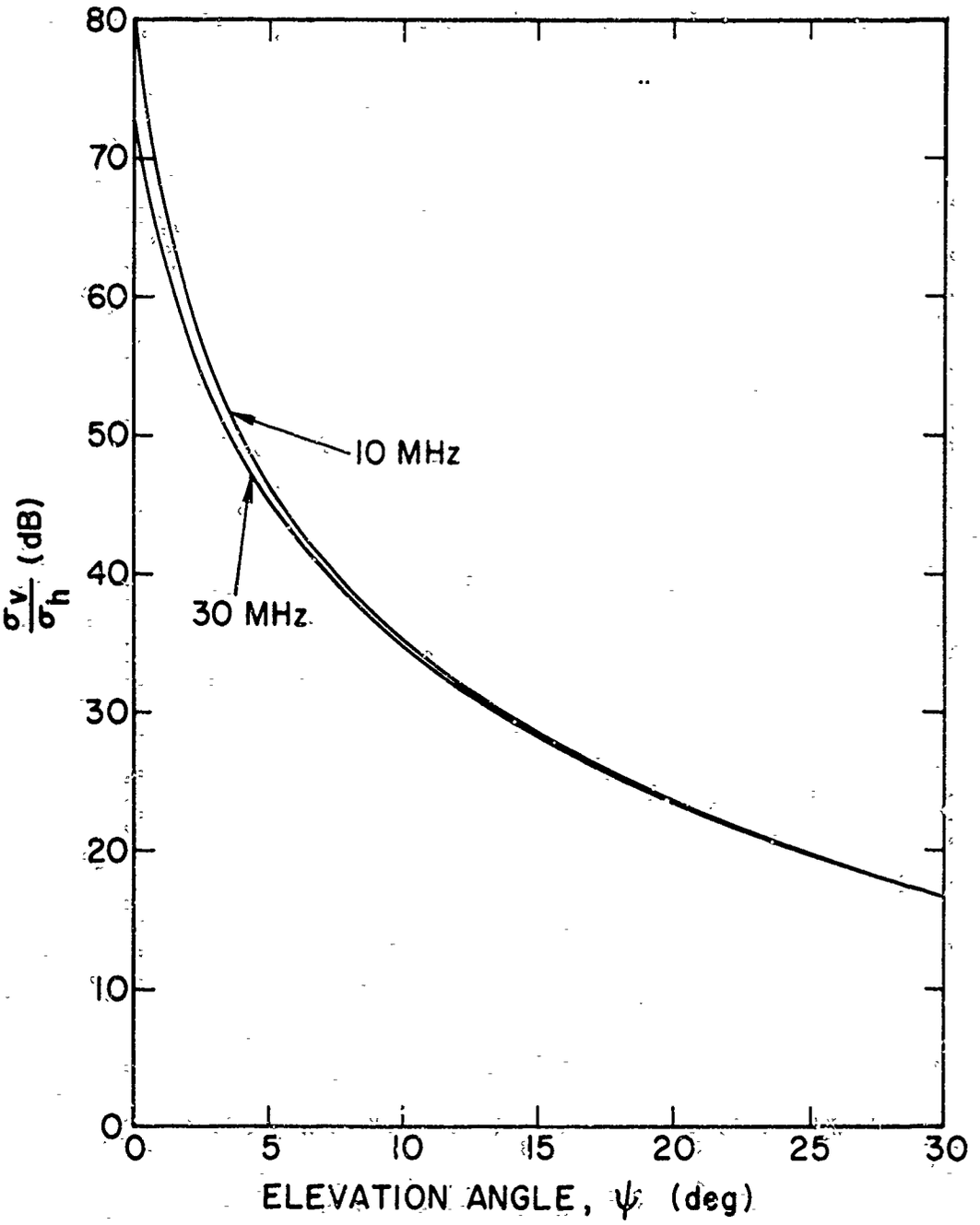

Figure 3. Theoretical sea cross-section magnitude gain for vertical over horizontal polarization, after Barrick [Ref. 34].

heights equal to about 0.01 the radio wavelength.

Barrick and Peake [Refs. 33, 34] compare the theory to Wright's experimental data (as does Wright himself), and very good agreement is shown. It is clear, therefore, that at HF, the backscatter from sea waves only a few feet high will correspond with Wright's "model" measurements, hence with the theory. Barrick (private communication) says that the theory should hold for wave heights up to about 0.1 times the radio wavelength. Somewhere beyond this limit we should undoubtedly observe the ratio σ_v / σ_h to decrease.

D. THE MODEL FOR σ_0(sea)

When a large sea-backscatter area is observed, it will often be true that more than one sea state will be present. Using superposition (incoherently), the power returned from each sea state is added, and it will therefore be more difficult to measure a directional spectrum for the sea-wave energy. Because of the saturation principal, however, one expects to find little difference in the backscatter between single and multiple sea-state patches, so that the theory for the homogeneous sea still applies (Wetzel, private communication). It would appear, therefore, that the amplitude of sea backscatter should be very continuous--- varying little, or slowly, from point to point. This circumstance will be contrasted with the irregular behavior of land scatterers.

The perturbation theory appears to account very well for the magnitude and polarization dependence of backscatter from water waves at microwave frequencies. The conditions for applying the theory at HF are satisfied, and there is no good reason to suspect that it should not work. Within an order of magnitude or so, the theory appears to explain results already obtained at HF, but more experimental data must be taken to verify the magnitude and polarization dependence of HF sea backscatter.

It is clear, however, that a most reasonable (first-order) conclusion is that the sea's backscattering cross section per unit area, σ_o, is primarily vertically polarized, with a value of about $5(10)^{-3}$ at elevation angles normally encountered at HF.

The consideration of the sea's doppler spectrum and its relation to sea state is a separate topic, not directly related to this work. However, if the second-order backscatter ($L = \lambda, 3\lambda/2$) does become appreciable in storm-generated seas, the waves which are responsible for that scatter will be large, hence will manifest a different σ_o polarization dependence than for the first-order ($L = \lambda/2$) backscatter. This circumstance might alter the character of the "polarization modulation" on sea backscatter to be described below, which in turn would aid in storm detection using the HF backscatter. The detection of such a change would be facilitated if the first-order doppler returns could be filtered out, and the ionospherically-induced doppler shifts [Refs. 39, 40] accounted for.

In the remaining chapters of this study, the first-order-scattering polarization characteristics of σ_o will be used in understanding the way in which polarization rotation causes the amplitude of sea backscatter to fluctuate with time delay, frequency, and azimuth.

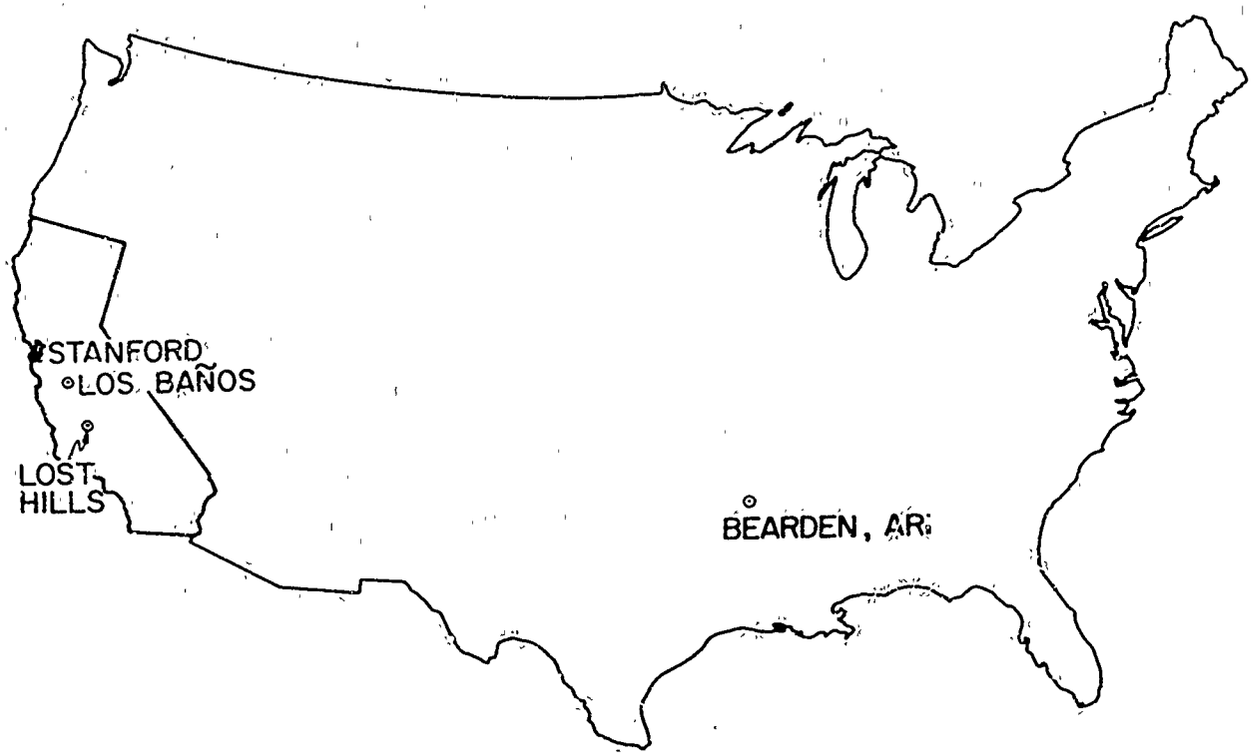

Figure 4. Location map: Stanford University field sites.

III. EXPERIMENTAL FACILITIES AND ANTENNA CHARACTERISTICS

In this chapter, the equipment, sounding waveforms, and antennas used in the backscatter work will be discussed, and mathematics will be presented to model the system sufficiently well to understand the experimental data. A map of the field sites is shown in Fig. 4. The receiving site is located near Los Baños, California (Lat. 37° 9' 39.0" N, Long. 120° 57' 9.5" W), and the backscatter transmitter is located at Lost Hills, California (Lat. 35° 41' 54.6" N, Long. 119° 57' 4.7" W). An additional transmitter is located near Bearden, Arkansas (Lat. 33° 44' 33.0" N, Long. 92° 37' 38.0" W), which provides oblique soundings of the ionosphere to the receiving site.

In the first section of the chapter, the equipment and sounding method will be described, while the antennas will be discussed separately in later sections. The purpose here is not to repeat work that has already been published; the reader will be referred to the many papers and reports written on the subjects.

A. THE SFCW SOUNDING METHOD

1. History

All of the experimental data on sea backscatter were taken using the "Sweep-Frequency-Continuous-Wave" (SFCW) sounding method. The technique is not new. It has been described under various titles such as "FMCW" and "chirp," and is discussed in most radar texts (see Ref. 41 for example).

a. HF Oblique Sounding

For application to HF sounding, the SFCW method was devised comparatively recently by R. B. Fenwick and G. H. Barry [Ref. 42], while working at Stanford. It has been used with great success in both oblique and backscatter sounding research. Fenwick and Barry [Ref. 43] first described its use in oblique sounding. Later, Epstein [Refs. 44, 45] used it in oblique soundings, with which he measured the effects of Faraday rotation with frequency. Sweeney [Refs. 46, 47] has described its utility in conjunction with mode-resolved reception of ionospheric signals on a wide aperture receiving array (to be described below). Fenwick and Lomasney [Ref. 48] used the SFCW waveform in vertical incidence soundings of the ionosphere.

b. HF Backscatter Sounding

The use of the SFCW waveform in backscatter studies is relatively new, and very little has been published on this application. The method is, however, identical to the one-way oblique ionospheric studies (just described), except that a sometimes more directive transmitting antenna and more transmitter power are usually used in the backscatter work. The reason for this is that backscatter energy is usually attenuated by 40 dB or more, as compared to energy propagated over the corresponding one-way path at the backscatter range. T. W. Washburn was the first to use the Stanford backscatter sounding system, and a preliminary analysis of his data was given at the 1968 Fall URSI meeting [Ref. 49]. In 1967, Croft extended his computer raytracing techniques (to be discussed later) to the interpretation of certain portions of Washburn's data, which established the presence of traveling ionospheric irregularities [Ref. 50]. A more recent example of an interpretation of earth backscatter SFCW data was given by Croft and Washburn [Ref. 51]. Reference 18

will contain a complete summary of the work done using the Stanford SFCW system as applied to the backscatter from the land--rather than from the sea. The work on sea backscatter, described herein, has not yet reached the open literature.

2. General Description of the System

The SFCW sounding method is accomplished by transmitting and simultaneously receiving (after a propagation delay on the order of several milliseconds) a CW carrier, whose frequency is swept linearly with time between two preset frequencies [Ref. 42]. The rate of the sweep may vary (in preset values) between less than 1 kHz/sec to as much as 10 MHz/sec, depending upon the equipment in use. The author used rates of 250 and 500 kHz/sec, which proved best for data reproduction. Photographs of the equipment used at the transmitter and receiver are shown in Figs. 5 and 6, respectively. A simplified block diagram describing the essence of the backscatter system is shown in Fig. 7.* The elements in this figure are very similar to those used before [Ref. 42, 43, 48]. The reader is referred to Ref. 43 for a description of the SFCW waveform generator.

The transmitter used at Lost Hills consists of three 10 kW automatically tracking units. When either of the large transmitting arrays is used (not described herein) all three transmitters are connected. When the crossed-LPA system is used, the output of a single transmitter is split, and 5 kW is fed into the feedline going to each antenna. The receiver at Los Baños is a Hallicrafters Manson (shown within the dotter area in Fig. 7), which is pretuned to 18 MHz. The instantaneous frequency f_t' of the SFCW generator at the receiver is therefore exactly 18 MHz higher than

---

* The equipment used for oblique sounding over the Los Baños/Bearden path (see Fig. 4) is exactly the same as that shown in Fig. 7, except that the transmitter is lower-power and wideband. Furthermore, a crystal rather than a cesium-beam standard is used at Bearden.

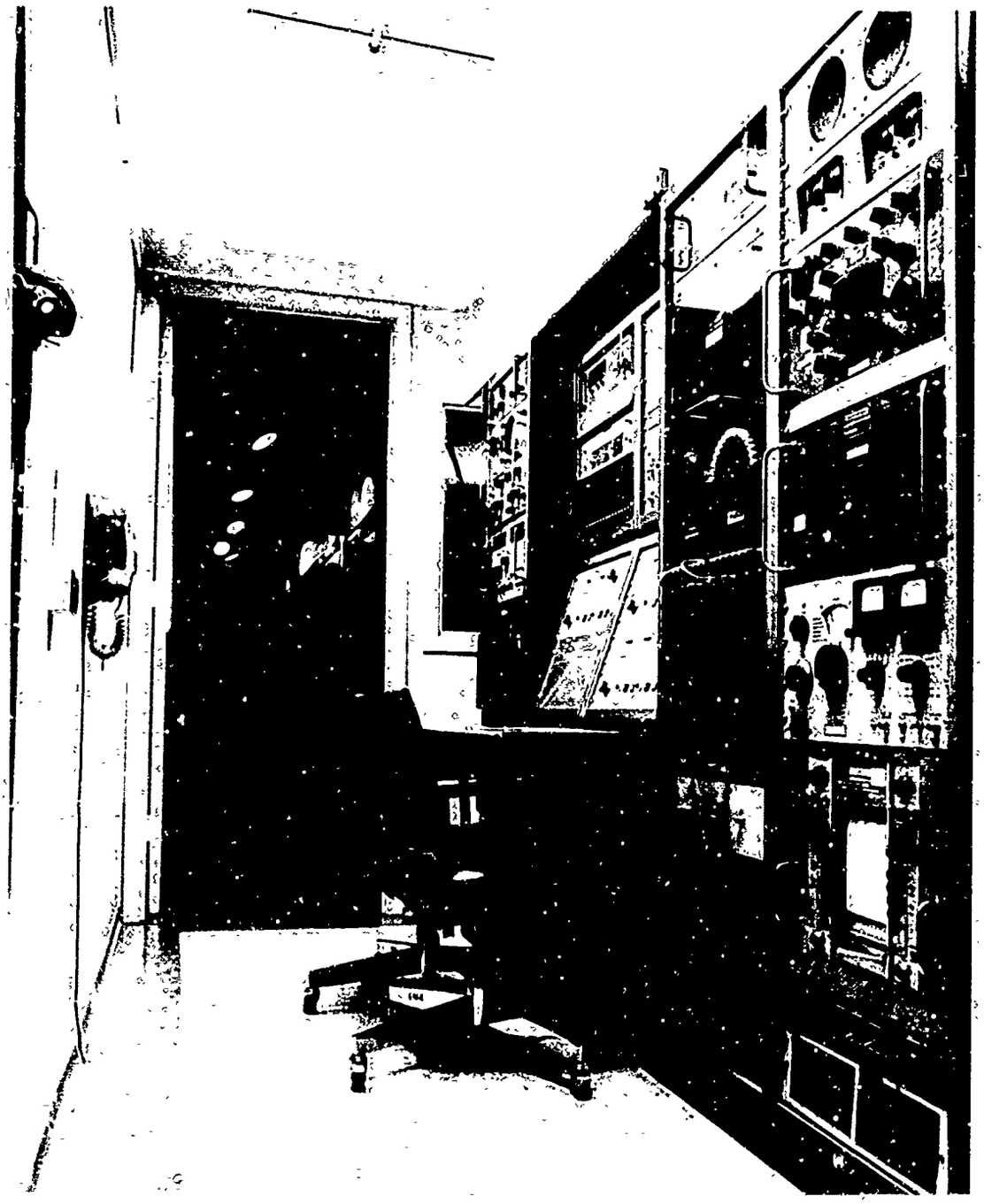

Figure 5. Transmitting equipment at Lost Hills, California.

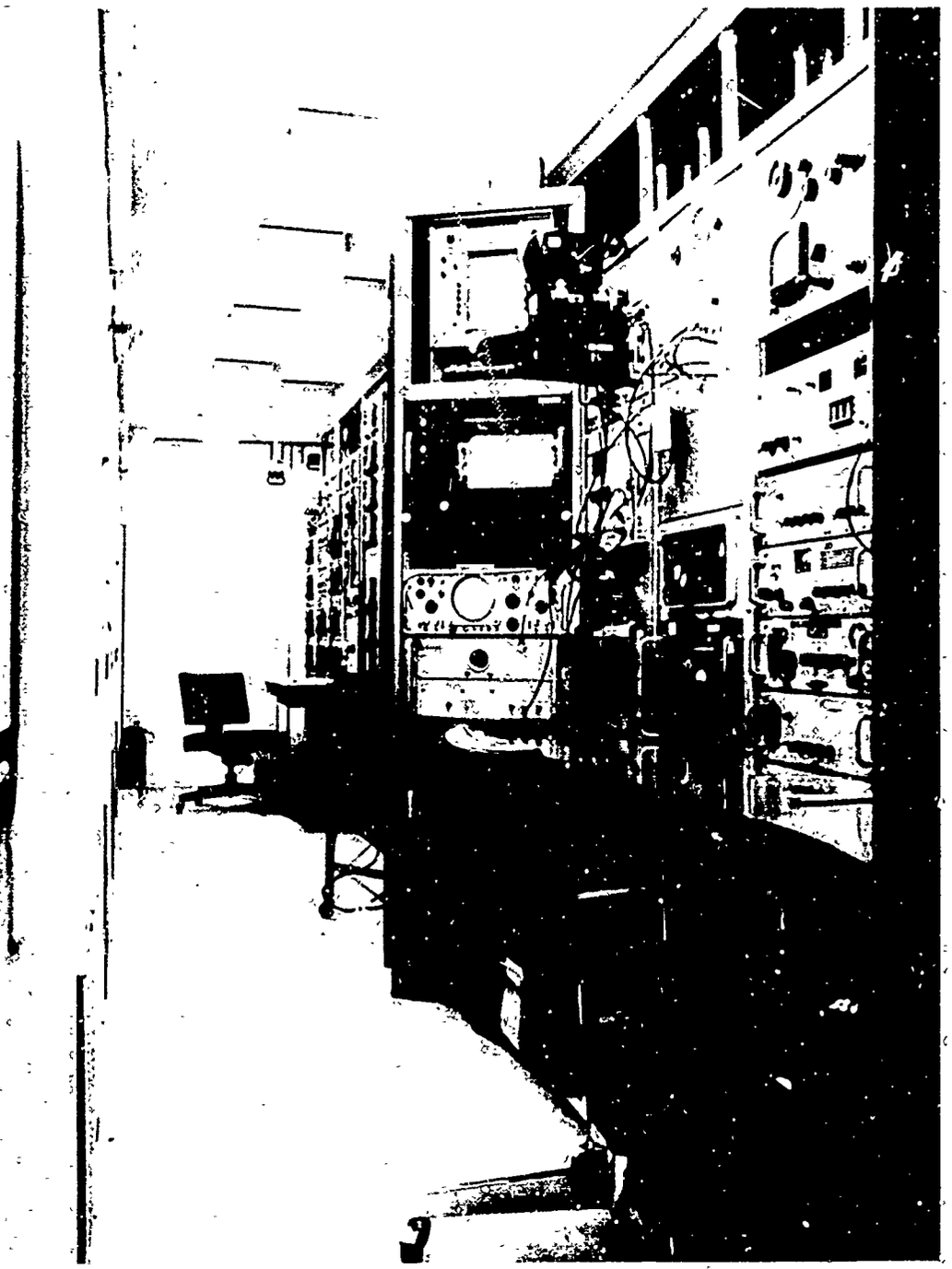

Figure 6. Receiving equipment at Los Baños, California.

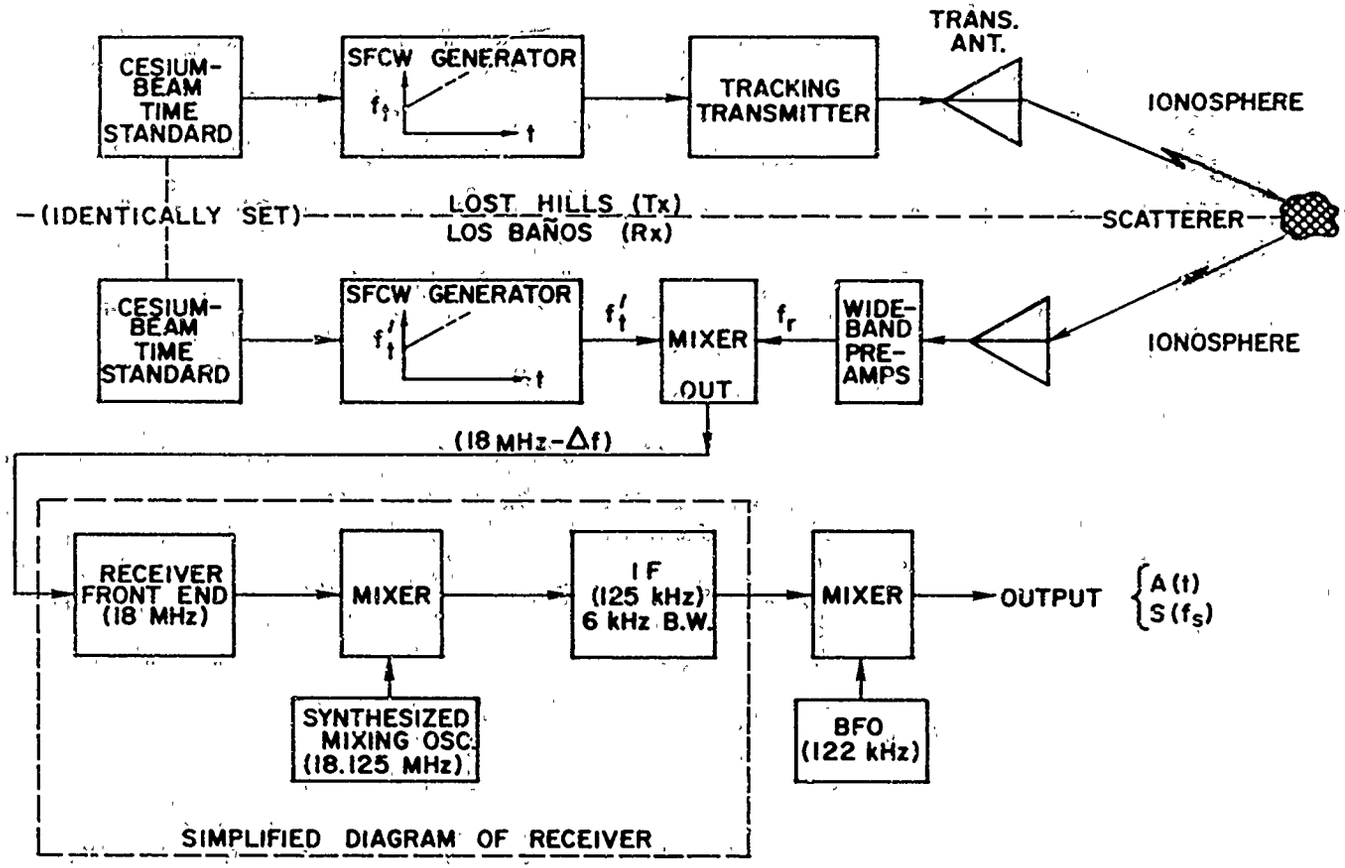

Figure 7. Block diagram of Stanford SFCW sounding system.

that at the transmitter site. This signal, when mixed with the transmitted (backscattered) signal yields a difference frequency which is very near to 18 MHz, but differs by an amount proportional to the propagation time delay, which will be discussed below. The receiver has a synthesized local oscillator, which is tuned to 18 MHz plus the intermediate frequency (IF) (125 kHz); the bandwidth of the IF section is set to 6 kHz. Finally, a synthesized BFO is set to exactly 122 kHz and mixed with the IF output in an external mixer. The output of this last mixer contains all the information one needs to deduce the time delay and amplitude of backscatter components.

The SFCW system just described differs from others in only one major aspect. Namely, both time and frequency are controlled with extreme accuracy. This is accomplished through the accuracy of the primary cesium-beam standards, which are periodically calibrated against one another. All frequencies used in the system are synthesized [using Hewlett-Packard (HP) model 5100A/5110A synthesizers], and their frequencies possess the accuracy of the cesium-beam standard. This accuracy is 1×10^{-11}, which is equivalent to an accumulated time inaccuracy of less than ± 1 μsec/day since calibration. This accuracy is mainly important in ensuring that the frequencies in use will be extremely stable with the passage of time--from minute to minute and from day to day, etc. As an additional benefit, the backscatter time delays may be measured to extremely good accuracy. This accuracy is, in fact, much better than is usually needed, because for most measurements neither the ground range to the backscatter area, nor the height of the ionosphere are known, so that neither angle-of-elevation nor actual range calibration is made.

3. Processing the Receiver Output

The signal output from the receiver in Fig. 7 will be represented by the variable A(t), where t is real time. To obtain the

backscatter information, A(t) is Fourier analyzed, so that it is necessary first to understand how the frequency spectrum of A(t) will behave.

a. The Frequency Spectrum

Suppose that the frequency sweeps at the transmitter and receiver begin at exactly the same time (as controlled by the cesium-beam frequency/time standards). Figure 8 compares the behavior of the frequency at the transmitter (f_t) to its value at the receiver (f_r) as a function of time; the difference between these two frequencies is denoted Δf. It is clear that f_r will always be less than f_t, and that Δf will increase for larger round-trip propagation times, τ. Since $f_t' = f_t + 18.0$ MHz, the output of the first mixer, which is fed into the receiver front end. is equal to $(f_t + 18.0 \text{ MHz} - f_r)$, which equals $(18.0 - \Delta f)$ MHz. The signal with the latter frequency is then amplified and passed through more mixing stages until it reaches the final intermediate-frequency (IF) amplifier whose frequency is 125 kHz.

The last IF output is mixed with the BFO frequency of 122 kHz. The output signal then contains the backscatter signal information which will pass through the 6 kHz IF bandwidth. It is found experimentally that the frequency of the output signal, f_s, is equal to 3 kHz - Δf. Thus if Δf exceeds 3 kHz an ambiguity in f_s exists, since negative frequencies then appear to be positive. If the BFO were set to any lower frequency, however, the amplitude of signals with frequencies such that $f_s = 0$ would be attenuated, since they would lie outside the passband of the last IF (which is ±3 kHz). Thus the limit on Δf is 3 kHz.

In order to allow for greater values of Δf, the start time of the receiver SFCW generator is delayed by an amount Δf. This is done simply by adjusting thumb-knobs on the cesium-beam standard

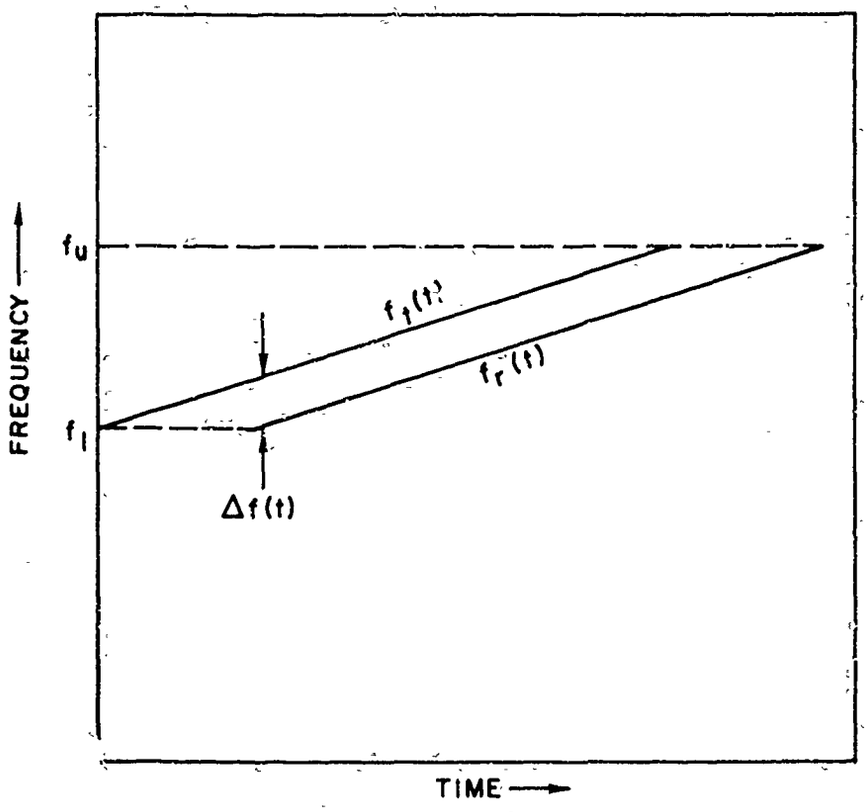

Figure 8. Simplified illustration of the frequency behavior of the transmitted and received signals, $f_t(t)$ and $f_r(t)$, respectively.

in as low as 1 μsec steps. Given that we know the sweep rate, $\dot{f} \triangleq K$ (kHz/sec), the equivalent change in Δf is equal to KΔT. Thus, allowing for the transmitter and receiver to begin sweeping at different times,

$$f_s = (3 + K\Delta T) - \Delta f \text{ kHz} \quad . \tag{1}$$

A(t) is then Fourier-analyzed in an electronic spectrum analyzer (the Federal Scientific model UA-7), which produces the signal spectrum $S(f_s)$.

b. Interpreting the Spectrum

For applications described herein, it is not necessary to preserve the phase of $S(f_s)$. The result of this analysis is that the backscatter amplitude is proportional to the magnitude of $S(f_s)$, while the time delay τ is proportional to Δf. From the many references on the SFCW technique, $\tau = \Delta f/\dot{f} = \Delta f/K$. From the spectrum analysis, we get finally:

$$\tau = [(3 + K\Delta T) - f_s]/K = \frac{3 - f_s}{K} + \Delta T \quad , \tag{2}$$

where frequencies are in kHz, and K has dimensions of kHz/sec. For sweep rate K = 250 kHz/sec, the quantity $d\tau/df_s$ has the value of 1/K = 4 msec/kHz, and for K = 500 kHz/sec, the value is 2 msec/kHz.

The backscatter records are thus a plot of spectrum frequency versus time, with amplitude as a third dimension which is displayed on a photographic grey scale with a dynamic range of 10 to 15 dB. The records are calibrated as a group time delay τ, vs frequency f, according to $f = f_t$. The latter is obtained from the property that $f_t = f(\text{starting}) + K(t - t_o)$, where t_o is the time at which a sweep begins.

c. The Equivalent Pulse Length, $\Delta\tau$

The equivalent pulse length which results from the spectrum analysis is the last remaining item of the SFCW technique which need be discussed. It has been customary to define the pulse length (or time-delay resolution) $\Delta\tau$ as the inverse of the frequency bandwidth over which the backscatter is integrated. Conversely, a pulse of length $\Delta\tau$ will have a frequency spectrum approximately $1/\Delta\tau$ wide, so that if a broad enough receiver bandwidth is used, the minimum resolution in time delay, $\Delta\tau$, will be realized. The receiver IF bandwidth of the SFCW technique is made purposely narrow (6 kHz in the present application) in order to improve the signal-to-noise ratio. Since the frequency of the sounder is always increasing, however, the equivalent bandwidth of a received pulse is simply proportional to how long an integration takes in the spectrum analysis process. The integration time is therefore inversely proportional to the equivalent receiver signal bandwidth. For the data presented herein, all of the spectrum analysis was performed on the electronic analyzer, which produces 500 discrete outputs which appear as 500 lines across the frequency band of analysis. Each line represents the output from an individual filter whose bandwidth is 1/500 of the total possible frequency range displayed. The bandwidth of each of these filters determines the integration time required to fill them up with energy. This integration time, when multiplied by the sweep rate, gives the frequency bandwidth over which the integration takes place. The inverse of the frequency bandwidth is the equivalent pulse length or minimum obtainable resolution cell. It is understood here that the energy from this pulse is by no means fully attenuated outside this bandwidth; however, the energy is so low that its peak may be determined within the bandwidth.

From the discussion above, the following expression may be used to calculate the equivalent pulse length, $\Delta\tau$:

$$\Delta\tau = \frac{W}{500}\frac{1}{K} \quad , \tag{3}$$

where W = spectrum-analyzer bandwidth. In the experiments it was always true that $\Delta\tau$ was small enough so that resolutions were limited by the ionosphere through dispersion and magnetoionic splitting [Ref. 45], or at least the observed changes in amplitude with time delay occurred over several pulse lengths. Therefore, it will really not be important to consider the effects of pulse length any further.

B. WIDE-APERTURE RECEIVING ARRAY

The most important factor determining the feasibility and success of the work described in this report was the use of an extremely wide-aperture receiving array. The design and construction of this array was supervised by L. E. Sweeney, Jr., and has already been described in great detail [Refs. 46, 47, 52]. A brief description will be given here, so that its characteristics may be understood well enough for application to the backscatter soundings.

1. General Characteristics

The antenna is a bidirectional broadside array of 256 vertical monopoles, spaced 10 meters apart; the over-all array length is 2.55 km. The array axis runs due north and south, so that its boresight reception is true east and west. Figure 9 is a photograph taken from the south end of the array. The terrain is relatively smooth and continuous, and the radiation vertical screening angle due to local foothills is on the order of 2 deg to the west and 0 deg to the east. The vertical monopoles are 18 ft high, and are fed with 52 ohm coaxial cable, which is grounded

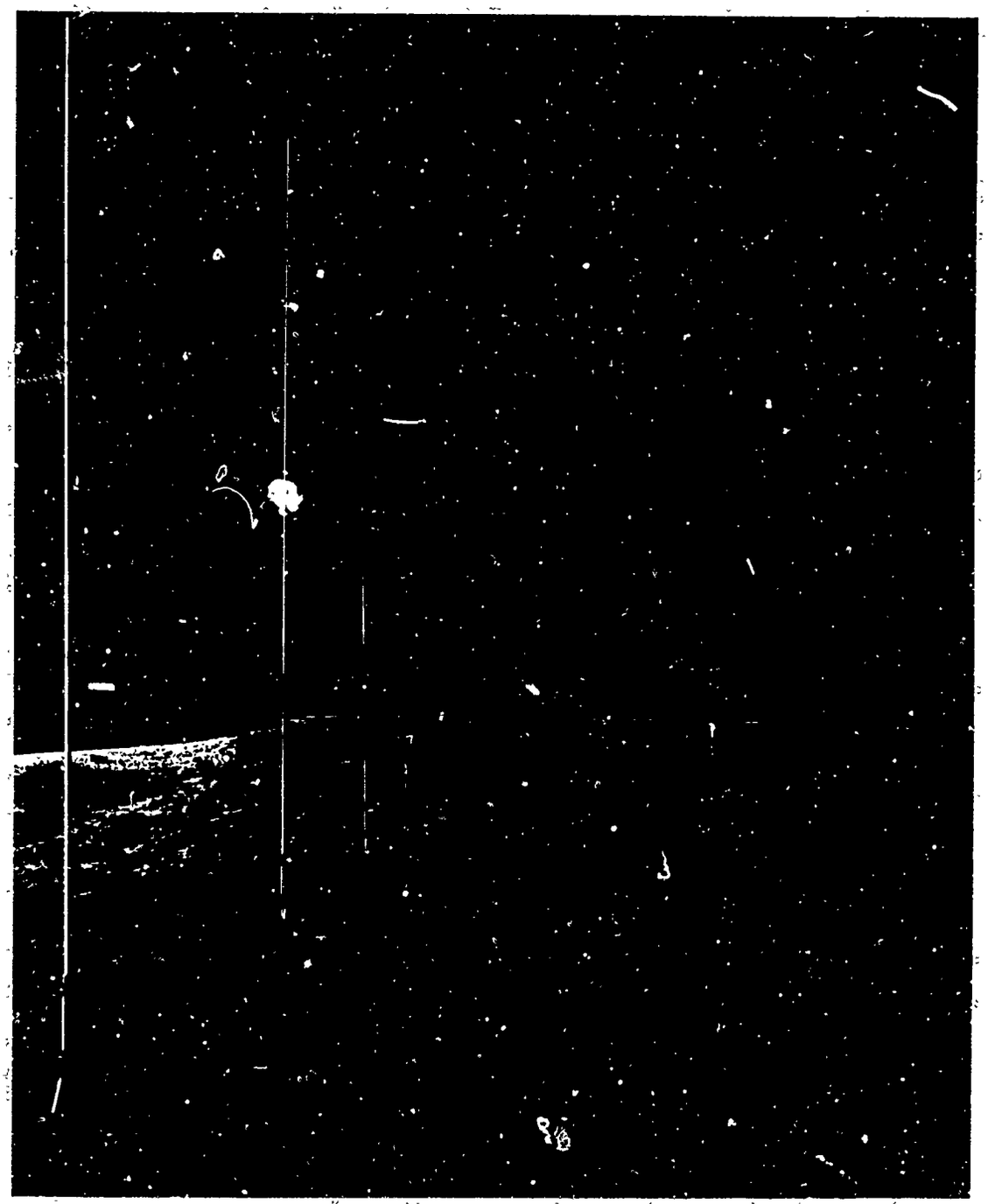

Figure 9. Wide-aperture receiving array at Los Baños, California.

by means of a strip of ground screen 72 ft wide running the length of the array. No attempt was made to match the impedance of the elements to the feed cables, which means that the absolute gain of the array should be a marked function of frequency. Quite to the contrary, however, no prohibitively deep nulls in the array gain appear in its direction of maximum "fire" (i.e., the main lobe) as the radio frequency is swept.*

The theoretical -3 dB beamwidth of the array varies from about 1 to 1/4 deg, between 7 and 30 MHz, respectively. The -6 dB beamwidth is 38 percent higher than these values. Thus, sufficiently continuous azimuth coverage between boresight and ±15 3/4 deg from boresight is achieved by phasing the elements so that their maximum reception occurs at intervals of 1/4 deg. This is accomplished by switching various lengths of coaxial cable in series with 255 of the 256 elements in order to properly phase the elements to achieve maximum gain in an off-boresight direction. This is called "slewing" the array and is quite common practice [Ref. 53, Chap. 4].

In order to economize on cable and switches, and in order to be able to taper its amplitude distribution, the array is first subdivided into 8 "subarrays", consisting of 32 elements each. A single feedline connects each subarray to the main equipment trailer, which is near the center of the array. Low-noise, wide-band preamplifiers are placed at each end of these 8 cables in order to overcome the losses introduced in the cables. In addition, certain amounts of attenuation are placed in series with each subarray in order to produce an amplitude taper across the array aperture.

---

* It might be conjectured that the mutual impedance between adjacent elements in the array causes sufficient coupling to modify the current distribution--hence improve the impedance match--of each monopole at the frequencies of non-resonance.

Each subarray consists of a "tree" of 32 elements [Ref. 47], whereby two elements are first paralleled, those two are paralleled with the adjacent pair, and so on, until 16 elements are finally fed in parallel with an adjacent 16. Each one of these connections forms a "sub-tree", which has its own slewing network of matching cables. This procedure allows substantial saving in the amount of phasing cables and in the number of switches required for slewing the array in 1/4 deg steps; and it reduces the probability of switch failure and total attenuation in the system. On the other hand, the saving in cable and switches results in a suboptimum element phasing which increases the sidelobe level of the array, but does not change the position at which the array's maximum gain occurs.

According to Sweeney, the sidelobe enhancement is nonexistent at slews of 0 and ±8.0 deg from boresight, and is relatively insignificant between boresight and ±12.0 deg (i.e., between bearing = 90 or 270 ±12.0 deg).

2. Mathematical Model

The uncertainties in the element gain and the effect of mutual coupling between elements of the array are of no consequence in the research reported here. However, the azimuthal dependence of the antenna gain is needed to determine the equivalent azimuthal angle over which, if the gain is assumed to be constant at its maximum, all of the received backscatter power would enter. It will be necessary to know that some portion of this equivalent beamwidth is small compared to a period of polarization rotation with azimuth when range and frequency are constant.

As mentioned above, the array is broken down into 8 subarrays, which are tapered in amplitude. Thus, the receiving antenna gain vs azimuth, $G_r(\varphi)$, may be calculated by summing the electric field phasors from each subarray, while considering each subarray gain pattern, $G_{SA}(\varphi)$, to be an element in the 8 element array [Refs. 47, 53]:

$$G_r(\varphi) = G_{ro} G_{SA}(\varphi) \left| \sum_{k=1}^{8} b_k e^{i(k-1)\gamma_{SA}} \right|^2 , \quad (4)$$

where G_{ro} is a constant which determined the maximum gain (for a given elevation angle and frequency), b_k is the tapering gain in the k^{th} subarray "element" shown in Table 1, and γ_{SA} is the phase angle on each subarray, given by

$$\gamma_{SA} = \frac{2\pi d_r}{\lambda} (\cos \theta - \cos \theta_o) , \quad (5)$$

where d_r = distance between centers of adjacent subarrays (320 m),

λ = the radio wavelength,

θ = angle between main lobe ("line of fire") and array axis,

θ_o = steer angle (slew) of the array.

Table 1

TAPERING GAIN OF THE SUBARRAYS

k	b_k	Attenuation (dB)
1, 8	0.35355	9
2, 7	0.56233	5
3, 6	0.79434	2
4, 5	1.00000	0

For low elevation angles, θ is very nearly equal to the projected azimuth, φ, of the incoming energy. θ is calculated exactly according to:

$$\cos \theta = \cos \psi \cos \varphi \quad , \tag{6}$$

where ψ is the elevation angle.

The calculation of G_{SA} (exactly) is not very straightforward, because of the non-optimum phasing of the array elements. As mentioned previously, however, the sidelobe enhancement is not very great for slews up to ±12 deg from boresight, so to a very good approximation for these angles, the well-known array factor may be used to describe the normalized gain of the 32 element subarray [Refs. 47, 53]:

$$G_{SA}(\varphi) = \frac{1}{32}\left[\frac{\sin (16\gamma_{EL})}{\sin (\gamma_{EL}/2)}\right]^2 \quad , \tag{7}$$

where

$$\gamma_{EL} = \frac{2\pi d_{el}}{\lambda} (\cos \theta - \cos \theta_o) \quad , \tag{8}$$

and d_{el} = element spacing (10 m).

For slew angles between ±12 1/4 and ±15 3/4 deg, Eq. (7) is considered to be at least a moderately good approximation [Ref. 47]. Figure 10 shows the behavior of $G_r(\varphi)/[G_r(\max)]$ as a function of azimuth for a slew angle of 0 deg (boresight), computed at a frequency of 22.35 MHz, assuming that $\psi = 0$ deg. As noted, the -3 dB beamwidth of this array function is 0.32 deg, and the -6 dB beamwidth is 0.50 deg.

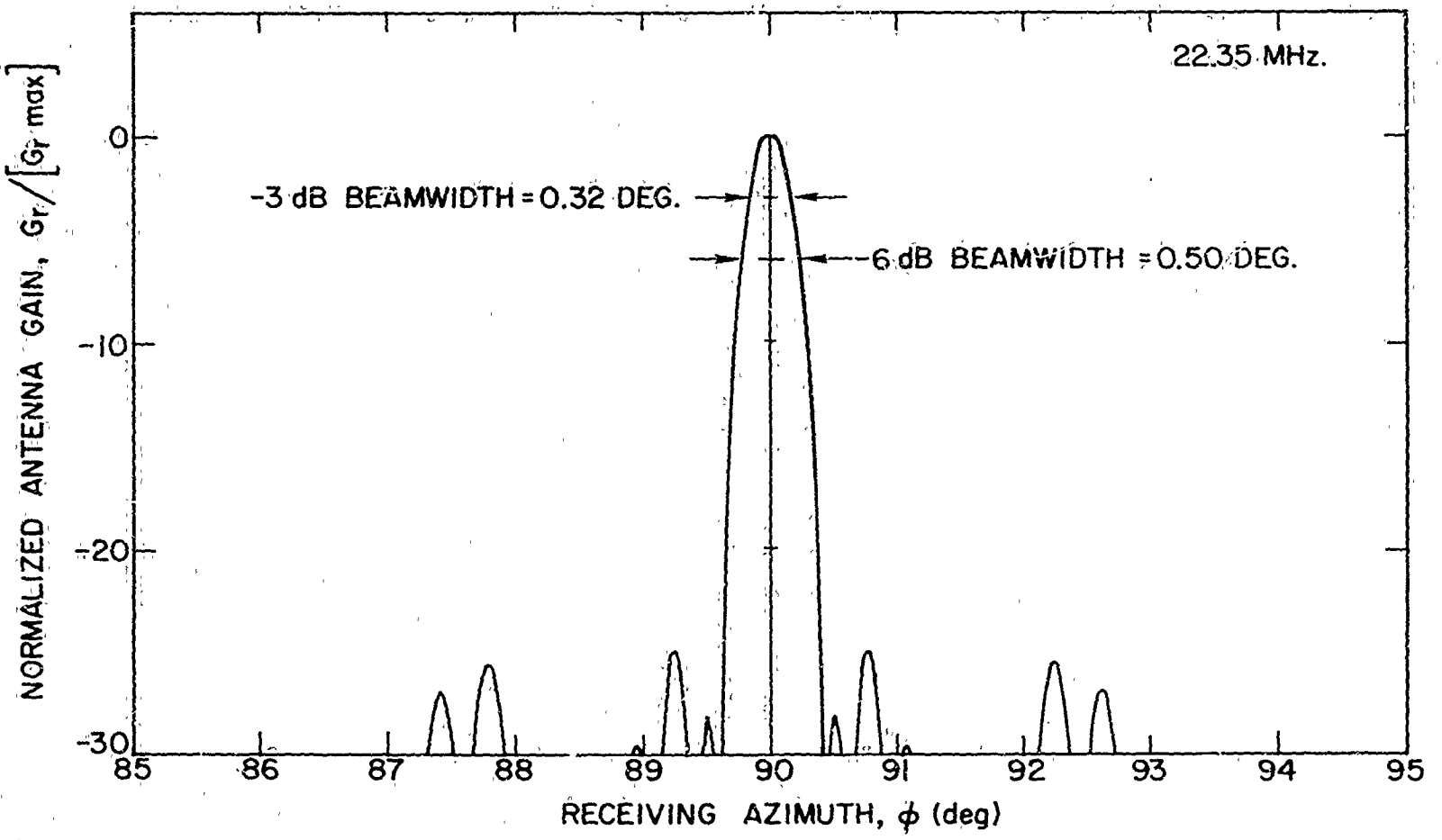

Figure 10. Los Baños array factor at boresight.

C. THE CROSSED-LPA TRANSMITTING ANTENNA

The transmitting antenna which proved to be most useful in the studies of polarization effects on backscatter amplitude was the crossed LPA antenna shown in Fig. 11. The LPA's were manufactured by Hy-Gain (Model LP-1007), cover a frequency range of 13 to 30 MHz, and exhibit negligible mutual coupling. The front-back-ratio (F/B) of each is 15 dB, and the horizontal beamwidth of these antennas is extremely broad compared to the receiving beam. The horizontal element is mounted 53.5 ft (16.3 m) and the vertical element, 76.0 ft (23.16 m) above the ground. As discussed by Epstein [Refs. 44,45], the antenna had already been used successfully in polarization studies of waves transmitted over one-way obliquely-incident ionospheric paths. The design of the crossed-LPA system and a preliminary analysis of its behavior has recently been published by Lomasney and Barnum [Ref. 54].

The antennas are unique in that: (a) the transmitted polarization may be switched from vertical to horizontal very quickly, and (b) the antennas can be fed together, but out of phase, in order to produce elliptical (ideally, circular) polarization, which matches the polarization of one of the magnetoionic components of the ionosphere (to be discussed later). When these antennas are operated separately (one at a time), it will not be necessary to consider their absolute gain behavior (since it is never needed in this case). Moreover, the polarization characteristic of each antenna is linear and well defined, being very nearly 90 deg removed from the other in space at all transmitting azimuths and elevation angles used.

By contrast, when the antennas are fed together in order to produce a given elliptical polarization, it is necessary to consider the relative magnitude and phase of the radiated fields from the elements in the presence of the ground. The desired polarization for matching the magnetoionic components in the ionosphere is circular under almost all

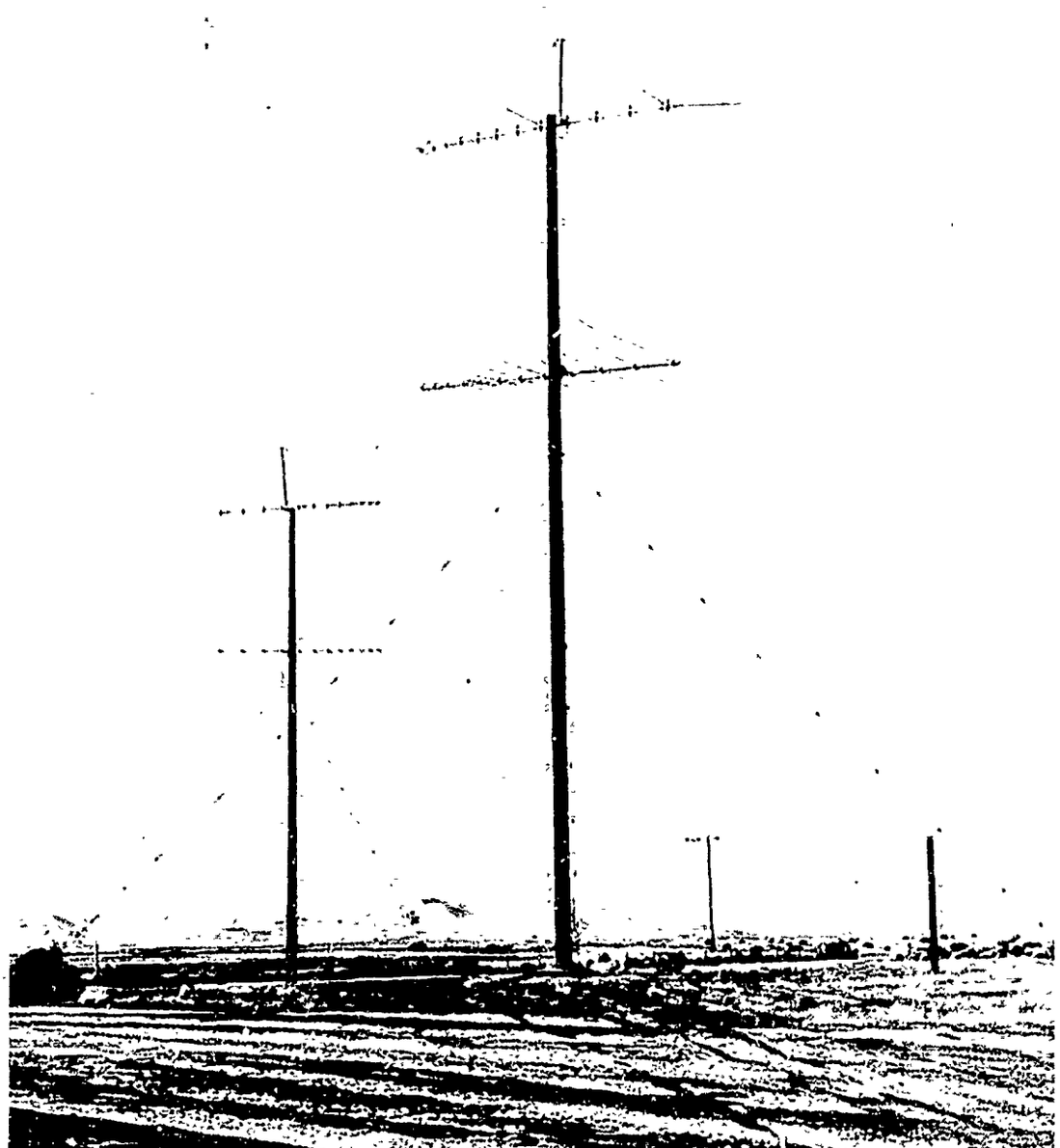

Figure 11. Crossed-LPA transmitting antennas at Lost Hills, California: westward-looking antenna in the foreground.

circumstances (to be shown later). As shown by Lomasney and Barnum [Ref. 54], however, such a condition is difficult to achieve over a broad range of frequencies and elevation angles. But it was also shown that nearly circular polarization may be obtained over the widest ranges by placing a phasing line (coaxial cable) in series with the vertical LPA element in order to adjust the relative phase between the antennas to be the necessary 90 deg. For the studies to be reported here, the electrical length of the phasing line was 27.27 ft or 8.313 m, and the antennas were fed with equal power; the phase was such that the top half of the vertical antenna was in phase with the right half of the horizontal antenna, while looking in the direction of "fire."

The ground underneath the antennas was flat farm land, but the soil was not "rich" and therefore cannot be assumed to be "good"; it was thus considered to be "medium" ground, with a conductivity of 10^{-3} mhos/meter, and relative dielectric constant of 10.

Using the approach described in Ref. 54, the relative magnitudes and phases of the two LPA's were calculated from the equations for their vertical pattern gains (magnitude and phases), while including the fixed phase difference introduced by the phasing cable. With this information, the calculation of the transmitted ellipticity, ϵ, and the tilt angle, θ_{ro}, (by which the major axis of the ellipse deviates from the horizontal) is straightforward.* This calculation was carried on by means of a digital computer. The output is plotted in Figs 12 and 13. The former shows how the ellipticity ϵ varies with elevation angle for different frequencies. Assuming a 300 km virtual height in the ionosphere, the approximate variation of ϵ with slant range is also

---

* If interested, the reader will find the derivation of the equations for ϵ and θ_{ro} in Ref. 55.

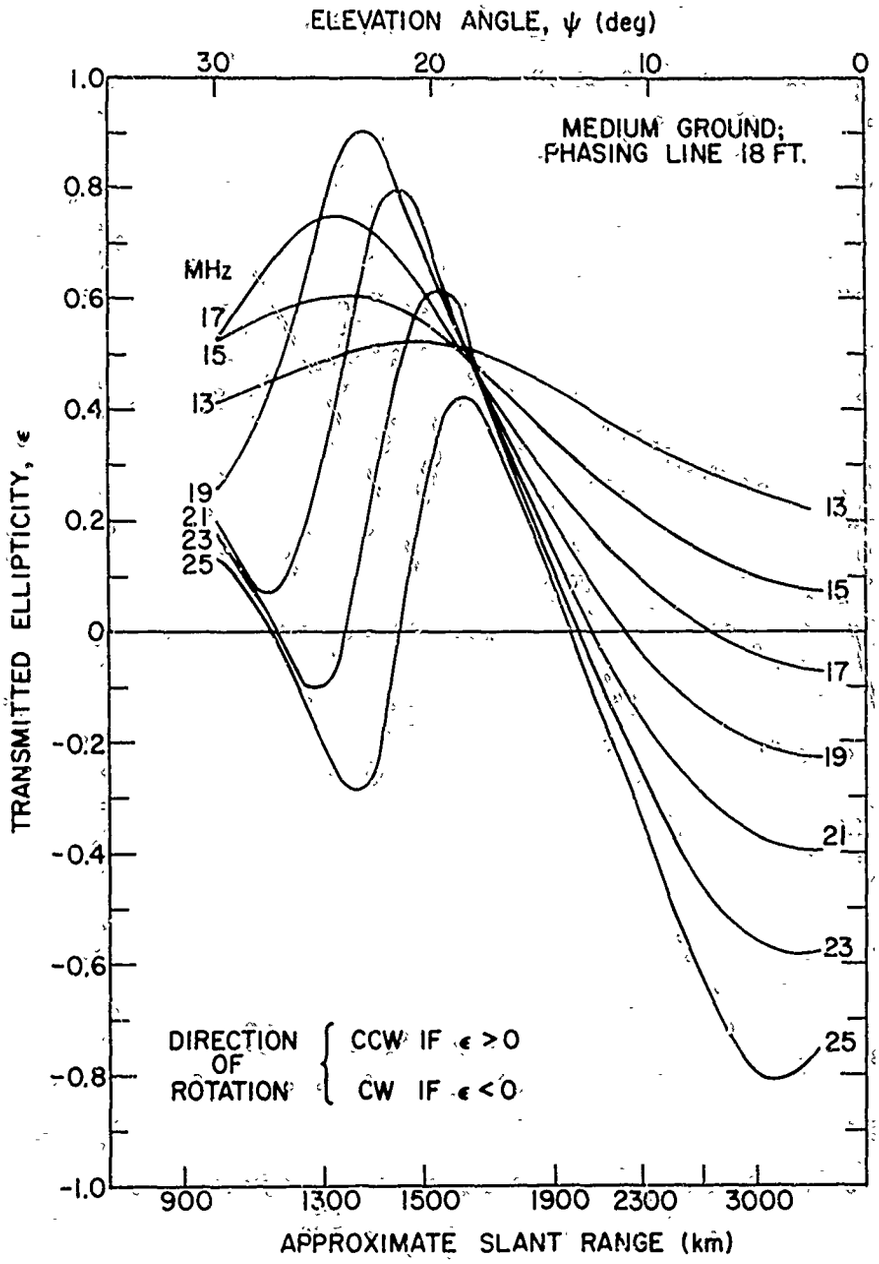

Figure 12. The ellipticity of polarization of waves transmitted by the crossed LPA's.

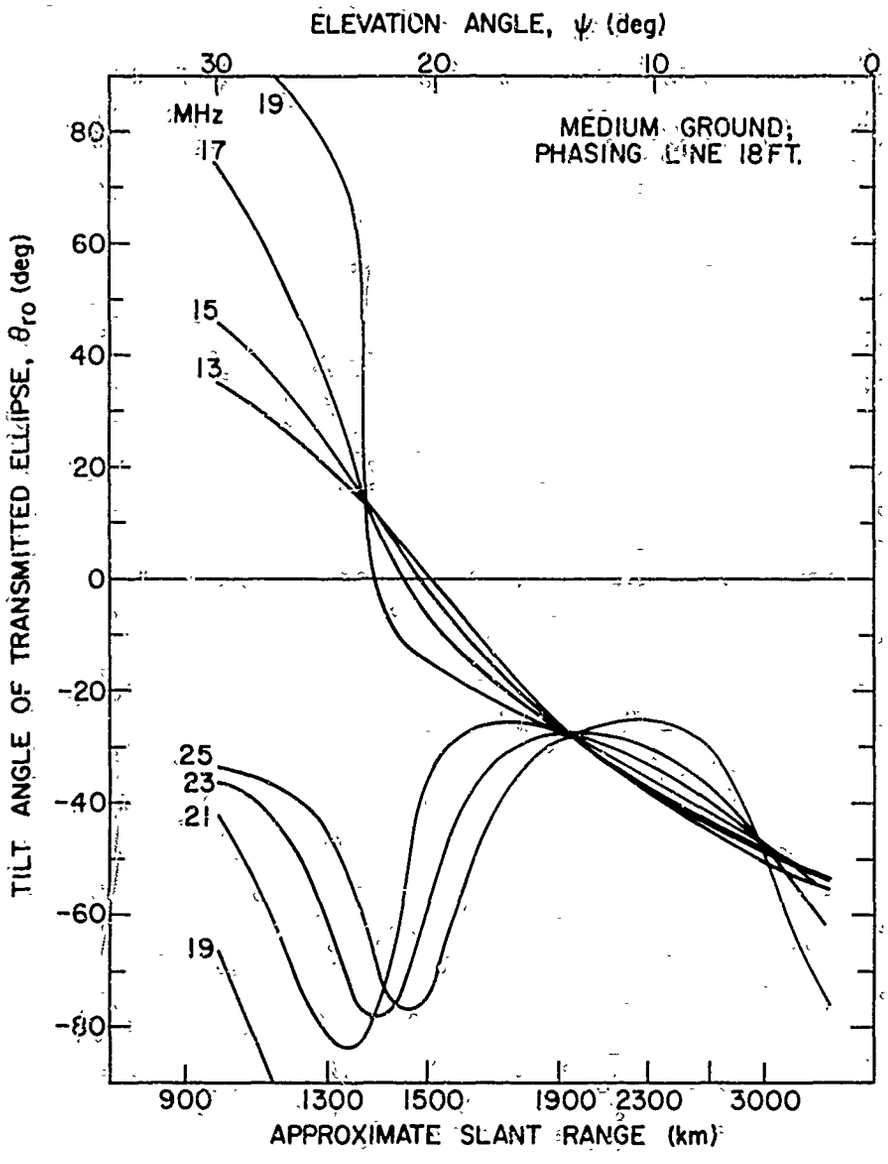

Figure 13. Tilt angle of major axis of the ellipse transmitted according to Fig. 12.

shown. The direction of rotation of the ellipse is given by the sign of the ellipticity--right-handed for a negative sign, and left-handed for a positive sign. If the phase of the antennas were reversed it would be necessary to reverse the direction of rotation [Ref. 54]. Figure 13 shows how ϑ_{ro} varies with elevation angle and slant range. When the ellipticity is less than 0.2 or so, the transmitted wave is nearly linear, and the tilt angle shows how much its plane of polarization differs from the horizontal. The significance of these figures will be discussed further when the experimental data are interpreted.

1. "Leading Edge" Focusing

Beginning at the lower left corner of the figure we see the 1, 2, 3, 4, and 5-hop vertical-incidence returns directly from the transmitter, via the (Fall) F layer, as we increase time delay. Beginning at 5 msec delay, the lower leading edge of the backscatter emanates from the 2-hop vertical-incidence return. This edge represents the "minimum time delay" of the backscatter, and is different from the delay to the skip-distance except at the longer ranges, as shown by Peterson [Ref. 7] and Dieminger [Ref. 8]. The 3-hop vertical-incidence trace produces a higher leading edge which is the two-hop backscatter. In between the 1- and 2-hop leading edge, a faint trace of a third edge is seen which has 2 components. This third edge is backscatter from the Pacific Ocean, via the westward lobe of the Los Baños receiving array. Its leading edge is far to the left of the eastward backscatter because the ionospheric density to the west is much lower than to the east at this time of day (0724 PST). The two components of the westward edge are undoubtedly due to magnetoionic splitting (by analogy with typical vertical-incidence data showing the "o" and "x" modes) [Refs. 48, 56, 57], which were apparently (but not clearly) observed by Silberstein [Ref. 58]. Judging from the relative strengths of the east and west backscatter, the effective F/B of the transmitting antenna is about 10 to 15 dB or more. The backscatter propagation viewed at these frequencies is entirely by the F layer, and no evidence of either normal or sporadic E propagation is apparent.

2. Discrete Echoes

The most important backscatter detail which appears to the left of the 1-hop leading edge in Fig. 14, can be divided into essentially two categories: The lines representing echoes from discrete echoes in land backscatter, and those representing focusing of the backscatter due

1. "Leading Edge" Focusing

Beginning at the lower left corner of the figure we see the 1, 2, 3, 4, and 5-hop vertical-incidence returns directly from the transmitter, via the (Fall) F layer, as we increase time delay. Beginning at 5 msec delay, the lower leading edge of the backscatter emanates from the 2-hop vertical-incidence return. This edge represents the "minimum time delay" of the backscatter, and is different from the delay to the skip-distance except at the longer ranges, as shown by Peterson [Ref. 7] and Dieminger [Ref. 8]. The 3-hop vertical-incidence trace produces a higher leading edge which is the two-hop backscatter. In between the 1- and 2-hop leading edge, a faint trace of a third edge is seen which has 2 components. This third edge is backscatter from the Pacific Ocean, via the westward lobe of the Los Baños receiving array. Its leading edge is far to the left of the eastward backscatter because the ionospheric density to the west is much lower than to the east at this time of day (0724 PST). The two components of the westward edge are undoubtedly due to magnetoionic splitting (by analogy with typical vertical-incidence data showing the "o" and "x" modes)[Refs. 48, 56, 57], which were apparently (but not clearly) observed by Silberstein [Ref. 58]. Judging from the relative strengths of the east and west backscatter, the effective F/B of the transmitting antenna is about 10 to 15 dB or more. The backscatter propagation viewed at these frequencies is entirely by the F layer, and no evidence of either normal or sporadic E propagation is apparent.

2. Discrete Echoes

The most important backscatter detail which appears to the left of the 1-hop leading edge in Fig. 14, can be divided into essentially two categories: The lines representing echoes from discrete echoes in land backscatter, and those representing focusing of the backscatter due

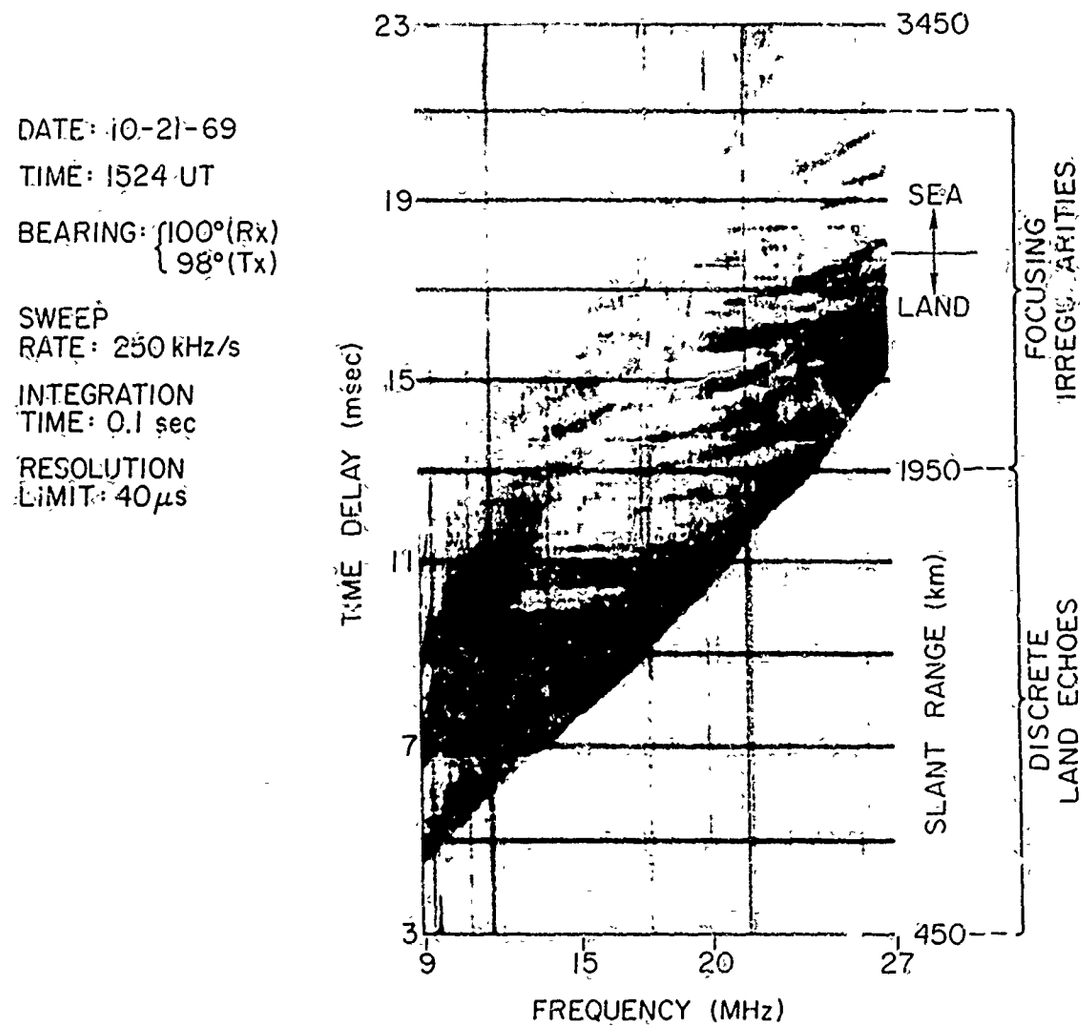

Figure 14. Example of SFCW backscatter data. (Subtract 8 hours from UT (Universal Time) to obtain local standard time at transmitter for all SFCW records.)

to ionospheric irregularities. The former, and to some degree the latter, are subjects discussed at great length by Washburn [Ref. 18]. There is a third mechanism which can modulate sea backscatter intensity, and which has an appearance similar to that of the focusing regions; however, its consideration will be presented in the next section.

The nearly horizontal lines in the lower half of the data are always seen in backscatter from the land, but never from the sea surface. This fact at once illustrates the first unique feature of sea backscatter, in that its cross section is a very smooth continuous function with azimuth. Washburn [Refs. 18, 19, 49] has identified certain echoes of these types as arising from mountains, and, in general, it is characteristic of these echoes to jut out to the left of the leading edge of the backscatter and to possess the shape of a forward oblique ionogram to the range of the scatterer (but with the time delay doubled). If the echo is strong enough it can be identified as such even with a relatively small antenna, as shown by Silberstein [Ref. 58]. By contrast, as Washburn showed, when a narrow beamwidth antenna is used, it is possible to resolve several ionospheric modes in the echo, and observe effects due both to the bistatic sounder geometry, and due to the passage of traveling ionospheric disturbances (TID's). It is characteristic of these echoes to be rather discrete in azimuth--within the beamwidth of the Los Baños receiving array. It is also clear from these echoes that the upper (Peterson) ray propagation is greatly attenuated, hence it may be ignored (except very near the leading edge).

3. Focusing From Ionospheric Irregularities

The second set of lines at the top of the data in Fig. 14 are seen in backscatter from both sea and land, without distinction (most of the data represent backscatter from the land). These lines are clearly distinguished from the discrete scattering echoes, in that they are

always broader in range extent, much less sensitive to changes in azimuth, and typically move with time. Furthermore, they are more nearly horizontal than vertical, but are rarely as smooth and straight as the land echoes. They appear here to be rather evenly spaced and almost parallel, but these lines will be distinguished from another (new) type to be discussed shortly.

Several authors have observed these fluctuations in backscatter intensity, in both fixed- and wide-swept-frequency data [Refs. 50, 51, 59-66] and some have considered their cause. In 1957 [Ref. 60] and 1961 [Ref. 61] Tveten reported seeing regularly-spaced striations in F_2-propagated backscatter signals, whose range varied with time. He associated these with TID's. Dueño saw similar variations [Ref. 62]. Using a more directive antenna, Hunsucker and Tveten [Ref. 63, 1967] showed that the variations are also a function of azimuth--they are usually tilted. Recently, Georges and Stephenson [Ref. 59] modeled these variations using 3-dimensional computer ray-tracing.

The appearance of the lines in wide-swept-frequency backscatter was reported by Bolgiano [Ref. 64, 1962] and Gilliland [Ref. 65, 1965]. It was characteristic for these lines to be very nearly horizontal when viewed with antennas having beamwidths of 2 deg (Bolgiano) with that of a single rhombic (Gilliland). In 1967 Croft [Refs. 50, 66] published an excellent analysis of the striations seen in Gilliland's data, and some data [Ref. 50] taken using the Los Baños array. Using computer raytracing, Croft showed that the effect of irregularities is to focus the radio waves onto the earth's surface, over a comparatively narrow range increment at a given frequency, thereby producing the striations. These irregularities almost always occur more often in the evening than the morning, and in general more so in the summer, less in the fall, and least in the winter. They are definitely correlated with magnetic storms in the ionosphere (probably the auroral electrojet [Ref. 63]),

and they occur more often when the sun shines on the ionosphere more directly.

B. A NEW BACKSCATTER FEATURE SEEN ONLY FROM THE SEA

This section will present data which reveal unique feature of ionospherically-propagated sea backscatter which has been recorded using the wide-aperture array. The cause of this feature will then be hypothesized, and the remaining chapters will prove it, and will demonstrate the way in which it may be controlled.

1. The Experimental Data

Figures 15 and 17-27 contain examples of wide-swept-frequency backscatter data which reveal this unusual phenomenon. These data were recorded in exactly the same fashion as for Fig. 14 except that different transmitting and receiving bearings were used, and for Fig. 17 onward (except Fig. 26), only a single LPA was used to transmit to the Pacific Ocean.

a. The Gulf of Mexico

The records shown in Fig. 15 were recorded by Washburn during a study of land backscatter. They are presented here, with his permission, in order to reveal some characteristics of backscatter from the Gulf of Mexico. The data were taken on 20 September 1968, with the Lost Hills array slewed to 94 deg. The times and receiver bearings are indicated at the top of each record, and the system parameters are listed below. The time delay corresponding approximately to the division between land and sea is also indicated on the data.

Applying knowledge already gained, we can then see that several echoes from discrete reflectors occur in the portion from the land, but none from the sea. There are also some heavy, wide families of focusing lines between (roughly) 16 and 20 msec. The abrupt change in

the 1-hop backscatter on the left-which resembles a leading edge--has been recently explained by Croft and Washburn [Ref. 51]. The difference in brightness change in the right half of each record is due to a manual adjustment of the receiver gain.

The new features in these data are two sets of line families which do not at all resemble the focusing lines, and which have only been observed in backscatter from the sea surface. These lines appear between 22 and 24 and 18 and 20 msec (approximately), in two different forms. The lines between 22 and 24 msec are clearest on the record for 1954 UT, and those between 18 and 20 msec are clearest on the other record. The former set are quite easily seen, but the latter set are less dark and more closely spaced--about 6 per msec--making them less discernible; more data will be shown, however, which bring this type out more clearly. It is characteristic of these lines to be tilted in the range-frequency display, becoming more nearly parallel to the leading edge as they approach it. When two layers are present, causing the second focusing edge on the left [Ref. 51], the lines tend to be parallel to it also, which means that they can become tangent to the horizontal somewhere between the two edges. This characteristic of the lines clearly distinguishes them from discrete land echoes.

Secondly, the new lines are usually quite parallel and regularly spaced. Because of this, the fact they are seen only over the sea, and the above characteristics, make them quite distinguishable from the focusing lines due to ionospheric irregularities.

Data taken at times near that in Fig. 15 represent the only records of backscatter from the Gulf of Mexico which show these lines clearly. It is still not absolutely clear why they occur relatively infrequently over this path.

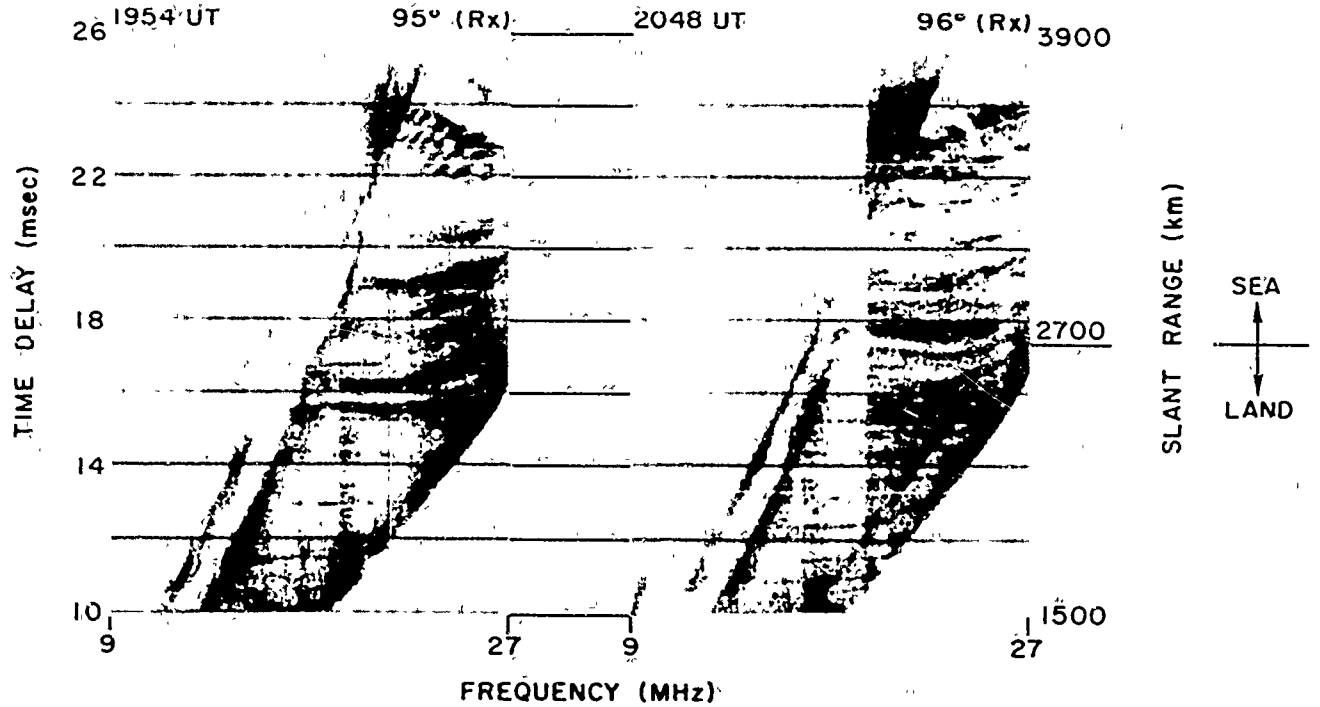

DATE: 9-20-68
BEARINGS: TRANSMITTER (Tx) 94 DEG.
RECEIVER (Rx) SHOWN ABOVE
SWEEP RATE: 250 kHz/sec
INTEGRATION TIME: 0.1 sec
RESOLUTION LIMIT: 40 μsec

Figure 15. SFCW backscatter from the Gulf of Mexico, showing a new type of modulation on sea backscatter echoes.

b. The Pacific Ocean

The backscatter paths to the Pacific Ocean, where the return from all azimuths, ranges and frequencies came from the sea surface, proved to be much better for studying these new lines, since the effect is associated with the sea's surface. Figure 16 shows the geometry of these paths. A beamwidth of 125 deg is indicated on Fig. 16 for the vertical element of the crossed-LPA's, ± 15-3/4 deg from boresight (270 deg), the single LPA was essentially omnidirectional to the west, with its radiation about 15 dB lower to the east.

(1) February 1969

Figures 17-20 are examples of data taken on 5 February 1969, shortly after the westward LPA's had been erected at Lost Hills. Referring to Fig. 17 first, it is evident that there are no discrete echoes (as we expect), and only one clear focusing line (between 15 and 17 msec and 20 to 25 MHz). The 1-hop westward leading edge is clear, and a faint trace of the eastward edge near the bottom of the data is also present. Between 11 and 15 msec, and 13 to 15 MHz, a second focusing edge is seen which is either 2-hop backscatter, or an E-layer leading edge. The latter seems to be the best interpretation.

The backscatter in Fig. 17 is comparatively smooth and continuous with range and frequency, except for the family of lines on the data which resemble a thumbprint. Once again, it is seen that these lines are parallel to both the left and right (E- and F-layer) leading edges, and are quite uniformly spaced. The thumbprint lines are horizontal only over a narrow frequency range where they curve down from one leading edge and up again to the other. Figures 18-20 show very similar behavior, except that the line patterns taken on different shapes as time-of-day progresses. Some lines appear below about 10 msec which are not as clear as those above, and which are very nearly horizontal. It

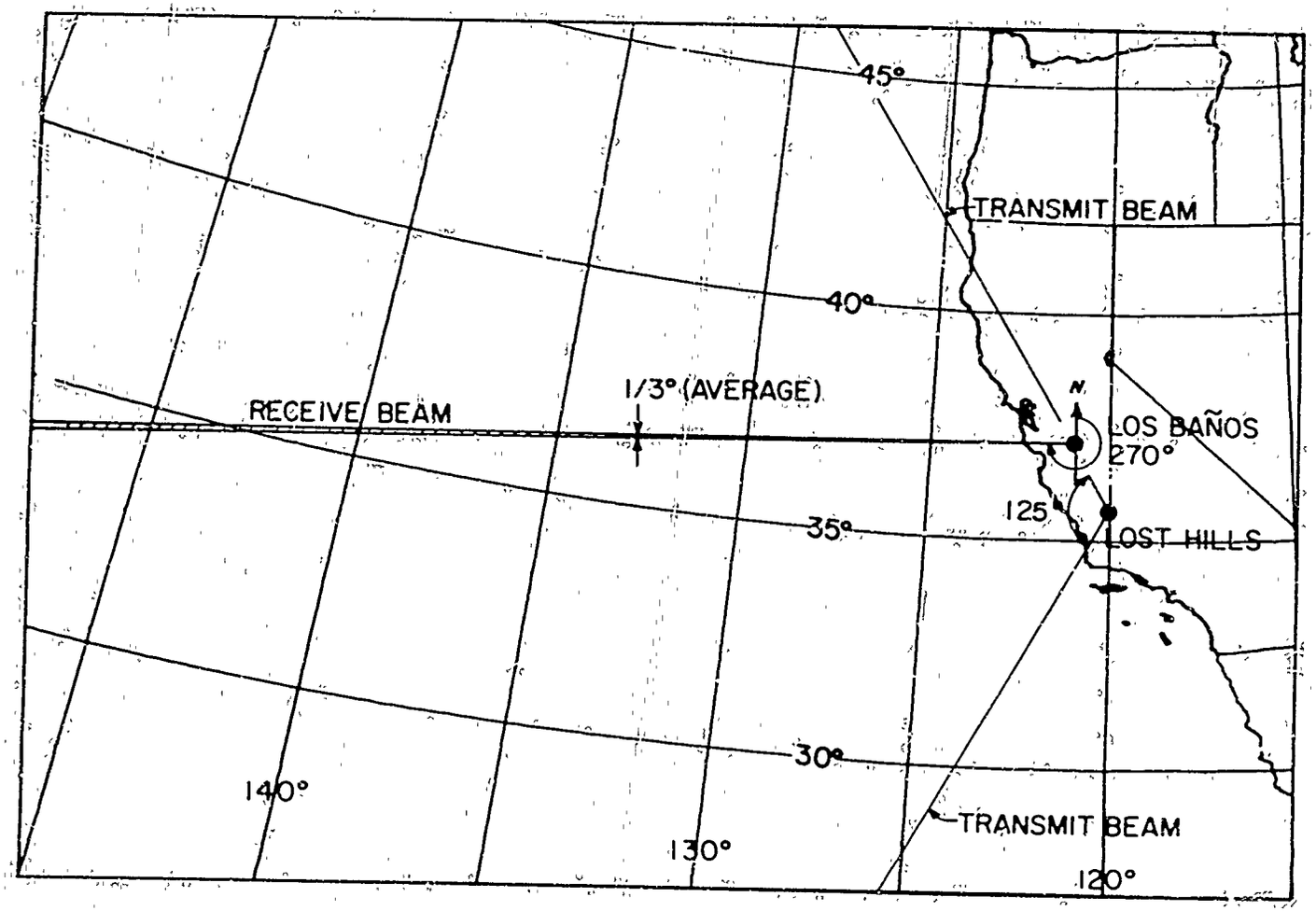

Figure 16. Map showing how the transmitter and receiver illuminate the Pacific Ocean. This geometry applies to all of the remaining data except Fig. 26.

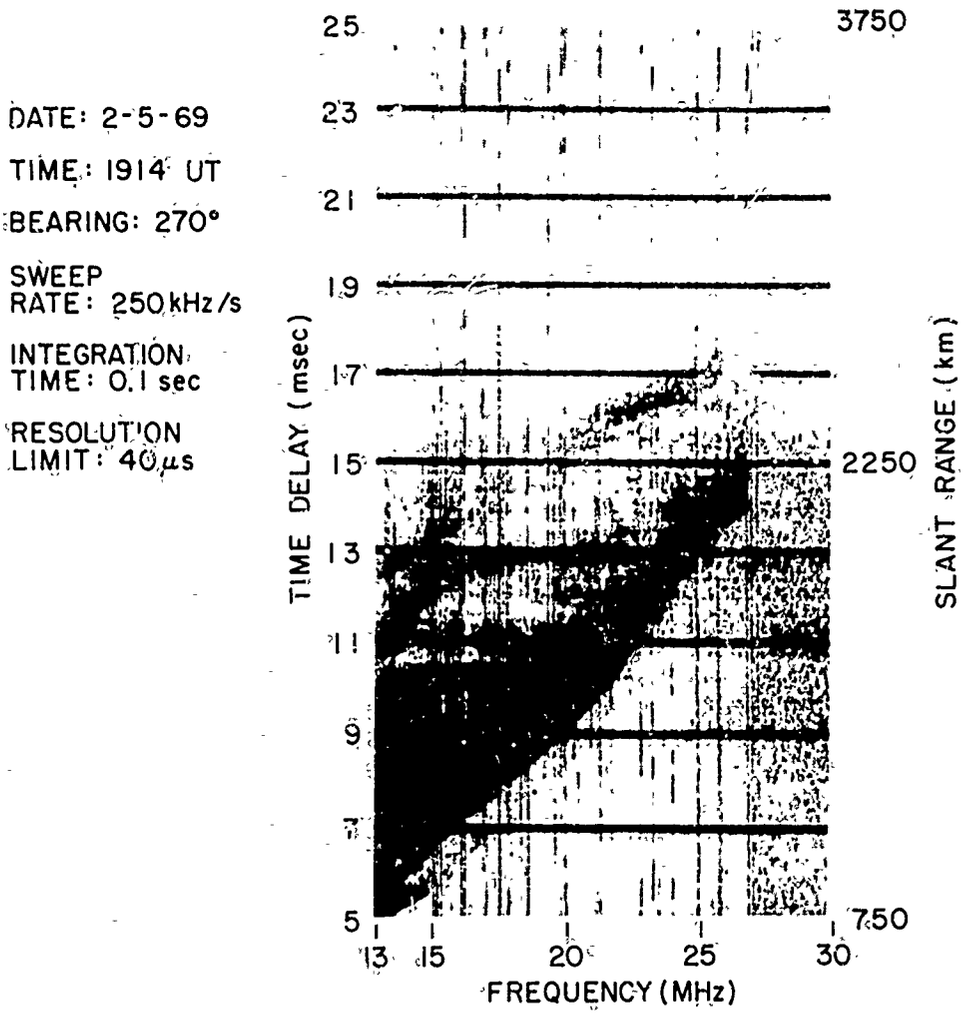

Figure 17. SFCW backscatter from the Pacific Ocean on 5 Feb. 1969 at 1914 UT.

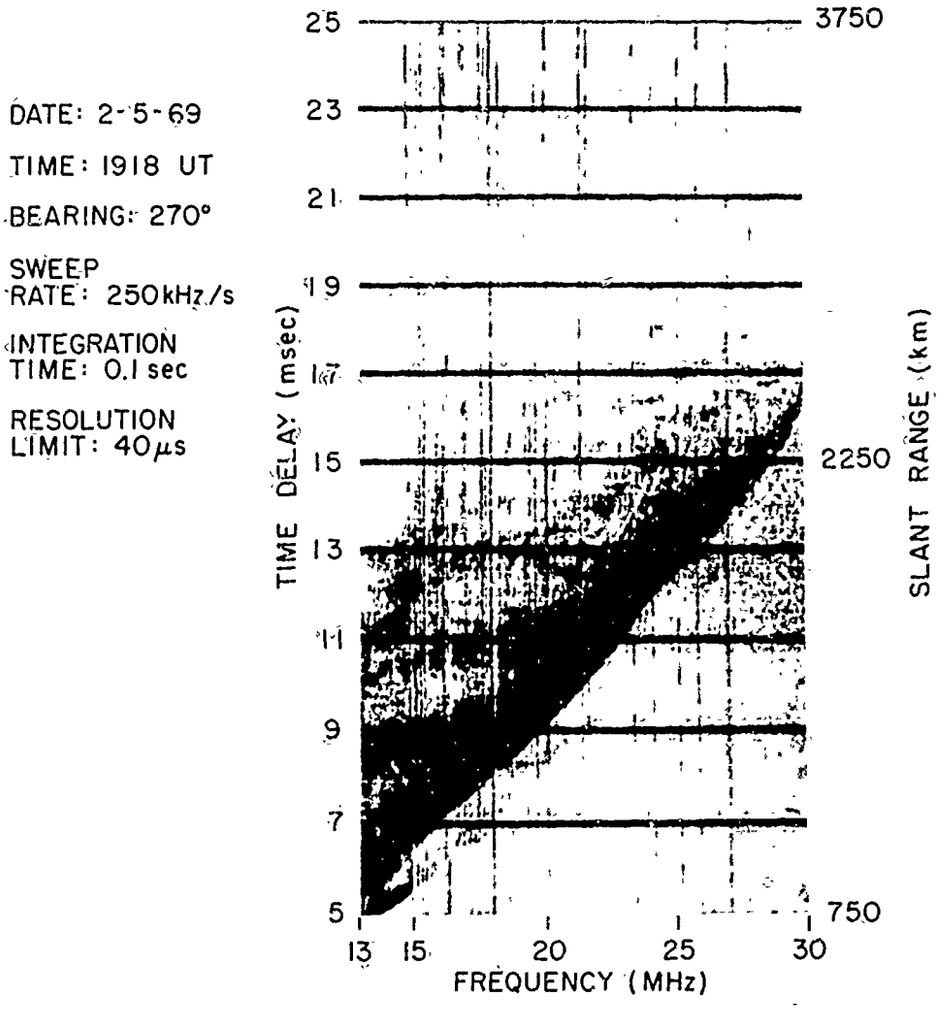

Figure 18. Same as Fig. 17, but taken at 1918 UT.

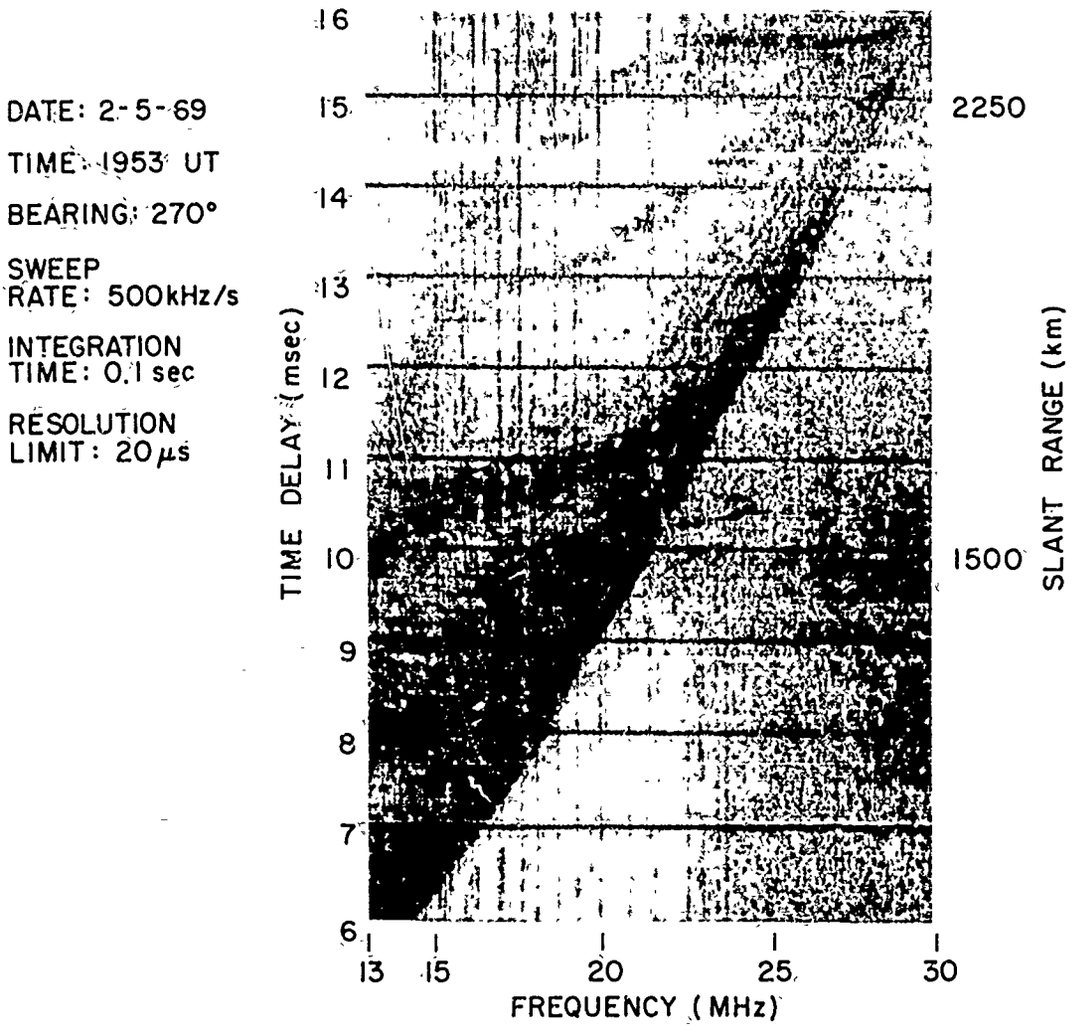

Figure 19. Same as Fig. 17, but taken at 1953 UT, and the sweep rate was doubled.

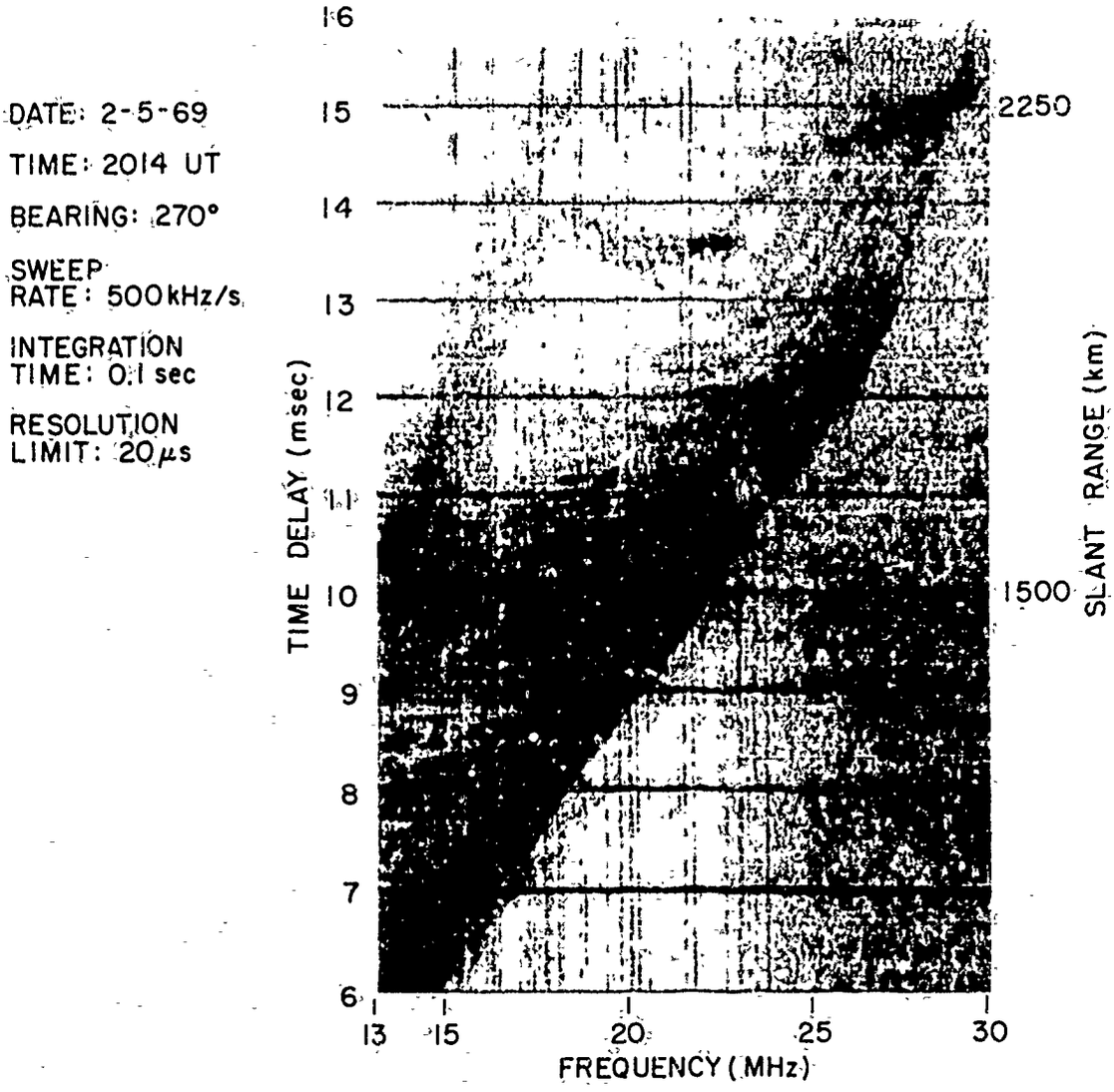

Figure 20. Same as Fig. 19, but taken at 2014 UT.

is probably true that these are not due to scatter from the east, and they are too regularly spaced to be focusing lines. It would appear therefore, that they are of the same type as those which are nearly parallel to the F-layer leading edge. Figures 19 and 20 show this distinction most clearly.

The data for February 5 were so encouraging that more experiments were run two days afterward; and as seen, Figs. 21-24 illustrate the same things as the above. On this same day, the transmitted polarization was changed in certain ways in order to see what effect it had on the characteristics of the thumbprint lines. This experiment gave positive results, but its discussion will be deferred, since it will be better understood after the theory for the lines is developed.

Figure 21 is very similar to Fig. 20, except for the following: On both figures (and on the others) there are lines down to 8 msec, but they are not horizontal on Fig. 21. Therefore, on the latter, they more nearly resemble the lines on the upper half of the data. Secondly, on each figure there is an E-layer leading edge, but on Fig. 21, a 2-hop F-layer leading edge emanates just to the left of that from the E-layer, and extends beyond 10 msec in time delay. When this extension occurs, the backscatter-frequency spectrum tries to cross zero frequency (at the top of the figures), hence begins to "fold over" into the figure, extending downward. The same is true here for the 1-hop F-layer leading edge. The seriousness of this effect diminishes quickly as it progresses downward in (apparent) time delay, since this energy lies outside the 6 kHz IF pass-band (Chapter III).

In order to examine the backscatter behavior at these higher time delays, the time delay window was reset 2 minutes afterwards, as shown in Fig. 22. By comparison with data taken with other systems, it is surprising that the backscatter intensity was high out to 3,400 km--since the effective radiated power was only 2 kW times the gain of a

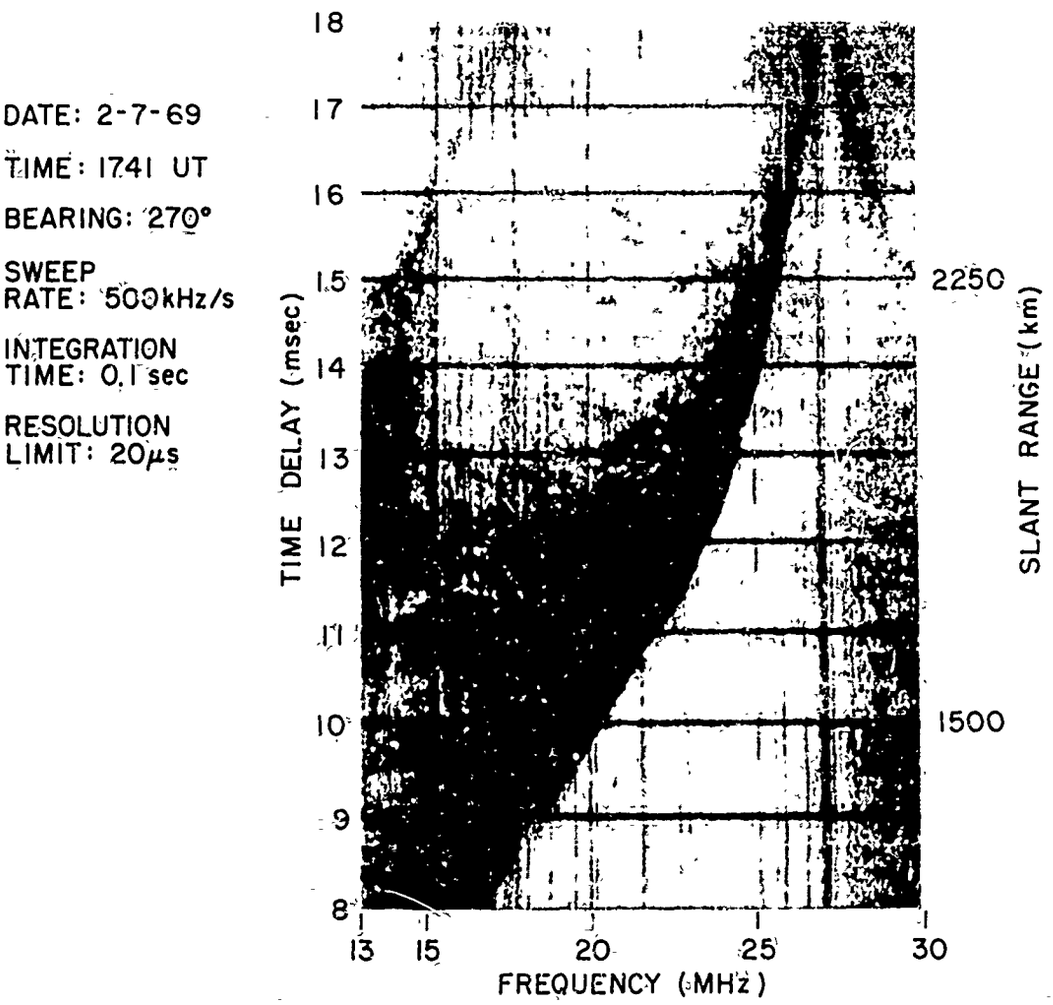

Figure 21. Same as Fig. 17, but taken two days later at 1741 UT, and the sweep rate is doubled.

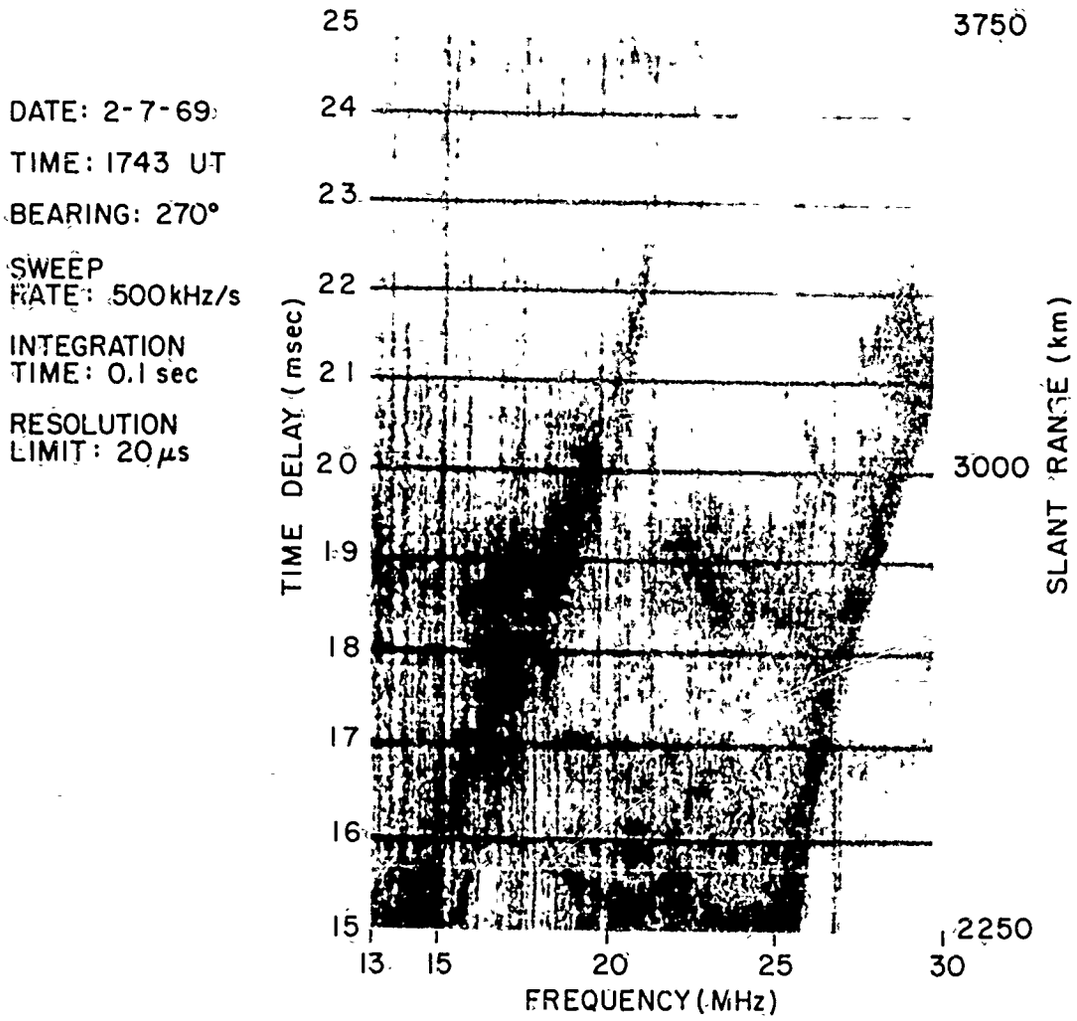

Figure 22. Same as Fig. 21, but taken at 1743 UT. The polarization modulation at the higher time delays is now revealed.

single LPA. It has become clear, however, that the receiving array discriminates against interference from other users, which increases the signal-to-interference ratio. Figure 22 reveals that the lines are absent in the 2-hop return (left), but appear almost vertical in the 1-hop backscatter between about 17 and 21 msec. It is clear then that they can occur out to 3,000 km ranges.

Figures 23 and 24 show the behavior of the new line families most dramatically. Figure 24 is an expanded version of the data in Fig. 23 between 13 and 17 msec, taken two minutes later. The lines are seen to be almost parallel with the 1-hop leading edge, and decreases their width and spacing as it is approached. In Fig. 23 it is seen that the lines tilt less vertically toward the left, and their bottoms begin to curve. By comparison to the earlier data, it is conjectured that this curvature would continue if the lines were still resolvable, and that this effect is associated with the E-layer leading edge on the left of Fig. 22.

(2) July 1969

It will now be instructive to consider the behavior of these lines as a function of season. Figure 25 shows SFCW data taken on 30 July 1969. The system was set nearly identically as for Figs. 17-24, and the receiving antenna bearing was the same (270 deg). The summer and winter ionospheres were much different, however, and at the same time the new type of line families cannot be seen. Evidence will later show that the lines might be seen at the longer ranges. To check this, the upper portion of the backscatter was expanded between 16 and 24 msec. There are a few vertical enhancements in this data, but most of these seem to be due to interfering stations. Some of the lines around 20 msec, and between 22 and 24 msec could be real. It is quite clear from this and other data, that, in general, the summer backscatter has a great deal more irregularity in its structure than in the winter, and correspondingly,

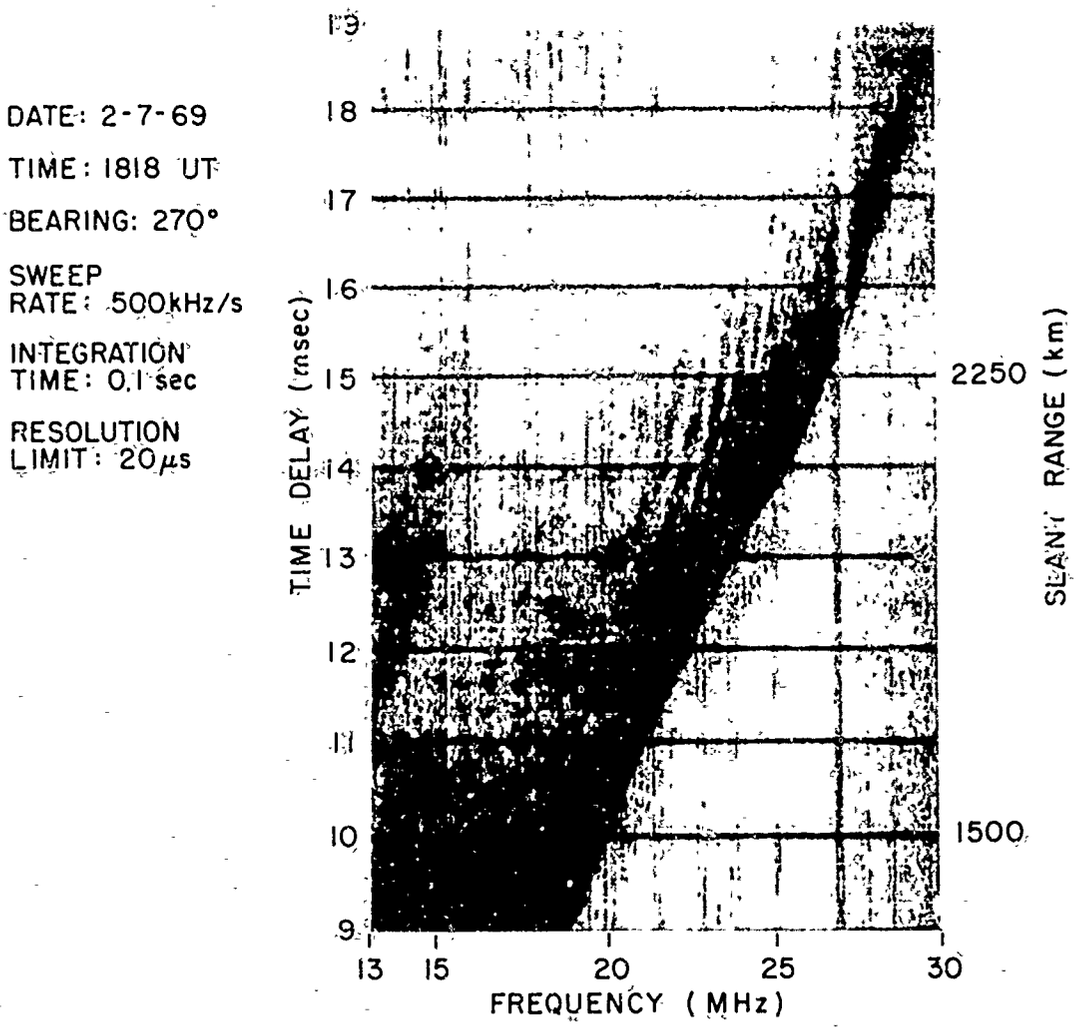

Figure 23. Same as Fig. 21, except at 1818 UT.

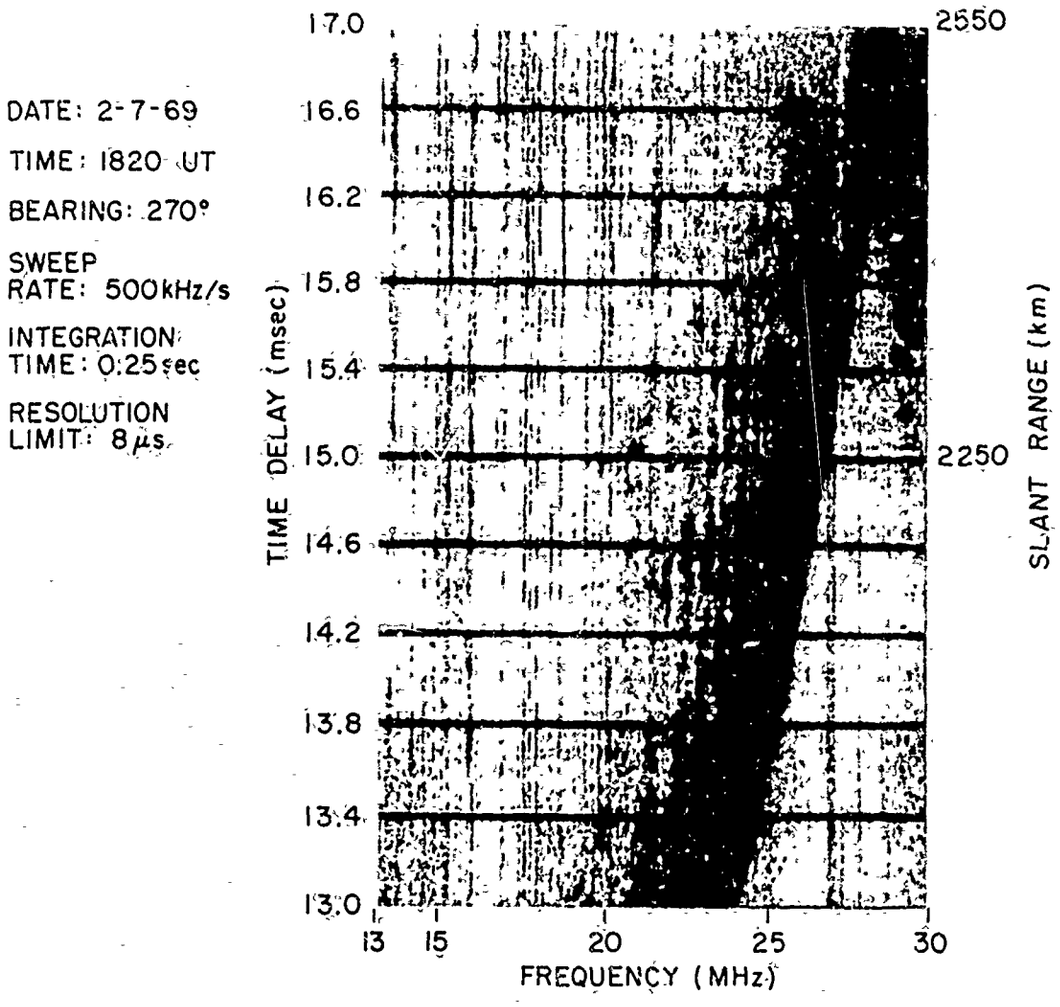

Figure 24. Same as Fig. 23, except that the time is two minutes later, and the portion of the data between 13 and 17 msec has been expanded to show more detail.

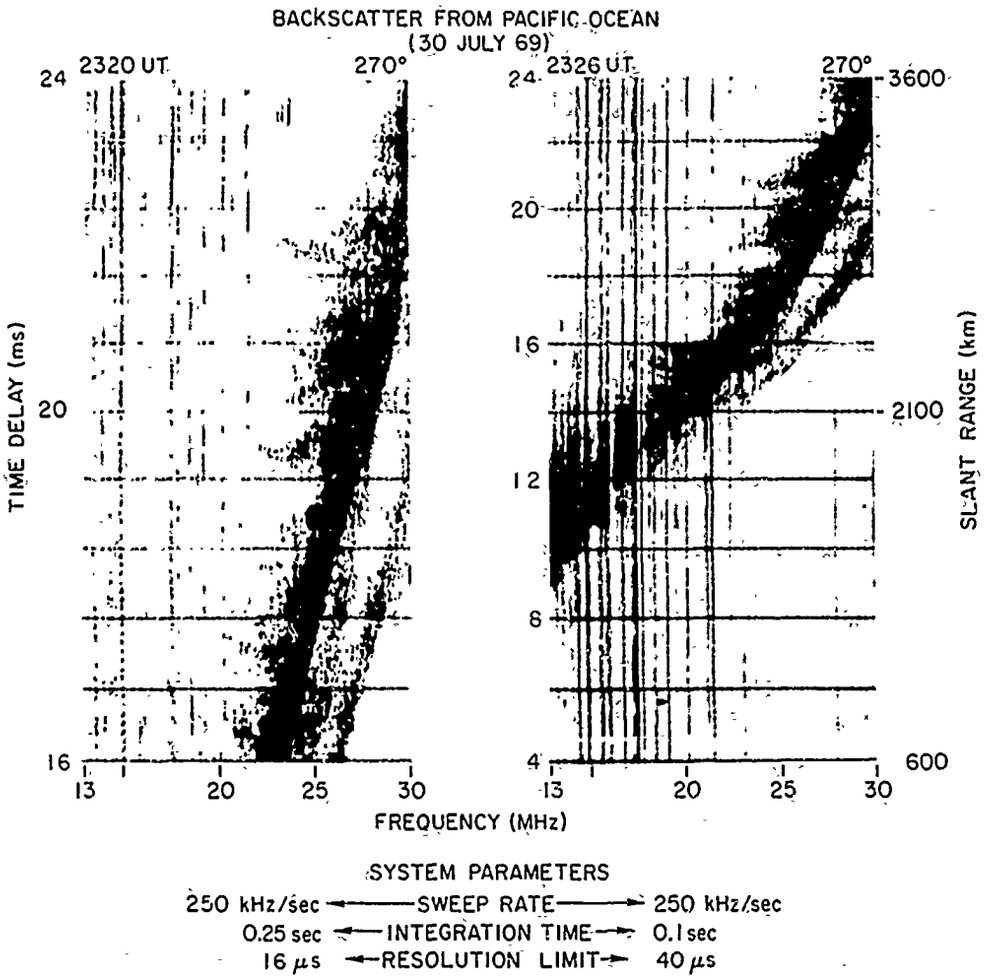

Figure 25. SFCW backscatter from the Pacific Ocean on 30 July 1969, showing that the new modulation was not detectable at that time.

many more focusing lines. It so far seems that the thumbprint-lines are simply not resolvable, except occasionally, in summertime backscatter.

(3) October and November 1969

By contrast, it was already shown that they were seen in September 1968 (Fig. 15), and Figs. 26 and 27 show that once again they appeared in the autumn. The data in Fig. 26 were taken by transmitting from Stanford, rather than Lost Hills, using a bi-directional rhombic antenna. Because it was late in the afternoon (locally 1714 PST), it was possible to isolate the westward backscatter from the east as designated on the figure. Once again, the line families appear in regular spacings, nearly parallel to the leading edge. It is also noteworthy in Fig. 26 that the lines can be seen right up to the edge of backscatter--which usually does not happen. The explanation for this is that the upper- (Pederson) ray propagation was attenuated all the way to the backscatter focusing edge, which may have resulted from reduced radiation at the higher elevation angles by the rhombic antenna.

The data in Fig. 27 were also taken in the afternoon, but several days later, using the single LPA at Lost Hills. These data look very similar to those in Fig. 18, except that there are less focusing irregularities present in the latter.

2. Conclusions

It may generally be concluded from the data that:

(a) The newly observed line families are never seen in backscatter from the land.

(b) They are nearly always seen in the autumn and winter during daylight hours, in backscatter from the Pacific Ocean.

(c) They are very rarely seen in the summer, and then only vaguely.

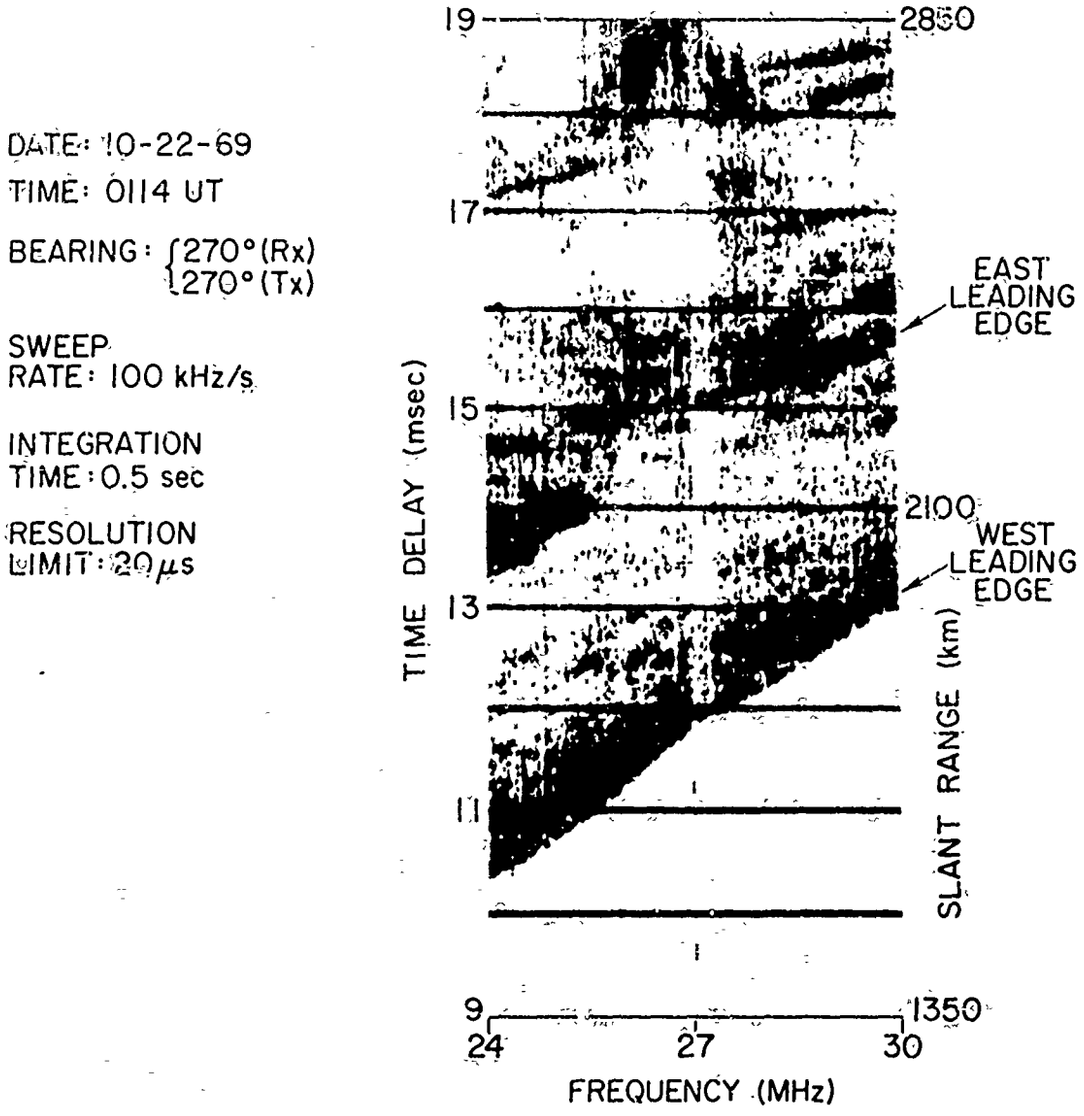

Figure 26. SFCW backscatter from the Pacific Ocean on 22 October 1969: transmitter at the Stanford campus rather than Lost Hills. The backscatter from east and west is separated by virtue of the late time of day (0114 UT, 1714 local time at transmitter.)

DATE: 11-5-69
TIME: 0052 UT
BEARING: 270°
SWEEP RATE: 250 kHz/s
INTEGRATION TIME: 0.1 sec
RESOLUTION LIMIT: 40 μs

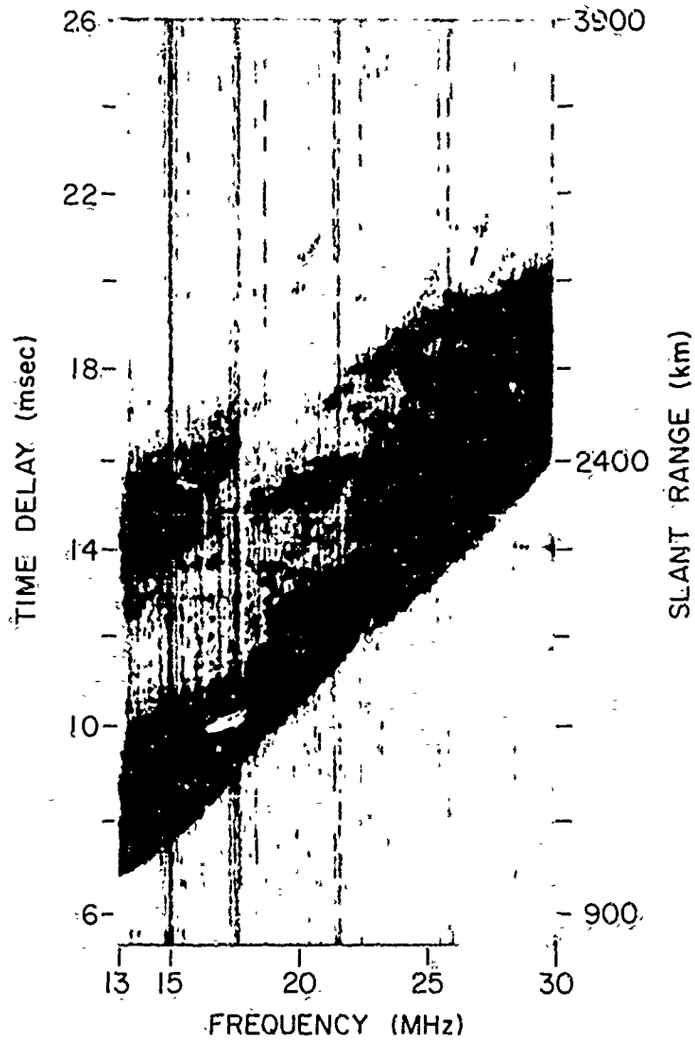

Figure 27. SFCW backscatter from the Pacific Ocean on 5 Nov. 1969. Transmitter at Lost Hills.

(d) It is characteristic of the lines to be more nearly parallel to the main leading edge of the backscatter, and to increase in number as they approach it.

(e) They are clearly distinguishable from both discrete echoes and focusing lines; however, they can become horizontal over a certain frequency range when an E-layer leading edge is also present, since they can curve around in a manner resembling a thumbprint.

(f) They are most clearly seen at ranges below 2,500 km, but they can also appear at ranges beyond this.

3. Hypothesis

To form a hypothesis to explain these lines we must first ask ourselves what is different about the scattering behavior of the sea surface, and we must account for the fact that the lines have probably never been seen before.

a. Continuity of the Sea's σ_o and the Effect of Swells

The conclusions of Chapter II predict the sea surface to have a nearly uniform, or slowly varying cross section per unit area with azimuth and range. This model should hold true except when large wave swells travel through the scattering area under observation, since these swells are not predicted by theory, and they can represent a sizable discontinuity in the sea surface structure. The backscatter from these swells should have a high doppler shift (since they move faster) when the radio wavelength is correct for coherent (Bragg) reflection. Additionally, if the surrounding (steady-state) sea is moderately calm, the amplitude of the backscatter from the swells should be quite strong at those correct frequencies. Following this line of thought further, imagine a swell wave train emanating from a point source, thereby causing the wavefronts to expand outwards in concentric shells. Suppose that one

then illuminates this whole system of waves with a relatively broadbeamed antenna (like a rhombic). The scatter from the swells will be a maximum when the wave spacing--normal to the direction of radio-wave propagation--is an integral number of half the projected radio wavelength. But, the range at which this constructive interference occurs exactly should be frequency dependent. Thus, there will be a line of amplitude enhancement in a range-frequency display of backscatter, for each harmonic number of radio half-wavelengths. This could result in families of lines which could then be tilted with a negative or positive slope, depending upon the direction from which the swells came (which way the wind was blowing). Muldrew [Ref. 32] believes that he saw this exactly, and the above explanation is his. He was stationed in Ottawa, and used a rhombic antenna. He believes that the lines could not have been caused by any ionospheric phenomena, and gives good evidence to support the Atlantic-Ocean swell hypothesis. His arguments are quite appealing, and evidence will be given later which suggests that a rhombic antenna is much too small to use in seeing lines like those revealed in Figs. 17-27.

Muldrew's observation is the only one of its kind. His proposed technique could very well be used as another aid to the detection of storms at sea which generate large swells. For the present, it is sufficient to note that his type of observation is not seen nearly as regularly as the thumbprint phenomena. Moreover, the appearance of the swell lines is different, in that they are not parallel to the backscatter leading edge, and they sometimes bend in the opposite direction. It is safe to say that the sea surface normally does not contain large swells travelling through it, with sufficient amplitude to override the backscatter from the more numerous, more closely-spaced sea-wave components--as assumed by the theory. It is therefore safe to say that the thumbprints are <u>not</u> due to backscatter from swells.

b. The Polarization Dependence of the Sea's σ_o

The other property unique about the sea surface is that not only is its scatter magnitude relatively constant over a large area, but as shown in Chapter II, it follows that its polarization dependence will be also. In fact, the sea should be most nearly a vertically-polarized reflector at low elevation angles, except perhaps for extremely rough seas.

By contrast, reflectors on the land can, statistically speaking, favor any polarization. It has been felt by some [Refs 15, 17] that on the average the land also favors vertical over horizontal polarization. This may be true, but measurements of localized areas do not seem to confirm this. Indeed, Ranzi [Ref. 67] found that the "background" scatterers seemed to favor vertical polarizations, while large discrete echoes from power lines and mountains favored horizontal polarization. It is therefore true that when a narrow beam antenna is used, the small slice of terrain appearing in one resolution cell can have a polarization dependence different than the adjacent cell--such as when comparing scatter from vertical metal poles or trees, to horizontal power lines.

c. Hypothesis

Lastly, it must be considered that the thumbprint lines have probably never been seen before, and a very important difference between the author's sounder and others, is that the Los Baños array is the widest-aperture antenna ever built to operate at HF. The apperance of the lines is therefore probably associated with antenna beamwidth.

Because of the last property, the lines may be presumed to be associated with some phenomenon in the ionosphere. The only phenomenon which might be sensitive to antenna beamwidth is that which causes the plane of polarization of down-coming radiowaves to rotate with

range, frequency, and azimuth--Faraday rotation. The fact that the sea cross section and its polarization dependence is uniform from one position to the next, makes it possible for the amplitude of sea backscatter to be a function of range and frequency according to the instantaneous value of the radio wave polarization. For instance, providing that the polarization does not rotate appreciably across the main receiving beam, then if at a fixed frequency and range the polarization comes down horizontal, very little sea scatter will originate. By contrast, if the polarization comes down vertical, and if the receiving antenna's polarization is correct, a maximum in backscatter amplitude will be achieved (ignoring focusing and scattering irregularities in the ionosphere). Thus, the fact that the antenna is big enough makes this phenomena possible, and the continuity of the sea's cross-section magnitude and polarization dependence make it appear only in sea backscatter. This is the hypothesis, and the remaining chapters will introduce strong evidence in its favor.

V. THE MODULATION OF SEA-BACKSCATTER AMPLITUDE BY POLARIZATION ROTATION (THEORY)

The purpose of this chapter is to provide a theory, based on the hypothesis stated at the end of the last chapter, which will be used to explain the "thumbprints" in swept-frequency sea backscatter records. The first section will discuss the concept of "polarization rotation," which will be applied in the development of the theory. The theory assumes only that ordinary and extraordinary modes are equally attenuated in the ionosphere, and that they are circularly polarized when exciting the ionosphere. The simplification due to a monostatic sounding geometry will then be shown, and the fourth section will express the conditions under which the "polarization modulation" will be present. The last section will demonstrate the use of an aproximate computer-raytracing technique to synthesize model backscatter data which show the new modulation. The next chapter will show experimental data which verify the theory.

A. THE ROTATION OF POLARIZATION AFTER AN IONOSPHERIC REFLECTION

It has long been known that the earth's magnetic field will affect the propagation of radio waves. Ratcliffe [Ref. 68], Budden [Ref. 57], and others have given excellent historical accounts of the development of ionospheric research. Ratcliffe points out that the work of his book was mainly based on the theoretical work published by Appleton in 1927 [Ref. 69]. Appleton's theory derived an expression for the complex refractive index in the ionosphere, which was fully published by 1932 [Ref. 70]. In 1934, Booker [Ref. 71] interpreted the equations with regard to polarization, and his conclusions are summarized by Ratcliffe

[Ref. 68]. In 1952, Snyder and Helliwell [Ref. 72] published a "Universal Wave Polarization Chart for the Magneto-ionic Theory," which is quite helpful in visualizing the behavior of the polarization of radio waves.

In Appleton's results from Ratcliffe [Ref. 68], it is seen that the earth's magnetic field causes the energy of a linearly polarized wave to split into two elliptically polarized waves, which travel with different phase and group velocities, and in general do not follow the same ionospheric paths. The process is called magnetoionic splitting. The two waves have the "characteristic polarizations" of the ionosphere; these are usually denoted the "ordinary" and "extraordinary," for the waves which are least and most affected by the earth's magnetic field, respectively.

In the event that an elliptically polarized wave is transmitted into the ionosphere, it will also be broken down into the two characteristic waves, but the components will have unequal amplitude. In fact, if one transmits a wave which exactly matches one of the characteristic polarizations of the ionosphere, the other component will not be excited (except to a small degree, perhaps, due to the fact that the ionosphere is not completely homogeneous). This will be discussed later.

When both magnetoionic components are excited, two phenomena occur. If the experimenter transmits a short enough pulse of energy over a one-way path through the ionosphere (and if the ionosphere will support the necessary pulse bandwidth), he will observe that the received energy will be split into two pulses, delayed by 0 to 4 μsec, due to the difference in the group velocity of the "o" and "x" modes. Usually, one sees a delay of 1 to 2 μsec. On the other hand, if the transmitted pulse is longer than the time-delay separation or the "o" and "x" modes, if the receiver bandwidth is too narrow to resolve the Fourier spectrum of the short pulses, or if a range-extended backscattering surface is used, one will observe that the energy from the two characteristic waves

will add. In the author's work, it will always be assumed that the "o" and "x" modes are never resolved in group time delay; however, if the reader is interested in considering the effects of the latter, and the implications on usable receiver bandwidth, he is referred to the excellent work done by Mark Epstein while working at Stanford [Refs. 45, 73].

When the energy from the "o" and "x" modes add, the difference in their phase velocities, cause the resultant polarization to vary according to the phase difference between the two modes. Assuming that the attenuation of the two magnetoionic components is equal (which is especially true at higher frequencies), then the resultant polarization will be linear, and its orientation can be anywhere between vertical and horizontal. When one uses a linear antenna he will see the amplitude of a received voltage vary with time, and it will reach a maximum when the arriving polarization is aligned with the antenna. Eckersley [Ref. 74] observed this as early as 1929, after Appleton's theory had just been published. In 1935, Martyn and Green [Ref. 75] measured the polarization of downcoming radiowaves from near vertical incidence.

A clear demonstration of the effect of o-x splitting (when the two modes are not resolved in time delay) was given in 1958 by Hedlund and Edwards [Ref. 76]. These workers used 100 μsec pulses, which were transmitted over a 1000 mile oblique path, using only 1-hop F-layer, lower ray propagation. The pulses were received on both vertical and horizontal antennas, from which it was observed that the signal amplitudes faded with the same period, but exactly out of phase. This is usually called "Faraday rotation," and has been described in detail by several authors [Ref. 77 as an example].

Appendix A is included at the end of this report in order to show how Faraday rotation develops. An unambiguous expression is given with which the instantaneous value of polarization rotation, Ω_i, can be computed. This is given by

$$\Omega_i = \frac{\pi}{\lambda_o}(P_o - P_x)\left[\frac{R_x}{i\,|R_x|}\right]_{EXIT} \quad , \tag{A15}$$

$$\text{Which is} \begin{Bmatrix} \text{CW if} > 0 \\ \text{CCW if} < 0 \end{Bmatrix} ,$$

where λ_o is the freespace radio wavelength, and R_x is the polarization of the extraordinary (x) wave when exciting the ionosphere (given in Appendix A). Usually the QL approximation holds, so that when the downcoming waves are parallel to the earth's magnetic field, $R_x = +i$, and when they are anti-parallel, $R_x = -i$. When $X \ll 1$ (Appendix A) the phase paths P_o and P_x are given by

$$P_o = \int_{o\ path} \mu_o ds$$

$$P_x = \int_{x\ path} \mu_x ds \quad , \tag{A12}$$

where the o and x paths are in general different. The refractive indices for the o and x modes, μ_o and μ_x, are functions of the radiofrequency, f, the electron density, N, the earth's magnetic field intensity, H, and the direction of propagation, θ, as commonly noted in ionospheric texts [e.g. Ref., 68]. It is also seen that $\mu_o \geq \mu_x$, but it not necessarily true that $P_o \geq P_x$ between two points, as sometimes assumed.

The expression for Faraday rotation is denoted by the instantaneous value, Ω_i, not the total value, Ω_t, as it is usually referred to [e.g., Refs. 44, 81, 77], since the latter only has meaning when it can be shown

that R_x does not change sign during the integration to determine P_o and P_x. Dulk [Ref. 77] used a technique which sometimes overcomes this problem, which will be discussed later. For the present purpose, it is sufficient to note that the concept of "polarization rotation in the ionosphere" is fictitious for oblique ionospheric propagation, since the o and x modes follow different paths, and it is therefore necessary to consider polarization rotation as the sum of two separate circular waves, according to Eq. (A15).

Hereafter, the subscript "i" will be removed from Ω_i, but it is understood that the instantaneous value of polarization rotation is still assumed.

B. THE MODULATION OF SEA-BACKSCATTER AMPLITUDE BY POLARIZATION ROTATION

Since the expression for Ω is a function of f, N, H, and θ, integrated through the ionosphere, it is clear that P_o and P_x (hence Ω) are functions of frequency, range (or time delay, τ) and azimuth, φ. Indeed, by constraining the range and azimuth to be constant, Epstein [Refs. 44, 45, 78, 79, 80] observed the variation of Ω with changes in frequency. Croft [Refs. 81, 82] wrote a computer program based on Dulk's method [Ref. 77], with which he approximately calculated Ω versus range at a constant frequency and azimuth. Using the same program it can also be shown that Ω varies with azimuth at a constant range (or time delay) and frequency.

Returning to Eq. (A15), the effect of polarization rotation on backscatter amplitude must in some way be derived from the way in which ordinary and extraordinary modes return to the receiver and interfere--according to their phase path differences. Additionally, this interference must be contained in some expression which can be integrated over the frequency bandwidth (Δf), the time delay resolution ($\Delta\tau$), and the

azimuthal beamwidth ($\Delta\varphi$) specified by the sounder, in order to yield the received power.

Qualitatively, the process by which the backscatter modulation is produced is as follows: a wave is transmitted via the ionosphere, and if its polarization is linear, it generates equal-amplitude o and x waves which travel to the rough surface of the sea. In general, there are an infinite number of such "rays" which emanate from all elevation angles and azimuths. Each of the characteristic waves strikes the sea surface, and if its polarization is linear, it scatters new o and x waves which are returned to the receiving antenna. The net result is that the receiving antenna sees o and x waves, which add up to produce a linear wave whose orientation could change to produce an amplitude modulation on the received echoes; this is termed "polarization modulation." By comparison, if the transmitted polarization is circular, only one characteristic mode is excited, and if the sea were polarization-independent, only one mode would be reflected--thereby causing no modulation at the receiver. If in the latter case, the sea still generated o and x modes from the single mode transmitted, the interference at the receiver would exist, but would be different than in the first case. The same would be true if the sea were polarization-independent, but the transmitter excited both characteristic modes.

To model this behavior, it must first be realized that each mode which is returned to the receiver is gated out in time delay by the equivalent pulse resolution (and averaged), so that the constraint on these modes is that their time delays are all equal. This may be contrasted to the one-way communication path, in which the ranges of the modes are equal. Therefore, let us consider a particular time delay, using a fixed frequency. Furthermore Sweeney [Ref. 47] has shown both experimentally and by using the 3-dimensional raytracing program developed by ESSA [Ref. 83], that the lateral deviation of o and x rays is less

than the beamwidth of the receiving array, so that a particular azimuth may also be assumed at which the o and x modes will have equal amplitude. Since the scattering surface has uniform characteristics from one point to the next, it scatters exactly the same from point to point, so that the constraint of constant ground range need not be made.

Thus we will assume constant f, τ, and φ, and derive an expression for the amplitude of the received energy for these particular parameters. (Later, the expression will be integrated over the sounder's Δf, $\Delta\tau$, and $\Delta\varphi$.) To form such an expression, we must account for the modes which arrive at the receiver with exactly the same time-delay. There is a transmitted ordinary mode (o_t) which scatters and produces (in general) both an o and an x mode. Assume that the o mode is received at the correct time and label it o_r. The x mode will, however, not return with the correct time delay, so it is necessary for another transmitted o mode, labeled o_t', to produce the received x mode (x_r') which will derive the correct time delay. Likewise, the x_t mode produces an x_r mode, and the x_t' produces the o_t' mode. Therefore, in general, the receiver adds 4 modes (o_r, o_r', x_r, x_r') to produce the net amplitude of the received energy.

Figure 28 depicts the model just discussed, except that, for convenience and simplicity, a monostatic sounder geometry is depicted and the relative separation between the sounder and scattering points is greatly exaggerated. It is indicated that the o_t and o_r modes follow exactly the same path (since their time delays are equal by reciprocity), but this does not in general hold true for the bistatic geometry. This is also true for the x_t and x_r modes. As seen, these modes land on (and scatter from) different ground ranges, but it is remembered that the total group paths for the returned modes are equal. Likewise, the x_r' mode is scattered from somewhere in between the o_r and x_r modes, in order for the time delay of all three modes to be equal. The same is true for the o_r' mode. By symmetry, for the mono-

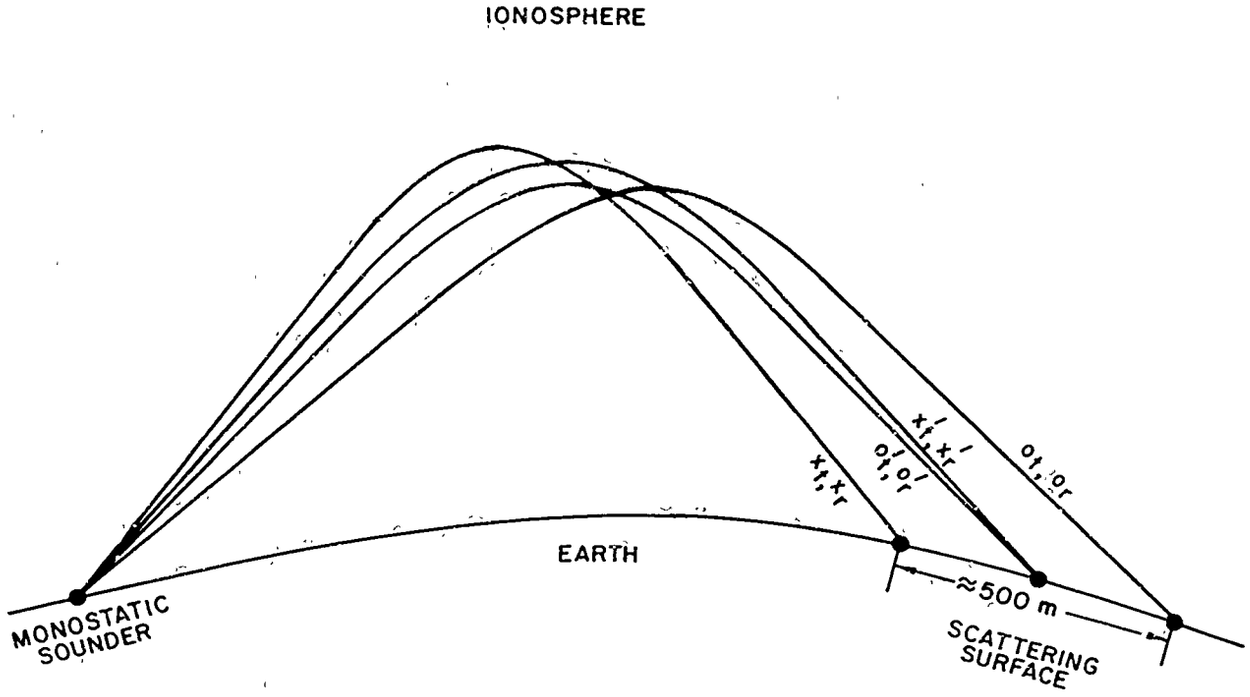

Figure 28. Sketch showing the propagation of the ordinary (o) and extraordinary (x) modes which contribute to the received backscatter. A monostatic sounder is assumed, and the mode separation is greatly exaggerated.

static sounder, the o_r' and o_t' modes follow identical paths, as do the x_t' and x_r' modes. This will not hold true for the bistatic case, however.

Thus, in general, there are 4 transmitted modes, 4 points of reflection, hence 4 received modes for the bistatic geometry, as depicted in Fig. 29. The four mode combinations are depicted as $(o_t -- o_r)$, $(x_t -- x_r)$, $(o_t' -- x_r')$, and $(x_t' -- o_r')$, the time delays of which are equal. This case will be considered first; then the next section will illustrate the simplifications which result when using a monostatic sounder.

We can proceed to define the phase paths, hence the equivalent polarization rotation of the returned mode combinations. It will be convenient, however, to divide this into 3 classes: 1) The sounding antennas and scatterer are linearly polarized, which proceeds directly from the above; 2) the scatterer is polarization-independent, but the sounder is linear; 3) the scatterer is linear, but one of the sounding antennas is circularly polarized.

1. Sounding Antennas and Scatterer Linearly Polarized

The total phase paths of the two returned o modes, P_{o1} and P_{o2}, and of the x modes, P_{x1} and P_{x2}, can be written as:

$$\begin{aligned} P_{o1} &= P_{ot} + P_{or} \quad , \\ P_{o2} &= P_{x't} + P_{o'r} \quad , \\ P_{x1} &= P_{xt} + P_{xr} \quad , \\ P_{x2} &= P_{o't} + P_{x'r} \quad , \end{aligned} \tag{9}$$

where P_{ot} denotes the phase path of the o_t mode; P_{or}, the o_r mode, etc. A fixed frequency, time delay, and azimuth are still assumed. For reference purposes, assume that all of these phase paths are calculated or measured when the sounding antennas and scatterer are all vertically

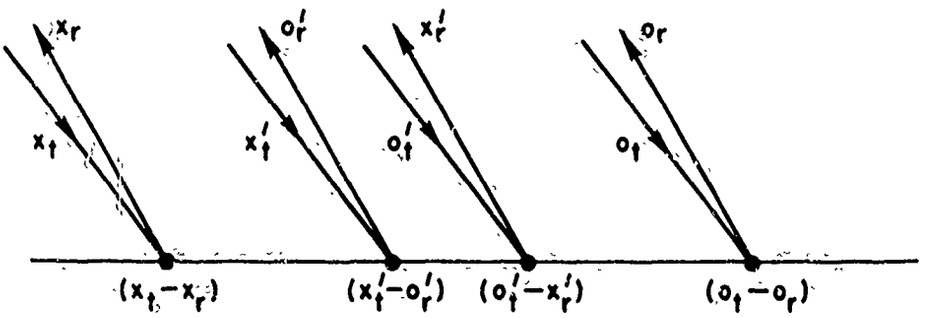

Figure 29. Characteristic-wave modes at the backscatter surface, for a bistatic sounder.

polarized. The effect of other linear polarizations will be accounted for later. We can then sum two pairs of o and x modes, to form two linearly-polarized resultant waves at the receiving antenna. This summation is most easily understood by taking $P_{o1} - P_{x1}$ and $P_{o2} - P_{x2}$, which gives (after rearranging terms):

$$\begin{aligned} P_{o1} - P_{x1} &= (P_{or} - P_{xr}) + (P_{ot} - P_{xt}) \quad , \\ P_{o2} - P_{x2} &= (P_{o'r} - P_{x'r}) - (P_{o't} - P_{x't}) \quad . \end{aligned} \tag{10}$$

Equivalent polarization-rotation angles, Ω, are defined from these phase paths according to:

$$\begin{aligned} \Omega_1 &\triangleq \frac{\pi}{\lambda_o} [(P_{or} - P_{xr}) + (P_{ot} - P_{xt})] \frac{R_x}{i|R_x|}_{EXIT} \quad , \\ \Omega_2 &\triangleq \frac{\pi}{\lambda_o} [(P_{o'r} - P_{x'r}) - (P_{o't} - P_{x't})] \frac{R_x}{i|R_x|}_{EXIT} \quad . \end{aligned} \tag{11}$$

The term $R_x/i|R_x|$ is equal to 1.0 times the sign of R_x, and it will be the same for Ω_1 and Ω_2, since all four modes arrive at the receiver very closely spaced. In order for the sign to be different, it would be necessary for a downcoming mode to be "QL" with cos θ positive in one case, and negative in the other (Appendix A); this condition is not likely to occur. Furthermore, in order to verify that the sign of R_x did not change for <u>all</u> of the experimental conditions used by the author, R_o and R_x were calculated at the bottom of the ionosphere (height = 80 km), assuming $X \ll 1$, for the antenna bearings, frequencies, and elevation angles used in the experiments. It was found that from Lost Hills and Los Baños the sign of R_x was <u>always negative for reception</u>,

and positive for transmission into the ionosphere to the west. These signs are reversed when sounding to the east. Moreover, it was determined that the "QL" approximation was always valid for the exiting or entering waves--which means that they were nearly circularly polarized all the time. Allowing for the sign of R_x to be (+) or (-), but the same for all modes, we can define the following equivalent polarization rotation angles:

$$\begin{aligned}
\Omega_r &= \pm \frac{\pi}{\lambda_o} \left(P_{or} - P_{xr}\right) \quad , \\
\Omega_t &= \pm \frac{\pi}{\lambda_o} \left(P_{ot} - P_{xt}\right) \quad , \\
\Omega'_r &= \pm \frac{\pi}{\lambda_o} \left(P_{o'r} - P_{x'r}\right) \quad , \\
\Omega'_t &= \pm \frac{\pi}{\lambda_o} \left(P_{o't} - P_{x't}\right) \quad ,
\end{aligned} \tag{12}$$

such that $\Omega_1 = \Omega_r + \Omega_t$ and $\Omega_2 = \Omega'_r - \Omega'_t$. It is not clear how the paths for P_{or} and P_{xr}, and the others, are determined, since the constraint of constant time delay applies to the resultants given by Eq. (9). Thus it may be difficult to calculate these angles for the bistatic geometry. For the moment, however, it is only necessary to see that they exist, and that their net signs are determined by whether the difference in their respective phase paths is positive or negative. Section 4, below, will discuss this further.

Thus, one receives the equivalent of two linearly-polarized waves, which, when they rotate with time, frequency, time-delay, or azimuth can produce a modulation on the received power. However, note that the reference at which the various phase path differences are measured or

calculated, has been defined as that for which the sounding antennas and scatterer are all vertically polarized. To account for this, it is first noted that Ω_r and Ω'_r have phase path terms which include only o and x paths from the scatterer to the receiver. Likewise, Ω_t and Ω'_t contain terms for o and x modes sent from the transmitter to the scatterer. Hence, if the transmitting antenna is rotated from the vertical by some angle, this angle will modify the phase paths forming Ω_t and Ω'_t by an amount which is equivalent to a polarization rotation. Thus, if one stands behind the transmitting antenna, the angle between its polarization and the vertical, measured in the CW direction, is equal to an equivalent positive polarization rotation, denoted $\Delta\Omega_t$. Then, if the scatterer is linearly polarized, and if its angle relative to the vertical is measured CW when viewing it from the transmitter, then this angle will tend to subtract from $\Delta\Omega_t$ (i.e. the scatterer and transmitter polarizations become more nearly aligned). Call this scatterer angle $\Delta\Omega_{st}$, which is thus positive when measured in the CCW direction as viewed from the transmitter. Following the same reasoning, the energy is retransmitted from the scatterer with a polarization-rotation "lead" in the positive direction when measured in the CCW direction when viewed from the receiver. This angle is denoted $\Delta\Omega_{sr}$, and is equal to $\Delta\Omega_{st}$ when the scatterer has the same polarization when viewing both the transmitter and receiver. When the receiving antenna is approached, its angle from the vertical, measured in a CW direction as viewed from behind it, will add an amount $\Delta\Omega_r$. Calling Ω_{rn}, Ω'_{rn}, Ω_{tn}, and Ω'_{tn} the "net" polarizations, then all of this is summed up as

$$
\begin{aligned}
\Omega_{rn} &= \Omega_r + \Delta\Omega_r + \Delta\Omega_{sr} \quad , \\
\Omega'_{rn} &= \Omega'_r + \Delta\Omega_r + \Delta\Omega_{sr} \quad , \\
\Omega_{tn} &= \Omega_t + \Delta\Omega_t + \Delta\Omega_{st} \quad , \\
\Omega'_{tn} &= \Omega'_t + \Delta\Omega_t + \Delta\Omega_{st} \quad ,
\end{aligned}
\tag{13}
$$

where $\Delta\Omega_r$ and $\Delta\Omega_t$ are positive when measured CW and when standing behind the antennas looking toward the scatterer. Likewise, Ω_{sr} and Ω_{st} are CW positive when looking toward the sounder from behind the scatterer.

Assuming that the downcoming modes are circularly polarized, we can now write down the general expression which describes the way in which polarization rotation will modify the received backscatter amplitude. We note that we receive the equivalent of two linearly-polarized waves, whose planes of polarization have rotated through angles of $(\Omega_{rn} + \Omega_{tn})$ and $(\Omega'_{rn} - \Omega'_{tn})$ respectively, with respect to the position of the receiving antenna. Hence, if we define

$$
\begin{aligned}
\Delta\Omega &= \Delta\Omega_r + \Delta\Omega_t + \Delta\Omega_{sr} + \Delta\Omega_{st} \quad , \\
\Delta\Omega' &= \Delta\Omega_r - \Delta\Omega_t + \Delta\Omega_{sr} - \Delta\Omega_{st} \quad ,
\end{aligned}
\tag{14}
$$

then the relative (RMS) receiver voltage, V_r, (normalized to 1.0) is given by

$$
V_r = \tfrac{1}{2}\left|\cos\left(\Omega_r + \Omega_t + \Delta\Omega\right) + \cos\left(\Omega'_r - \Omega'_t + \Delta\Omega'\right)\right| \quad . \tag{15}
$$

(Sounding antennas and scatterer linearly polarized)

This expression is generally applicable when the sounding antennas and scatterer are linearly polarized, but not necessarily in the same way.

This result is very interesting, because one could change one or both of the sounding polarization and then note a change in the backscatter power at some frequency, time delay, and azimuth. As an example, suppose that the receiving antenna and scatterer are vertically polarized and fixed, but that the transmitting antenna is switched from vertical to horizontal. From the above, when the transmitter (T_x) is vertical, $\Delta\Omega = \Delta\Omega' = 0$, but when it is horizontal $\Delta\Omega = \Delta\Omega' = \pm \pi/2$, so that

$$\begin{aligned} V_r\,(T_x \text{ vert}) &= \tfrac{1}{2}\left|\cos\,(\Omega_r + \Omega_t) + \cos\,(\Omega_r' - \Omega_t')\right| \quad , \\ V_r\,(T_x \text{ horiz}) &= \tfrac{1}{2}\left|\sin\,(\Omega_r + \Omega_t) + \sin\,(\Omega_r' - \Omega_t')\right| \quad . \end{aligned} \tag{16}$$

Thus, in general, a noticeable change in receiver voltage will occur when the transmitter polarization is switched between vertical and horizontal--providing that the condition of "fixed" frequency, time-delay, and azimuth is approximated.

2. Sounding Antennas Linearly Polarized, Scatterer Polarization Independent

If the scatterer is said to be "polarization independent," it is meant that it will scatter the same mode which impinges upon it. An example of such a reflector is a large, flat copper sheet. If a CW-circular wave strikes it, it is reflected as a CCW mode (when viewed from behind the waves in each case). Both the incoming and reflected waves will satisfy the condition in the ionosphere which enables both of them to propagate as o modes or x modes; (i.e., the sign of cos θ is different for each direction, thus accommodating the different rotations of the two modes). Hence, an o mode will be reflected as an o mode, and an x mode

as an x mode. Therefore, the cross-coupled modes combinations, $o_t' -- x_r'$ and $x_t' -- o_r'$, are eliminated.

Then, referring to Eq. (12), $\Omega_r' = \Omega_t' = 0$, so that

$$V_r = |\cos(\Omega_r + \Omega_t + \Delta\Omega)| \quad , \tag{17}$$

(Scatterer polarization independent, antennas linear)

where it is also true that $\Delta\Omega_{sr} = \Delta\Omega_{st} = 0$, so that $\Delta\Omega = \Delta\Omega_r + \Delta\Omega_t$. If we specify the receiver to be vertically polarized, then $\Delta\Omega = \Delta\Omega_t$. Hence, when the transmitter is vertical, $\Delta\Omega = 0$, and when it is horizontal, $\Delta\Omega = \pi/2$, so that

$$\begin{aligned} V_r(T_x \text{ vert}) &= |\cos(\Omega_r + \Omega_t)| \quad , \\ V_r(T_x \text{ horiz}) &= |\sin(\Omega_r + \Omega_t)| \quad . \end{aligned} \tag{18}$$

This expression says that the peaks and nulls will <u>exactly</u> interchange in the (hypothetical) backscatter record--manifesting changes in $(\Omega_r + \Omega_t)$ with changes in time delay, frequency, or azimuth--when the transmit polarization is switched from vertical to horizontal.

We see that if the scatterer were polarization-independent, and if (at least) one of the sounding antennas were circularly polarized, then we eliminate the reception of all but one of the four modes. In this case polarization rotation would not occur. Likewise, if both the transmitter and receiver were circularly polarized, polarization rotation would again be eliminated. Hence only one more case needs to be considered.

3. Scatterer Linearly Polarized, One Sounding Antenna Linear, the Other Circularly Polarized

In this last case, we receive only two modes. If the receiver is vertical, and the transmitter circular, the received phase paths are P_{o1} and P_{x2}, or P_{o2} and P_{x1} [Eq. (9)], depending upon whether the transmitter excites an o or x mode (respectively). If we reverse these polarizations, then the received phase paths are P_{o1} and P_{o2}, or P_{x1} and P_{x2}.

We must now combine these phase paths, subtracting them in such a way that a difference between an o and an x mode exists. The results have a different form than before, and new angles, denoted Ω''_j must be defined. These may be listed in the same order above, as:

$$\Omega''_1 = \pm \frac{\pi}{\lambda_o} \left[(P_{ot} + P_{or}) - (P_{o't} + P_{x'r}) \right] \quad \begin{matrix} R_x\text{-LINEAR} \\ \cdots\cdots \\ T_x\text{-o MODE} \end{matrix}$$

$$\Omega''_2 = \pm \frac{\pi}{\lambda_o} \left[(P_{x't} + P_{o'r}) - (P_{xt} + P_{xr}) \right] \quad \begin{matrix} R_x\text{-LINEAR} \\ \cdots\cdots \\ T_x\text{-x MODE} \end{matrix} \qquad (19)$$

$$\Omega''_3 = \pm \frac{\pi}{\lambda_o} \left[(P_{or} + P_{ot}) - (P_{x't} + P_{o'r}) \right] \quad \begin{matrix} R_x\text{-o MODE} \\ \cdots\cdots \\ T_x\text{-LINEAR} \end{matrix}$$

$$\Omega''_4 = \pm \frac{\pi}{\lambda_o} \left[(P_{o't} + P_{x'r}) - (P_{xt} + P_{xr}) \right] \quad \begin{matrix} R_x\text{-x MODE} \\ \cdots\cdots \\ T_x\text{-LINEAR} \end{matrix} .$$

To account for different orientations of the linear elements ($\Delta\Omega''$), note first that when the transmitter is circularly polarized $\Delta\Omega_t \equiv 0$, and a difference between an o and x mode occurs over the receiving path. Thus, $\Delta\Omega_r$ and $\Delta\Omega_{sr}$ contribute to $\Delta\Omega''$. It is also true in this case that the difference between like transmit modes occurs.

Therefore, the effect of adding a phase to one of these modes by rotating the scatterer polarization from vertical is cancelled when the other (like) mode is subtracted. Thus, $\Delta\Omega_{st} = 0$ when the transmitter is circularly polarized.

The same reasoning may be applied when the receiver is circularly polarized and the transmitter linear, to yield $\Delta\Omega'' = \Delta\Omega_t + \Delta\Omega_{st}$. Summarizing, we have:

$$\begin{aligned} \Delta\Omega''_1 &= \Delta\Omega''_2 = \Delta\Omega_r + \Delta\Omega_{sr} \quad , \\ \Delta\Omega''_3 &= \Delta\Omega''_4 = \Delta\Omega_t + \Delta\Omega_{st} \quad . \end{aligned} \tag{20}$$

Hence,

$$V_r = \left|\cos\left(\Omega''_j + \Delta\Omega''_j\right)\right| \quad . \tag{21}$$

(Scatterer linear, either T_x or R_x is circular, the other linear.)

In this expression $\Omega''_j + \Delta\Omega''_j$ are determined from equations (19) and (20) as $\Omega''_1 + \Delta\Omega''_1$, $\Omega''_2 + \Delta\Omega''_2$ etc. where j = 1, 2, 3, or 4. It is clear that if the transmit polarization were switched from linear to circular, a marked change in V_r would occur, as when comparing Eq. (15) or (17) to (21). More will be said about this later.

4. Further Interpretations: The Sign of "$P_o - P_x$"

The results of Appendix B show that an o mode will always accumulate more "phase path length" compared to "group path length" than will an x mode when both modes travel through nearly the same ionosphere in nearly the same direction. Thus, when these conditions are

satisfied, and when the group paths (i.e., time delays) of an x mode and o mode are equal, it will be true that $P_o \geq P_x$. This means also that when the time delay of a sum of x modes equals that of a sum of o modes, then $\Sigma P_o \geq \Sigma P_x$.

Therefore, referring to Eqs. (10), (11), and (12) we can say that the sign of $(\Omega_t + \Omega_r)$ is equal to the sign of R_x. For the bistatic geometry, however, we cannot be sure that this always holds true for Ω_t and Ω_r individually.

Secondly, if incoming modes with equal time delay involve the combinations of o and x modes, then it will be true that the mode combination which contains the greatest number of o modes will have the greatest total phase path. However, for the bistatic geometry (at least), we cannot determine which is the greater of two modes which have the same number of o and x modes. Therefore, we cannot specify the sign $(\Omega_r' - \Omega_t')$ in general.

We can, however, say the following, referring to Eqs. (9):

$$P_{x1} \leq P_{x2} \quad \text{and} \quad P_{o2} \leq P_{o1}$$

$$\text{(or)} \tag{22}$$

$$(P_{xt} + P_{xr}) \leq (P_{o't} + P_{x'r}), \; (P_{x't} + P_{o'r}) \leq (P_{ot} + P_{or}) \quad .$$

Therefore, referring to Eq. (19), the sign of Ω_j'' is the same as $(\Omega_r + \Omega_t)$, since the difference between the phase paths, determining both angles, is greater than zero. Furthermore, since $|\Omega_r + \Omega_t| = |P_{o_1} - P_{x_1}|\pi/\lambda_o$, and since $|\Omega_j''|$ always involves the difference between o and x modes (or o + o or x + x modes), it is true that

$$0 \leq |\Omega_j''| \leq |\Omega_t + \Omega_r| \tag{23}$$

This last result means that if the receiver and scatterer were linear, and the transmitted polarization were switched from vertical to circular, then comparison of Eqs. (15) and (21), in light of Eq. (23) shows that the period of one cosine component would be reduced--that is, the changes in $(\Omega_t + \Omega_r)$ and Ω_j' with changes in time delay, frequency, or azimuth. The consideration of a monostatic geometry will shed more light on this.

C. SIMPLIFICATIONS WHEN THE SOUNDER IS MONOSTATIC

Under monostatic conditions, Fig. 28 applies directly. Therefore, $P_{ot} = P_{or} = P_o$, $P_{xt} = P_{xr} = P_x$, $P_{o't} = P_{o'r} = P_{o'}$, and $P_{x't} = P_{x'r} = P_{x'}$, so that $\Omega_r = \Omega_t = \Omega$, and $\Omega_r' = \Omega_t'$. Furthermore, $\Delta\Omega_{sr} = \Delta\Omega_{st} = \Delta\Omega_s$.

The time delays--hence, the "group" paths, P'--of the o--o and x--x mode combinations are equal. Thus, $P_o' = P_x'$, and using the notation of Appendix B, the paths of the o and x are determined using

$$\int_{\text{o path}} \frac{d(\omega\mu_o)}{d\omega}\, ds = \int_{\text{x path}} \frac{d(\omega\mu_x)}{d\omega}\, ds \quad , \tag{24}$$

which holds for $X \ll 1$. If the latter condition is not satisfied, $P_o' = P_x'$ still holds, but the equation for P' is more complicated.

For the o′ and x′ modes, it is true that their ranges are equal, and that the sum of their group paths equals twice the amount given by Eq. (24). Thus, to determine the o′ and x′ paths, in order to calculate $P_{o'}$ and $P_{x'}$, we have

$$\text{Range (o′ path)} = \text{Range (x′ path)} \tag{25}$$

and

$$\int_{\text{o′ path}} \frac{d(\omega\mu_o)}{d\omega}\, ds + \int_{\text{x′ path}} \frac{d(\omega\mu_x)}{d\omega}\, ds = 2\int_{\text{o path}} \frac{d(\omega\mu_o)}{d\omega}\, ds \ . \tag{26}$$

which specifies that the time delays of the mode combinations $o' - x'$, $x' - o'$, and $o' - o'$ are equal.

1. Sounding Antennas and Scatterer Linearly Polarized

Using the results from the last section, Eq. (14) becomes:

$$\begin{aligned} \Delta\Omega &= \Delta\Omega_r + \Delta\Omega_t + 2\Delta\Omega_s \\ \Delta\Omega' &= \Delta\Omega_r - \Delta\Omega_t \quad . \end{aligned} \tag{27}$$

Equation (15) becomes

$$V_{rm} = (1/2)\left|\cos(2\Omega + \Delta\Omega) + \cos(\Delta\Omega')\right| \quad , \tag{28}$$

where the subscript "m" denotes "monostatic." When the scatterer and receiver are vertically polarized, Eq. (16) becomes:

$$\begin{aligned} V_{rm}(T_x \text{ vert}) &= (1/2)\left|\cos(2\Omega) + 1\right| = \cos^2(\Omega) \quad , \\ V_{rm}(T_x \text{ horiz}) &= (1/2)\left|\sin(2\Omega)\right| \quad , \end{aligned} \tag{29}$$

which shows that nulls appear at the position of the peaks in V_r, when the polarization is switched from vertical to circular, and the peaks double in number.

2. Sounding Antennas Linearly Polarized, Scatterer Polarization-Independent

Equation (17) becomes

$$V_{rm} = \left|\cos(2\Omega + \Delta\Omega\right| \quad , \tag{30}$$

and (18) is simplified to

$$\begin{aligned} V_{rm}(T_x \text{ vert}) &= \left|\cos(2\Omega)\right| \quad , \\ V_{rm}(T_x \text{ horiz}) &= \left|\sin(2\Omega)\right| \quad . \end{aligned} \tag{31}$$

3. Scatterer Linearly Polarized, One Sounding Antenna Linear, the Other Circularly Polarized

Equations (20) become

$$\begin{aligned} \Delta\Omega''_1 &= \Delta\Omega''_2 = \Delta\Omega_r + \Delta\Omega_s \quad , \\ \Delta\Omega''_3 &= \Delta\Omega''_4 = \Delta\Omega''_t + \Delta\Omega''_s \quad , \end{aligned} \tag{32}$$

and Eq. (21) is still given by

$$V_{rm} = \left|\cos\left(\Omega''_j + \Delta\Omega''_j\right)\right| \quad , \tag{33}$$

where, from Eq. (19)

$$\begin{aligned} \Omega''_1 &= \Omega''_3 = \pm\frac{\pi}{\lambda_o}\left[2P_o - (P_{x'} + P_{o'})\right] \quad , \\ \Omega''_2 &= \Omega''_4 = \pm\frac{\pi}{\lambda_o}\left[(P_{x'} + P_{o'}) - 2P_x\right] \quad . \end{aligned} \tag{34}$$

From Eq. (23):

$$0 \le \left|\Omega''_j\right| \le \left|2\Omega\right| \quad . \tag{35}$$

When the receiver and scatterer are vertically polarized, and the transmitter polarization is switched from vertical to circular, we note first that $\Delta\Omega = \Delta\Omega''_j = 0$, and V_{rm} takes the form

$$V_{rm} = \begin{cases} \cos^2(\Omega) \text{ --- } T_x \text{ vertical} \\ \\ \cos(\Omega''_j) \text{ --- } T_x \text{ circular} \\ \qquad (j = 1 \text{ or } 2) \end{cases} \quad . \tag{36}$$

It is again clear that the character of the receiver voltage fluctuations with changes in Ω and Ω''_j will be different for the two transmitter polarizations. For the monostatic sounder geometry, the following may also be noted: when an x mode becomes an x' mode, and an o mode an

o′ mode, such that the x′ and o′ modes cover the same ground range, it is reasonable to assume that the changes in phase path $(P_o - P_{o'})$ and $(P_x - P_{x'})$ are nearly equal, but opposite in sign. Stated otherwise, $(P_o + P_x) \cong (P_{o'} + P_{x'})$. Further justification for this relation is seen when it is considered that the o--o, o′--x′, and x--x mode combinations cover ground ranges which are very nearly equal (raytracing shows the o--o and x--x modes to be about 500 meters apart, and the o--x mode somewhere in between). Thus, changes in group path are very nearly equal to changes in phase path over these small range increments. But, since the total group path of the o′--x′ mode equals that of the sum of an o and x mode, and since each sum contains an "o" and "x" mode, it follows that the net phase paths should be approximately equal.

From this result, it is seen that

$$\Omega''_j \cong \Omega \text{ (monostatic)} \quad , \tag{37}$$

which satisfies Eq. (35).

Examination of Eq. (36) in light of (37) means that the character of V_{rm} changes from $\cos^2(\Omega)$ to approximately $|\cos(\Omega)|$ when the transmitter polarization is switched from vertical to circular. There may be a constant phase difference between Ω''_j and Ω, but this is neglected, as it is not important in determining the relative shape and period of V_{rm} when the polarization is switched. By symmetry, the same results will hold true if the receiver polarization is circular and the transmitter is linear.

D. THE CALCULATION OF TOTAL BACKSCATTERED POWER, INCLUDING POLARIZATION MODULATION

The last two sections have yielded formulas for the behavior of the received voltage in response to a backscatter signal which undergoes different amounts of instantaneous polarization rotation. These equations

for V_r were derived while assuming a particular time delay, frequency, azimuth, and time of day (all of which were constant). When an actual backscatter record is made, however, it will be true that any expression for backscatter power at discrete f, τ, and φ must be integrated over the frequency beamwidth (Δf), time-delay resolution ($\Delta\tau$), and the azimuthal beamwidth ($\Delta\varphi$) specified by the sounder. This integration determines the energy returned from the minimum-size backscatter resolution cell, and must be repeated for all frequencies, time delays, and azimuths encountered while recording the backscatter record. It will be assumed, however, that the data are recorded sufficiently rapidly to exclude the necessity of considering changes in Ω with time of day. This latter assumption is equivalent to saying that the integration time of the spectrum analyzer (see Chapter III) is much less than the time for Ω to change by $\pi/2$ radians. But the integration time was always less than 1 sec, and the time for the Ω change is typically 15 sec or more [Ref. 56], so the assumption is valid.

1. The General Technique

Much work has been done to describe the behavior of backscatter amplitude analytically, so that it may be calculated using computer raytracing. Croft [Refs. 84, 85] developed the general method applicable to two dimensions--no changes in the ionosphere with azimuth--while Georges and Stephenson [Ref. 59] extended the method to three dimensions. This previous work was quite justified in ignoring polarization modulation, since it has become clear that the smaller sounding antennas--normally encountered at HF--have beamwidths which are too broad to resolve the effects of polarization rotation. It is clear, however, that the present theory must account for the effect of the earth's magnetic field when calculating backscatter amplitude.

The backscatter power, dP_r, from the sea can be written as

$$dP_r = \mathcal{K} G_r G_t \sigma_o \, d\varphi \, d\tau \quad , \tag{38}$$

where the symbols have already been defined except for $\mathcal{K}$. The latter accounts for the transmitted power, range attenuation, antenna capture area, angle of elevation dependence, ionospheric focusing enhancements, and ionospheric absorption. It is here that Croft's techniques prove most valuable, in that computer raytracing can be employed to calculate the fluctuations in $\mathcal{K}$. To construct a synthetic backscatter record, a receiver bearing, frequency, and time delay are chosen, and dP_r is integrated over all azimuths and within the time-delay resolution $\Delta\tau$. Assuming that the bearing is constant, new frequencies and time delays are chosen and the process is repeated until the record is completed. In general, the transmitter azimuth φ' can be found from the receiver azimuth φ; and the time delay τ represents the sum of the time delays from transmitter to scattering point, τ_t, and that from scatterer to

the receiver, τ_r. If the bistatic separation is great, raytracing over both the transmit and receive paths may be necessary. For a monostatic, or nearly monostatic sounder, the integration in Eq. (38) is obviously greatly simplified.

2. Including Polarization Modulation

To include the effect of the earth's magnetic field, it is necessary in general to compute the deviation of the o and x modes from the "no field" rays, account for the differential absorption of these two characteristic waves, and finally to calculate the effect of polarization rotation on the receiver voltage. For the purpose of modeling "polarization modulation," it was already assumed that the lateral deviation of the modes and their differential absorption were small enough to be neglected. These assumptions appear to be very good in practice, and the only exception is that one occasionally observes a large difference in signal strength between the o and x modes. This circumstance is rare, however, as testified by the great amount of one-way propagation data containing signal fluctuations due to the interference between o and x modes causing polarization rotation.

Having made these assumptions, the expression for dP_r can be made to include polarization modulation by multiplying it by the appropriate expression for V_r^2 (or V_{rm}^2). Since V_r can vary rapidly with frequency, however, it is now necessary to compute its average over Δf. The equation for the average received power, $\langle P_r \rangle$, can then be written as

$$\langle P_r(f,\tau,\varphi) \rangle = \frac{1}{\Delta f} \int_{\Delta f} \int_{\Delta\tau} \int_{\varphi} K \sigma_o G_r G_t V_r^2 \, d\varphi \, d\tau \, df \quad . \tag{39}$$

3. The Ability to Detect Polarization Modulation

Since V_r^2 contains terms involving sines, cosines, and constants, if the heavily weighted part of the integration in Eq. (39) carries V_r^2 through one or more half cycles in Δf, $\Delta\tau$, or φ, one will not detect a noticeable difference in $\langle P_r \rangle$ between two time delays, frequencies, or azimuths, due to the rotation of polarization.

We can visualize this more clearly by first noting that the most heavily weighted portion of Eq. (39) is probably due to the antenna gain product $G_r G_t$. To investigate this, $G_r G_t d\varphi$ was integrated using a digital computer, as described in Appendix C. From this the equivalent beamwidth, $\Delta\varphi_e$, is computed which is defined as

$$\Delta\varphi_e \triangleq \frac{1}{[G_r G_t(\max)]} \int_0^{360^\circ} G_r G_t \, d\varphi \quad . \tag{40}$$

It is normally found that when $G_r = G_t$, $\Delta\varphi_e$ is the -3 dB beamwidth of the sounding antenna [Refs. 41, 86]. For the Los Baños-Lost Hills antenna system it is found that $\Delta\varphi_e$ is close to the -6 dB beamwidth of G_r, and this result should be independent of the radio frequency. It was also computed that the contributions to the integral were down 10 dB outside the main beam of G_r, and were down about 8 dB outside $\Delta\varphi_e$. Therefore, it is clear that the most significant portion of $G_r G_t$ is that spanning $\Delta\varphi_e$.

To first order, we can then estimate the expected variation in backscatter power due to polarization modulation. First, assume that $K\sigma_o G_r G_t$ changes very little over Δf and Δt; (i.e., that its average is equal to its "midband" value). This is a very good assumption. Secondly, assume that the contributions from this factor are negligible outside $\Delta\varphi_e$. Since σ_o to the east is from the land, its average value

should be at least one-tenth that over the Pacific. It is therefore really assumed that $\mathcal{K}$ is no larger to the east than 10 times its value to the west. A previous calculation [Ref. 21] shows that this is a good assumption. Having made these assumptions, $\mathcal{K}\sigma_o$ may be removed from the integration. Then, if $V_r = 1$ over $\Delta\varphi_e$ in one range cell, and $V_r = 0$ in another, the difference in amplitude between these two range cells will be at least 8 dB. But, if the backscatter from east and west is separated, (as in Fig. 26), this variation could be much greater.

As a consequence of the above discussion, we can define the following as the criterion for the detection of polarization modulation:

$$V_r^2(f,\tau,\varphi) \cong \frac{1}{\Delta f\ \Delta\tau\ \Delta\varphi_e} \int_{\Delta f}\int_{\Delta\tau}\int_{\Delta\varphi_e} V_r^2 d\varphi\, d\tau\, df \qquad (41)$$

where $\Delta\varphi_e$ is the -6 dB beamwidth of G_r. This specifies that the <u>average</u> of V_r^2 over the resolution cell ($\Delta\tau\,\Delta\varphi_e$) and frequency bandwidth is approximately equal to its value at discrete f, τ, and φ. As a pictorial example of this, consider the simple result for V_{rm} given by Eq. (29), and consider the transmitter polarization to be vertical, so that $V_{rm} = \cos^2\Omega$. The drawing in Fig. 30 intends to show lines of constant vertical polarization ($\Omega = 0, \pi, 2\pi$, etc.) in the $\Delta\tau\,\Delta\varphi_e$ plane at constant frequencies, $f_3 > f_2 > f_1$. When the lines are extended to new frequencies, surfaces of constant polarization in the $\Delta\tau\,\Delta\varphi_e\,\Delta f$ volume are traced out, as shown. In this case, we see that for a fixed location and value of $\Delta\tau$, and fixed $\Delta\varphi_e$, as f increases a given line moves toward lower τ until one line is lost, and a new one added. Since more than one surface intersects the volume in Fig. 30, Eq. (41) is not satisfied. If, however, $\Delta\tau$ were reduced by something greater than a factor of two--while not making $\Delta f = 1/\Delta\tau$ too large--it is evident that polarization modulation would be detected in the hypothetical backscatter record.

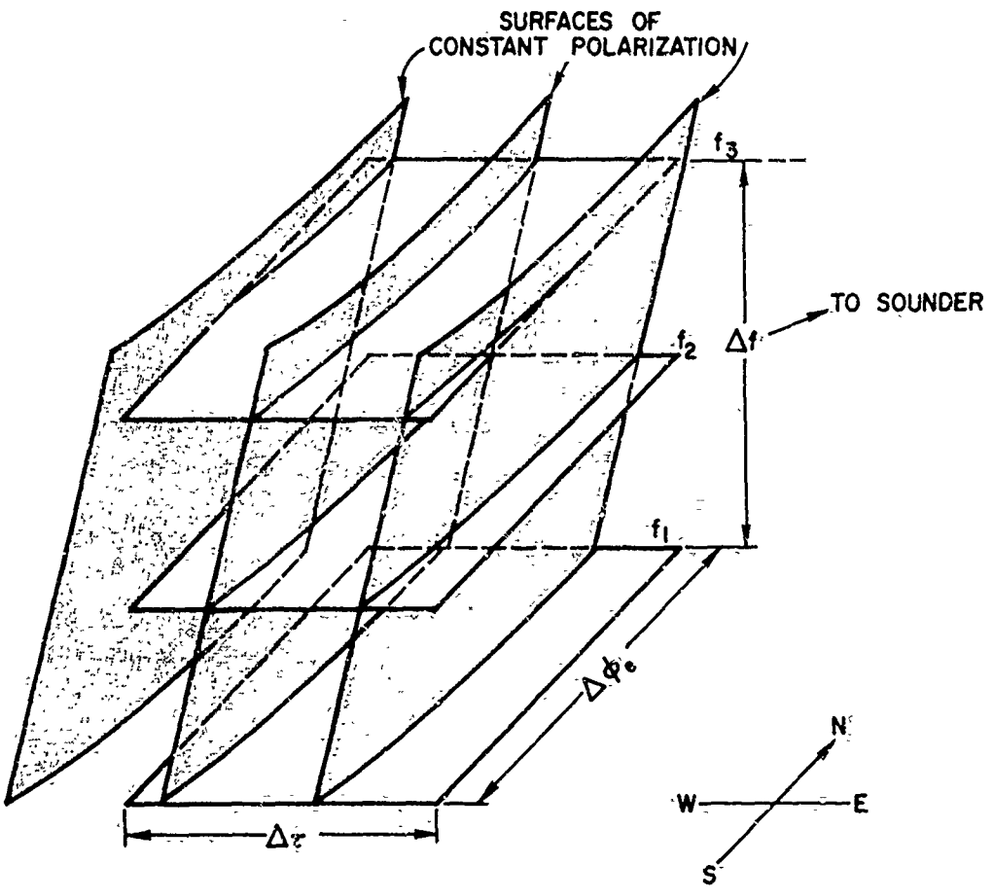

Figure 30. Sketch showing the way in which the ability to detect polarization modulation may be visualized. The shaded surfaces are those of constant polarization for the monostatic geometry.

E. AN APPROXIMATE COMPUTER-RAYTRACING INTERPRETATION

Using the computer program developed by Croft [Refs. 81, 82], which was referred to at the beginning of this chapter, one may compute approximately how polarization rotation varies with range, frequency, and azimuth. The method assumes that the "QL" approximation is valid over the entire ray paths--as is commonly true when tracing rays between the ground and satellites at very high frequencies. Dulk [Ref. 77] achieved good correspondence between measured and calculated polarization rotation using this method--even when rays became perpendicular to the earth's magnetic field lines. There is currently some debate about the reliability of this method when applied to oblique propagation, especially when radio waves do not really satisfy QL conditions. Epstein discussed this briefly [Refs. 44, 45]. Since the method often computes values of Ω which agree with those calculated by tracing individual o and x modes [Refs. 81, 82], the author is inclined to accept its results as providing at least a rough, first-order indication of the variation of Ω with time-delay, frequency, and azimuth. It is felt, however, that one should not attempt to use the method to compute a "total Faraday rotation" over a given oblique path unless it is known that the QL approximation is always valid, or at least that the ray does not become perpendicular to the earth's magnetic field.

The computer program traces a single ray through the ionosphere, using the no-field expression for μ (Appendix A), while the incremental increase in $P_o - P_x$ is calculated and summed along this path. One finds that a confusion over the proper sign of Ω can develop, but this will be of no consequence in what follows, since $\cos^2\Omega$ is evaluated. Two types of ionospheres were chosen: Those with an E and F layer, others with F_1 and F_2 layers. The first is typical for winter-daytime conditions, the second for the summer. The equation

for electron density, N, versus height, h is given by the Chapman function used by Croft [Refs. 81, 84] and Barnum [Ref. 87]:

$$N(h) = N_o \exp [1 - z - e^{-z}]$$

$$z = \frac{h - h_m}{h_s} \qquad (42)$$

h_m = height of maximum density, N_o

h_s = a scale height

Table 2

PARAMETERS USED FOR IONOSPHERES

Ionosphere		N_o elec/cm^3	h_m (km)	h_s (km)	h (km)
M61	E	10^4	130	30	$50 \leq h \leq 163$
	F	10^6	300	65	$164 \leq h \leq 300$
M62	E	10^5	130	25	$55 \leq h \leq 180$
	F	10^6	300	65	$181 \leq h \leq 300$
M63	F_1	$4.5\ (10)^5$	200	50	$50 \leq h \leq 227$
	F_2	10^6	300	65	$228 \leq h \leq 300$
M61K	same as M61, but with N_o replaced by 1.48 N_o				
M63K	same as M63, but with N_o replaced by 1.48 N_o				

Table 2 lists the parameters used for the different ionospheres. A dipole magnetic field was assumed for the earth, with its coordinates misaligned with the geophysical coordinates, placing its South pole near Thule, Greenland [Refs. 56, 88]. The upper (Pederson) ray propagation was assumed to be of lower amplitude, hence it was neglected.

The first set of raytracings was done with ionospheres "M61", "M62", and "M63", at a constant bearing of 270 deg. from Los Baños. Choosing constant frequencies between 10 and 28 MHz, Ω was calculated versus time delay and plotted as a family of curves parametric in frequency. Assuming a monostatic sounder geometry, and that the transmitter, receiver, and scatterer are all vertically polarized, $V_r = \cos^2\Omega$, Eq. (29). Thus, for this geometry it is meaningful to plot the locus of constant $\Omega = n\pi$, which therefore gives the position of maximum signal in the time-delay frequency plane. This was done graphically by stepping Ω in intervals of π radians (or 1/2 turns in rotation), and recording the time delays at which the parametric curves intersected each value of Ω. These points were then transferred to the time-delay frequency plane, and then connected by best-fit lines. The time-delay scale was doubled to account for the two-way backscatter propagation time. The results for these first three ionospheres are shown in Figs. 31 to 33. Each line represents a line of constant (vertical) polarization.

Neglecting all other properties which affect backscatter amplitude, it is still apparent that the periodicity and general character of the lines closely resemble those in the experimental data in Figs. 17 to 27. When the maximum density of the E layer was increased, Fig. 32 shows that a new leading edge (from the E layer) is seen on the synthetic record. This occurrence seems to explain the data in Fig. 23 quite well. Figure 33 shows that the summer ionosphere produces lines which are more closely spaced, and therefore more difficult to resolve. Moreover, the lines from the F_1 layer are superimposed on those from the F_2 layer over a large range of frequencies and time delays. To first order, this could explain why polarization modulation is not apparent on backscatter data recorded in the summer--except perhaps at the longest time delays.

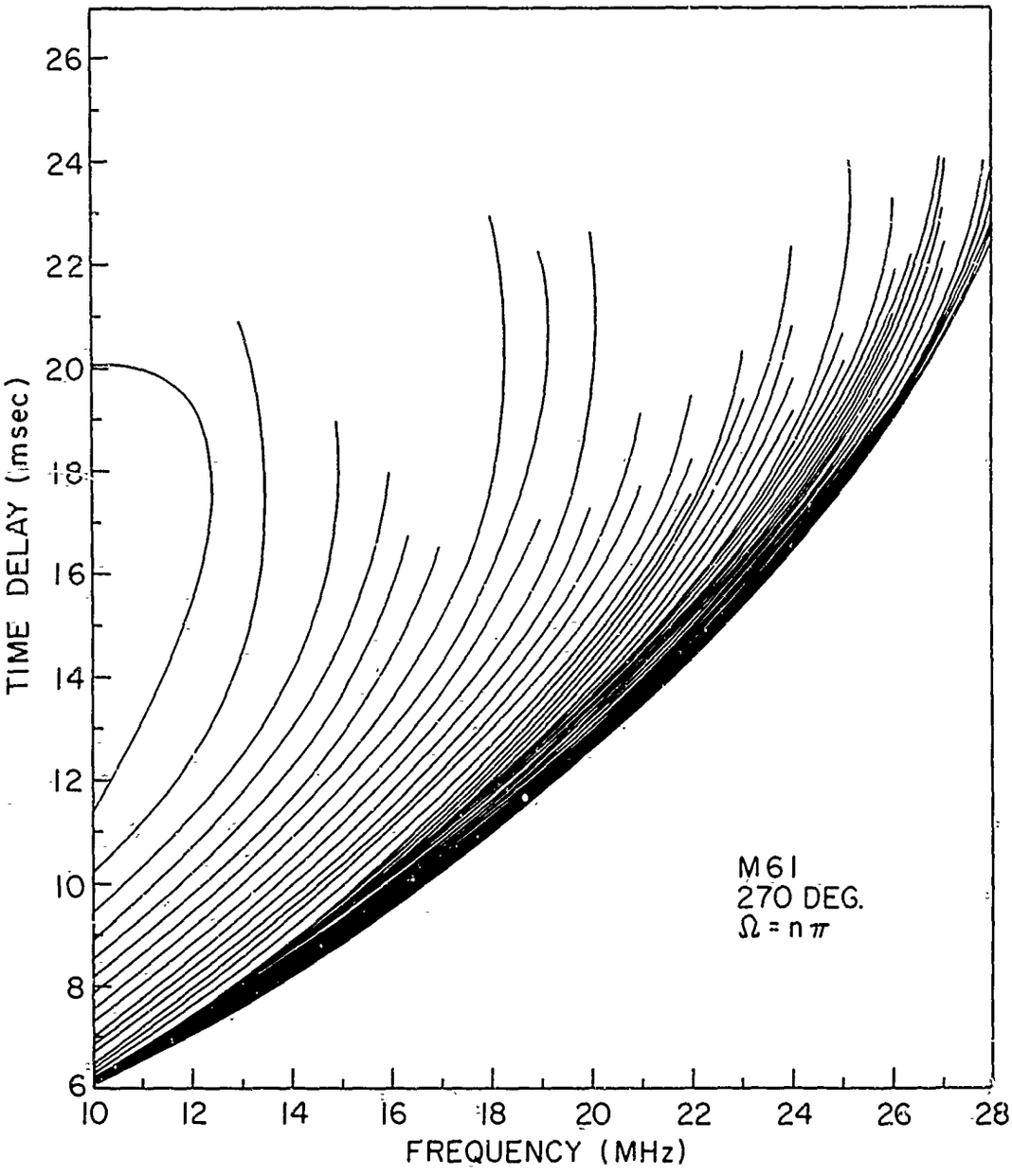

Figure 31. Synthetic backscatter plot showing lines of constant polarization. An F layer of 10^6 electrons/cm^3 and an E layer 100 times smaller are assumed for winter conditions.

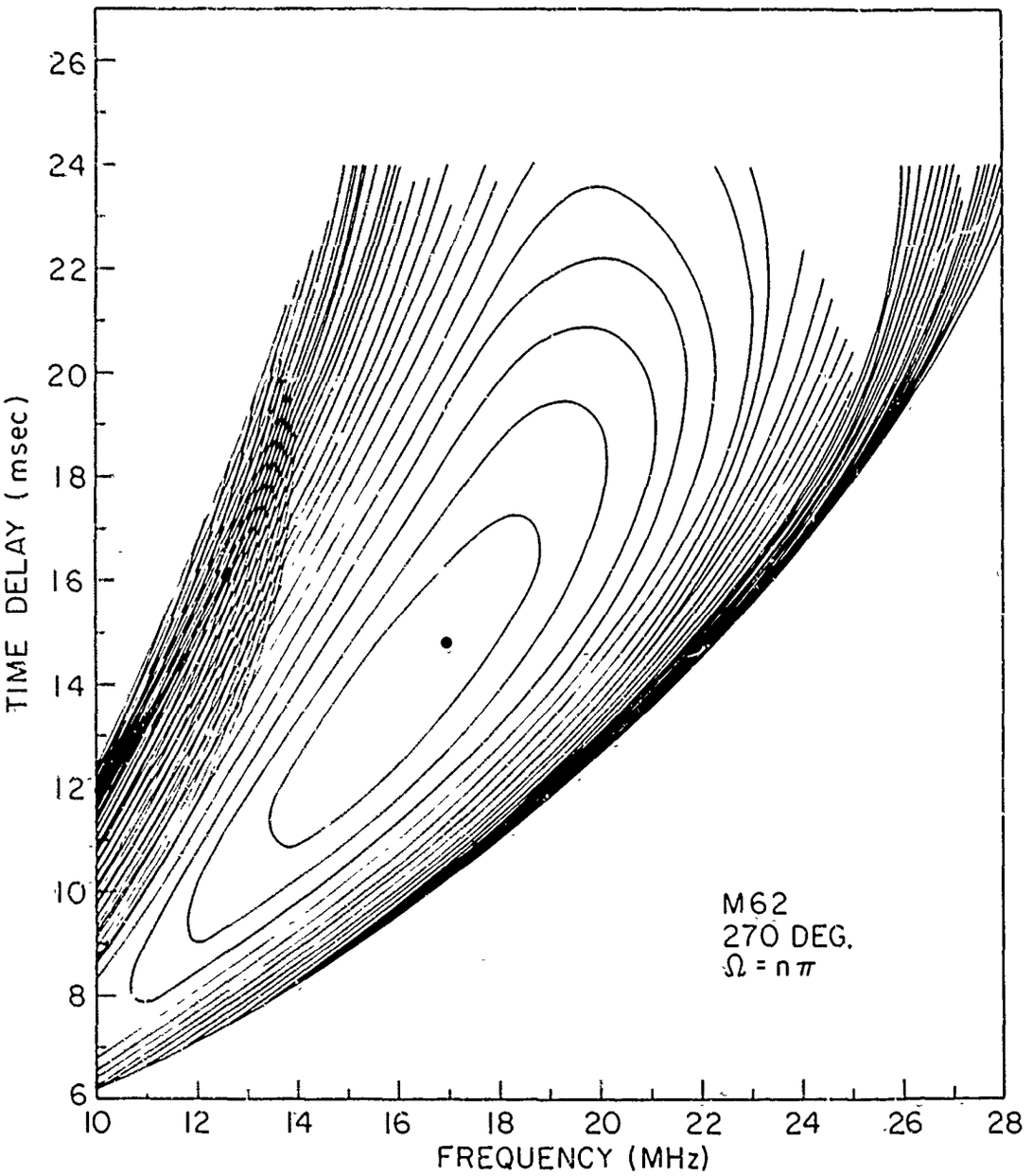

Figure 32: Same as Fig. 31, but the E layer is assumed 10 times larger. The "thumbprint" phenomenon correlates very well with experimental data.

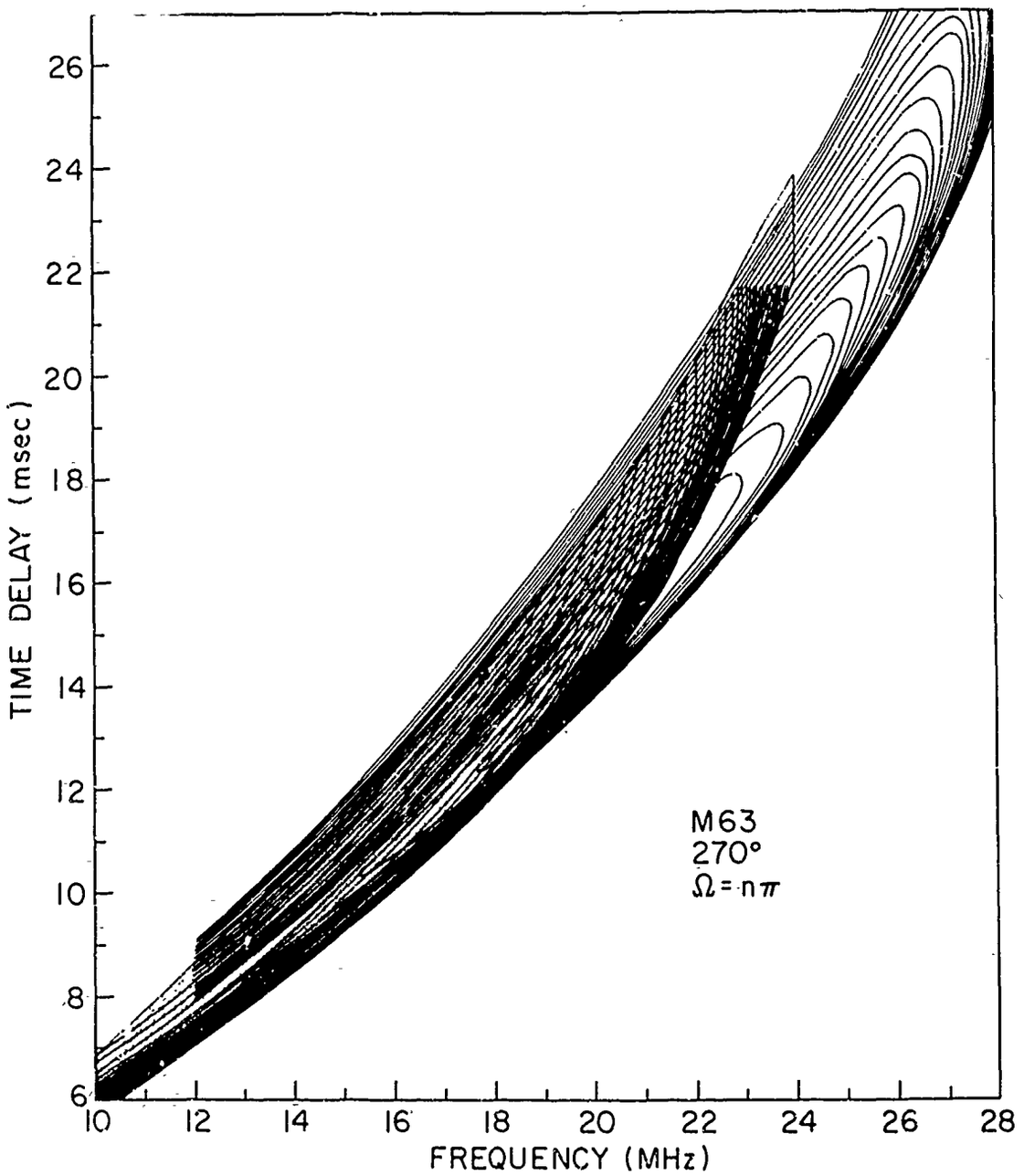

Figure 33. Same as Fig. 31, but a summer ionosphere is assumed.

The second set of raytracings was done at 20 MHz, using ionospheres "M61K" and "M63K". The new M61K is different from M61 in order to match the minimum time delay of the synthetic backscatter with certain experimental data. M63K was different from M63 in order to make a consistent F-layer size for Figs. 34 and 35. The effect of these changes is small, and for the present purpose we may ignore them entirely. The raytracings were done as before, except that different azimuths were used. Thus, the computer output was plotted as before, but parametric in azimuth rather than frequency. Values of $\Omega = n\pi$ were again assumed, and lines of constant (vertical) polarization were plotted in the time-delay azimuth plane. Assuming a 0.5 deg antenna beamwidth, it is apparent from Figs. 34 and 35 that Eq. (41) can be satisfied in the winter, but not during the summer at the time delays shown. Furthermore, the use of a 2 deg beamwidth or more would render the lines undetectable during the daytime for both seasons.

F. CONCLUSIONS

The theory just described could explain the observed periodicity and continuity of the new type of line families described in the last chapter. Since polarization modulation should become visible only when the magnitude and polarization properties of the scatterer are relatively constant, the fact that lines are seen only over the sea can be explained. The results using the approximate computer raytracing method show that the lines become more dense near the backscatter leading edge, and can curve around to resemble a thumbprint. These also agree with the experimental data.

The next chapter will give experimental proof that the new type of line families are caused by polarization rotation.

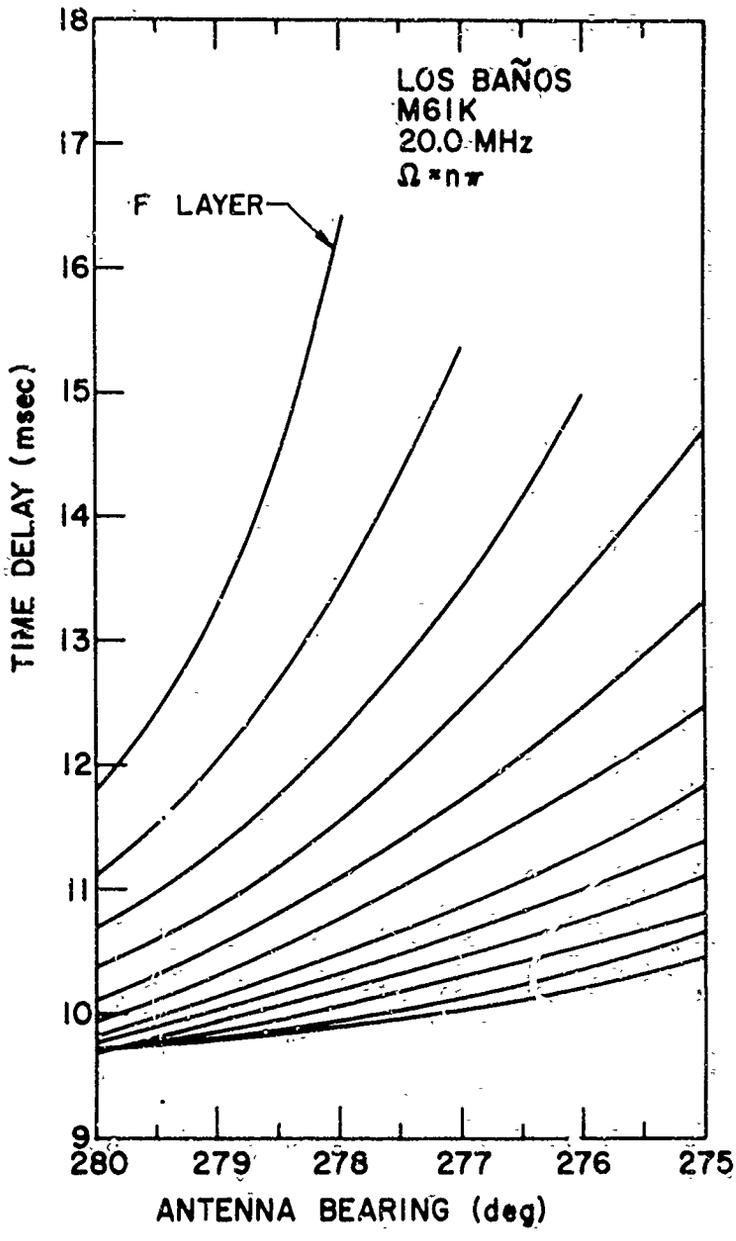

Figure 34. Synthetic backscatter showing lines of constant polarization in the time delay-azimuth plane, assuming a winter ionosphere. Shows why large antenna beamwidths cannot resolve polarization modulation.

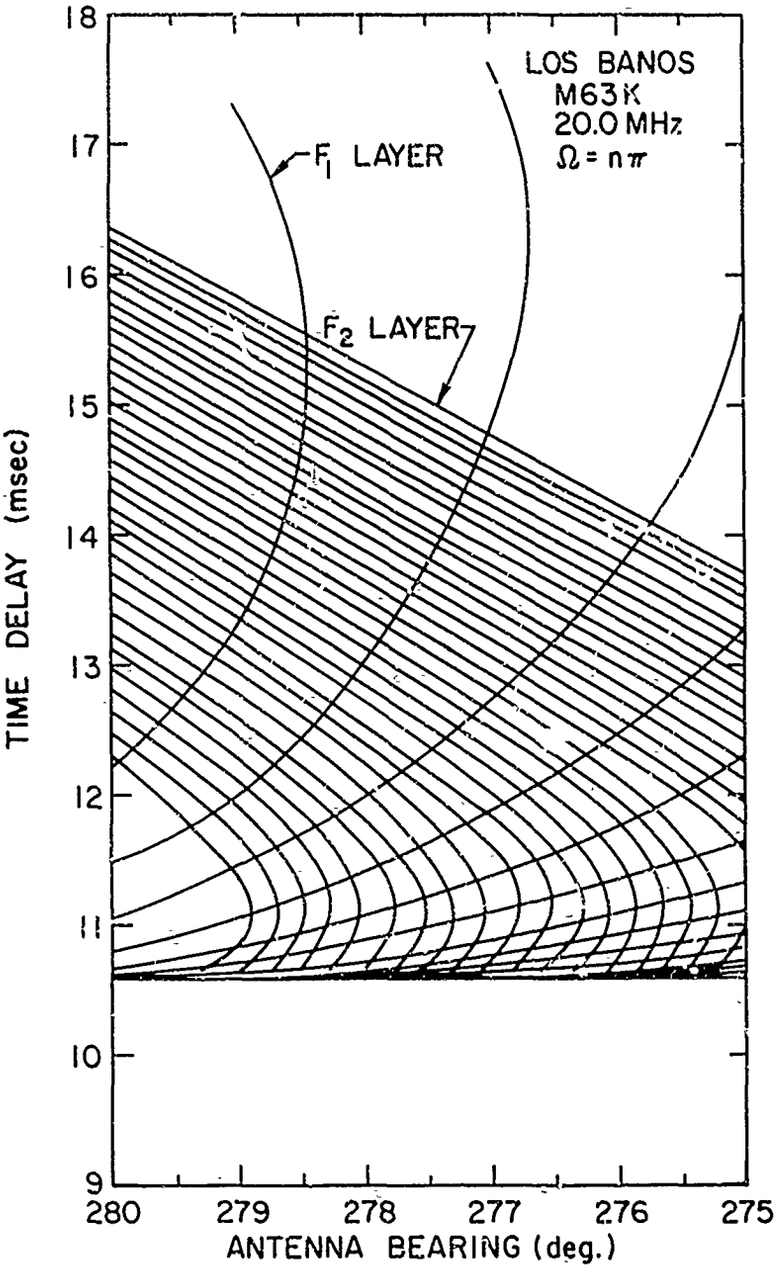

Figure 35. Same as Fig. 34, but using a summer ionosphere. Even the Los Baños array should not be able to resolve polarization modulation during the summer, as observed experimentally.

VI. EXPERIMENTAL EVIDENCE OF POLARIZATION-MODULATION ON SEA BACKSCATTER

The purpose of this chapter is to demonstrate the way in which controlling of the transmitter polarization affects the new type of modulation on sea backscatter. Two types of experiments were performed. In the first, the transmitter polarization was switched between vertical and elliptical polarization for alternate wide-swept frequency records. In the second experiment, narrow-band "fixed" frequency data were recorded, wherein the transmitter polarization was switched between vertical and horizontal every 10 seconds. The results corresponded with the theoretical predictions in the last chapter, and prove conclusively that the backscatter modulation was associated with polarization rotation.

A. TRANSMITTER POLARIZATION SWITCHED BETWEEN VERTICAL AND ELLIPTICAL

1. Experimental Data

Figures 36 and 37 show oblique ionograms taken between Los Baños and Bearden, Arkansas (i.e., to the east from Los Baños) on 5 and 7 February 1969, respectively. These data were recorded at nearly the same time of day, before each day's backscatter run. Figure 37 shows a modulation of the 1-hop (lower) trace due to polarization rotation with frequency [Epstein, Refs. 44, 45]. Figure 36 shows this condition clearly only near the maximum usable frequency (MUF); and it is conjectured that o and x modes were unequally attenuated over other portions of these data. Sweeney [Ref. 47] has shown a great deal of data which demonstrates that as a rule, polarization rotation with frequency is seen much more often than not. This has also been the author's experience while operating the system. It is therefore evident that the Los Baños receiving array is

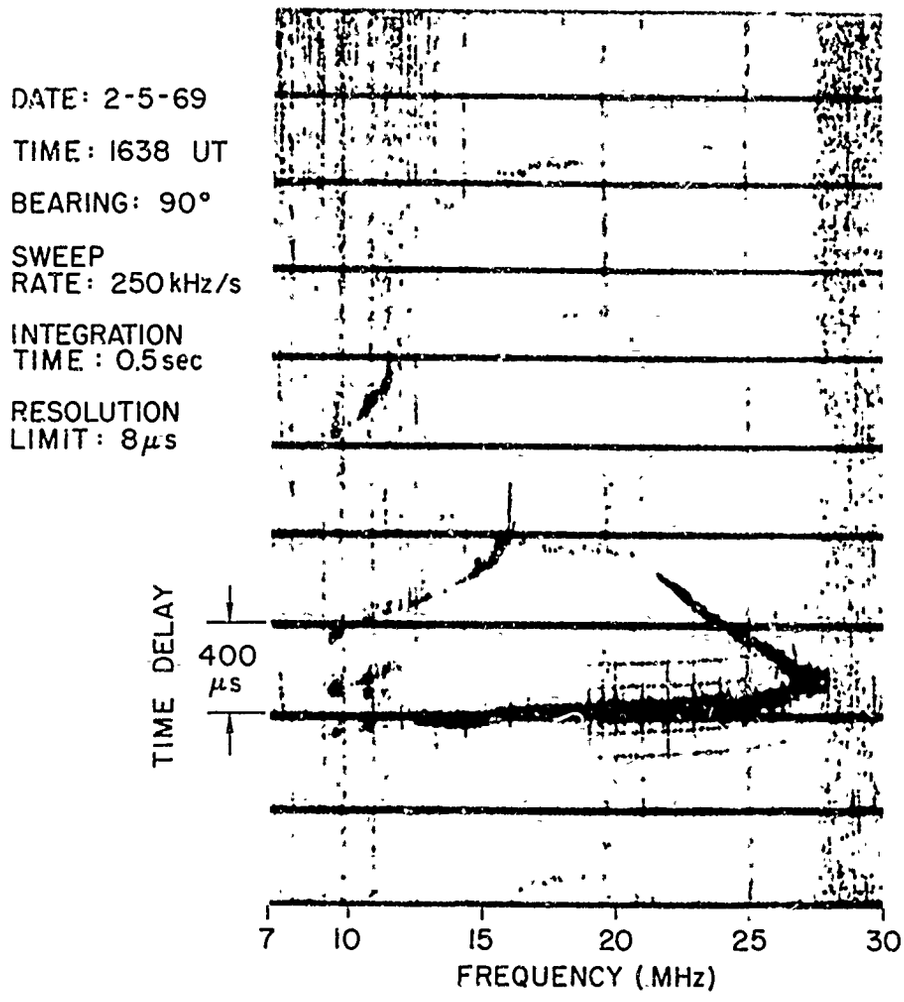

Figure 36. SFCW oblique sounding to the east (Bearden, Ark.), on 5 Feb. 1969.

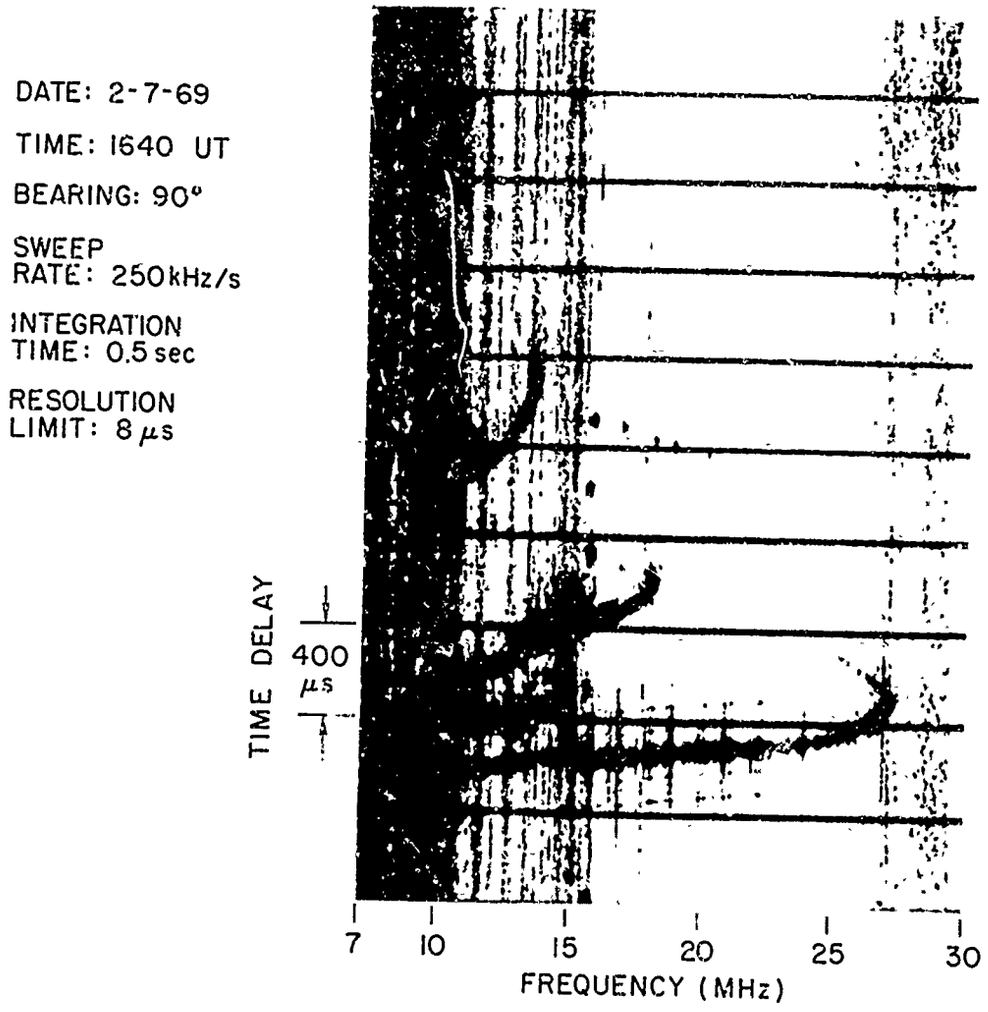

Figure 37. Same as Fig. 36, except taken on 7 Feb. 1969, at the same time of day.

usually not too large to discriminate against polarization rotation. Hence, during the period 5-7 February 1969, it was conjectured that the "thumbprint" line families appearing in the wide-frequency swept data of Figs. 17-24 were associated with polarization rotation. Indeed, the periodic nature of these lines closely resembles the expected behavior of V_r from the last chapter.

On both days, the crossed-LPA system was used at the transmitter, and it was relatively simple to feed these antennas one at a time, or together (out of phase). On 5 February 1969, it was found that switching between vertical and horizontal polarization on alternate records produced no consistent difference between the appearance of the lines--either their position or their spacings. It was believed that this was due to the 1 minute time lapses between these records, causing the lines to change because of the passage of time.

On 7 February 1969, the crossed LPA's were arranged so that they could also be fed simultaneously, out of phase, as described in Chapter III. It was desired to transmit nearly circular polarization over some portion of a backscatter record--at some frequency and slant range. Figures 38, 39 and 40 show the results of the experiment in which the transmitter polarization was switched between vertical (only) and the phased condition described in Chapter III. These data were obtained in exactly the same fashion as in Figs. 17-24. The system parameters are listed on the figures. When the transmitter polarization was elliptical it was denoted "circular", as the latter was the intended polarization. As for Figs. 21-24 taken on the same day, the sweep rate was 500 kHz/sec. However, the records in Figs. 38 and 40 were reprocessed at double the time taken to record the data, so that the effective sweep rate was 250 kHz/sec as noted. This circumstance represents only a reprocessing convenience.

From Fig. 38 it may be concluded that there is a noticeable difference between the thumbprint lines when the transmitting polarization

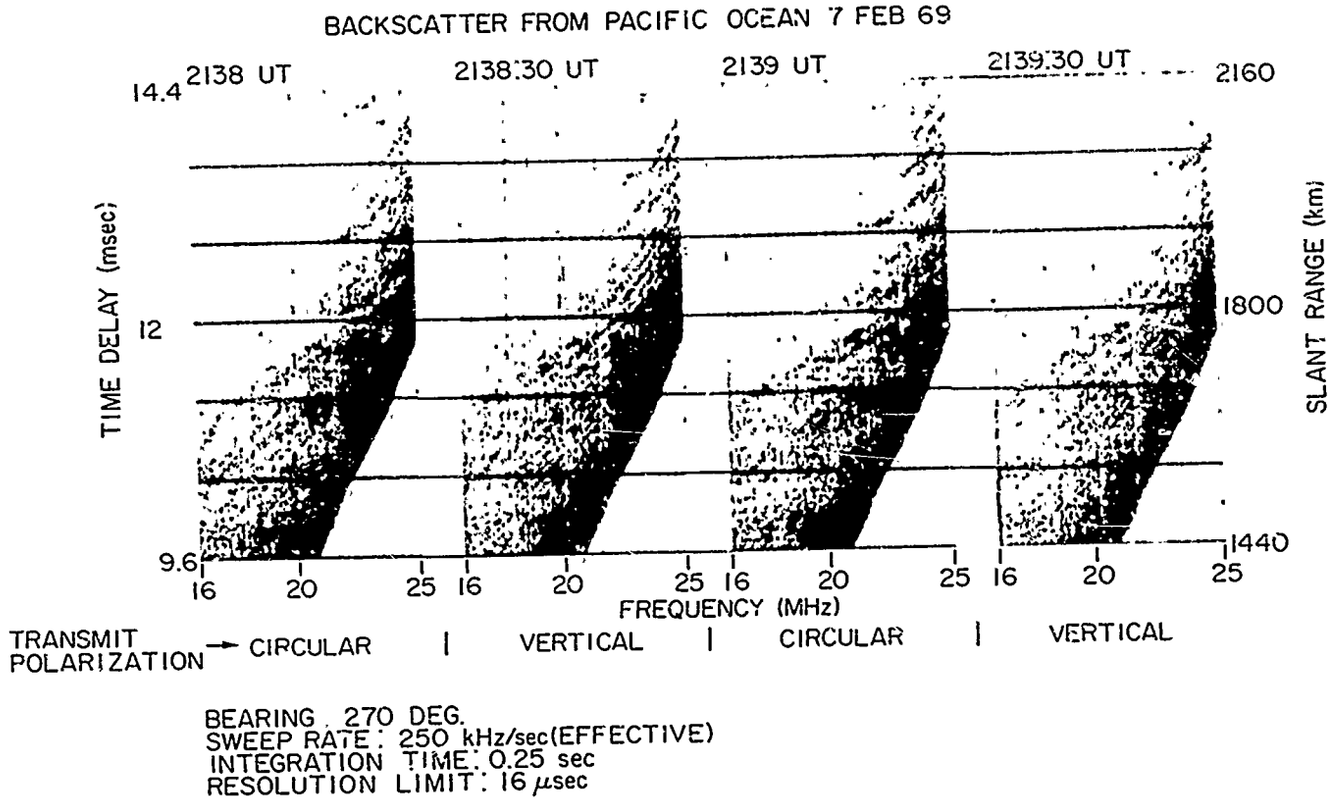

Figure 38. SFCW backscatter from the Pacific Ocean on 7 Feb. 1969 near 2138 UT, showing the way in which polarization modulation is changed when the transmitter's polarization is switched between vertical and "circular".

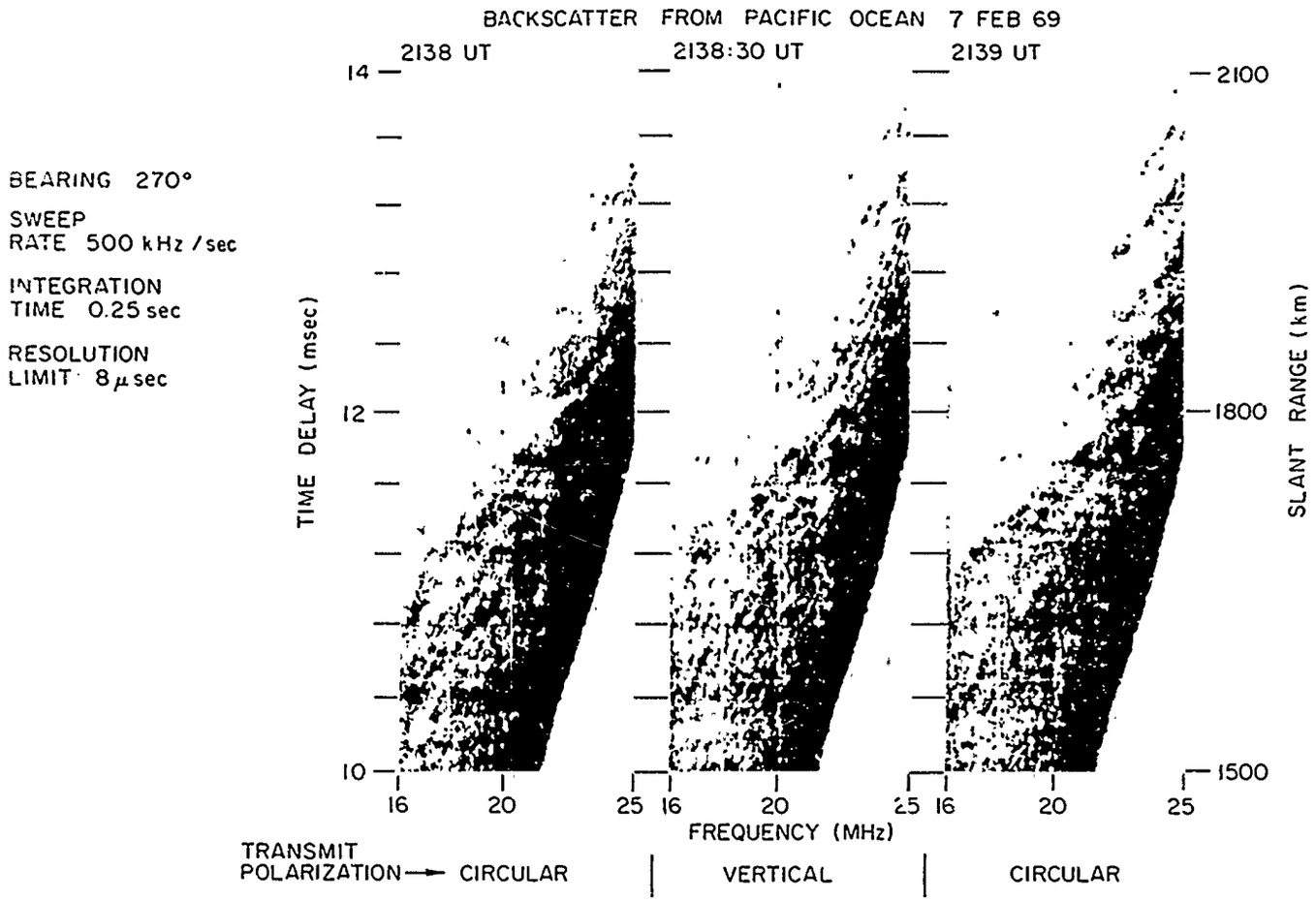

Figure 39. Same as Fig. 38, with the exception that three frames of the data were processed to improve resolution.

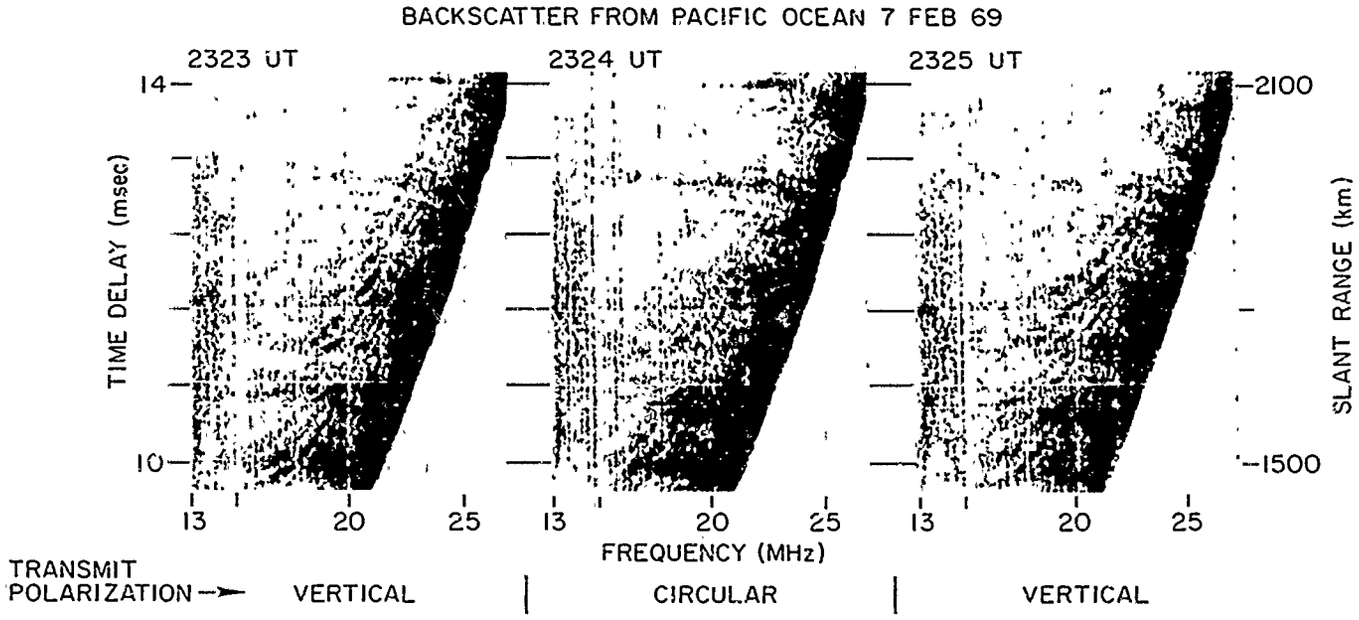

Figure 40. Same as Fig. 38, except taken at 2323-2325 UT.

is switched between vertical and so-called "circular". It is seen that the clarity of the lines is reduced when the polarization is "circular". From Chapter III, it may be concluded that circularity should be most nearly attained at the lower left and upper right portions of these data.

Figure 39 shows some of the data of Fig. 38, but more highly resolved. The same character of line clarity is seen, and near the top half of the data, the polarization lines are removed almost entirely--when the transmit polarization is "circular". Essentially the same thing was seen 3 hours later, as shown in Fig. 40.

2. Comparison With Theory

It is clear that when lines appear in the data their spacings in the time-delay and frequency dimensions are regular and periodic, as predicted by the expressions for V_r which contain sines and cosines. Referring to the work of the last chapter, the appropriate theoretical predictions of the character of received voltage, V_r, versus polarization rotation, Ω, are those for which the receiver polarization is vertical. It is most reasonable to assume that the sea also favors vertical polarization. Thus it is true that $\Delta\Omega = \Delta\Omega' = \Delta\Omega'' = 0$. (This will also hold if the sea is polarization-independent.)

The results for the monostatic sounder given by Eqs. (36) and (37) predict that enhancements in V_{rm} due to a favorable polarization alignment will be less discernable for circular transmitted polarization--as when comparing $\cos^2 \Omega$ to $|\cos \Omega|$. It appears that something similar to this simplified result has occurred, even though the Stanford sounder is bistatic.

The expressions for V_r when the sounder is bistatic, and when the transmitter polarization is switched between vertical and circular [Eqs. (15) and (21)], unfortunately do not lend themselves to ready interpretation or comparison.

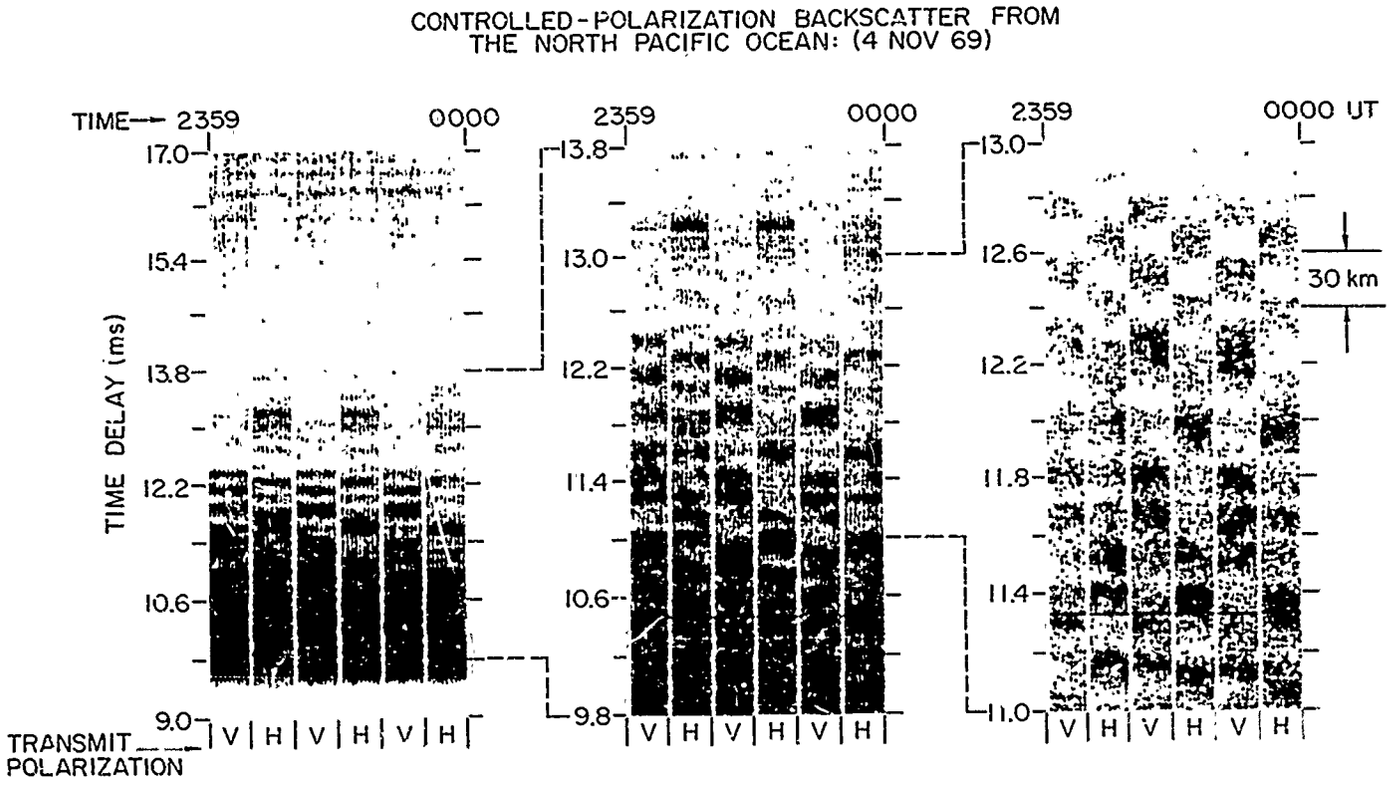

Figure 41. "Fixed-frequency" SFCW backscatter from the Pacific Ocean, in which the transmitter polarization was switched between vertical and horizontal polarization.

Just previous to the time at which these data were recorded, wide-frequency-swept data revealed "thumbprint" lines, so that the periodic backscatter enhancements shown in Fig. 41 represent a cross section of the lines in the time delay dimension, averaged over a 240 kHz bandwidth. Even though the 16 and 8 μsec data do not utilize the full Δf in the spectrum analysis, this type of display prohibits the realization of smaller Δf's--since the sweeps are repeated once per second and are closely spaced, thus causing the human eye to average over what might be a sequence of slanted lines at each enhancement.

The sweeps were short enough so that changes in the line structure from sweep to sweep were very small. Therefore, it was advantageous to switch the transmitter polarization between vertical ("V") and horizontal ("H") as noted on the data. This made the two polarization states well defined, thus escaping the uncertainties which arise when attempting to transmit circular polarization. For convenience in data display, the polarization was switched every 10 seconds as shown.

The results of Fig. 41 give conclusive proof that this type of modulation on sea backscatter is associated with polarization rotation. In fact, the amplitude of the backscatter from many time delays can be controlled by simply changing the transmitter polarization. It may be noted further that given backscatter enhancements for a given polarization slant downwards with the passage of time. Hence, at a constant time delay, the backscatter amplitude fluctuates with time of day. The period between a maxima and minima in this case is about 2 minutes (extrapolating) which agrees with past measurements of polarization fading on one-way-propagated signals. A discussion of the specific patterns of the polarization-modulation fluctuations will be given later. For the moment, it is sufficient to note that the fluctuations are regular and periodic, as predicted by the equation for V_r.

The dynamic range of the display in Fig. 41 is about 10 dB. This indicates that the difference in backscatter amplitude between a peak and a null is also about this much. To investigate this further, single sweeps occurring at 2359:59 and 0000:02 UT were reprocessed to display backscatter amplitude versus time delay (A scans). Figure 42 shows this. A portion of Fig. 41 is included for ease in reference. The record at 2359:59 UT is actually the last sweep recorded in the continuous-time data, at which time the polarization was horizontal. The second data, recorded 3 seconds later, was that for which the polarization had been switched to vertical. This segment of data reveals a periodicity in backscatter amplitude; and, if the scans for the two polarizations are carefully compared, one notes that a near minimum in backscatter amplitude shifts to a maximum after a period of just 3 seconds--during which the transmitter polarization was switched. The clearest examples of this occur between 10.6 and 12.2 msec. It is noted that the amplitude displays are linear in voltage, and that 10 dB excursions between adjacent peaks and nulls are not uncommon.

The data shown in Fig. 43 were recorded just a few minutes earlier than that in Fig. 42, and are presented now in order to demonstrate the dependence of polarization modulation on antenna beamwidth. As noted on the figure, approximately the left half was recorded using 1/8 of the full receiving array (i.e., a subarray) or a -6 dB beamwidth of 4.0 deg. Then, at 2351:45 UT the full array was switched in to operation, decreasing the beamwidth to 0.5 deg. In both cases, the receiver was AGC controlled, so that the average receiver output voltage was about the same. When the full array is used, the polarization modulation "bars" are clearly discernible. However, when a single subarray is used, it is difficult to identify this phenomenon. It is

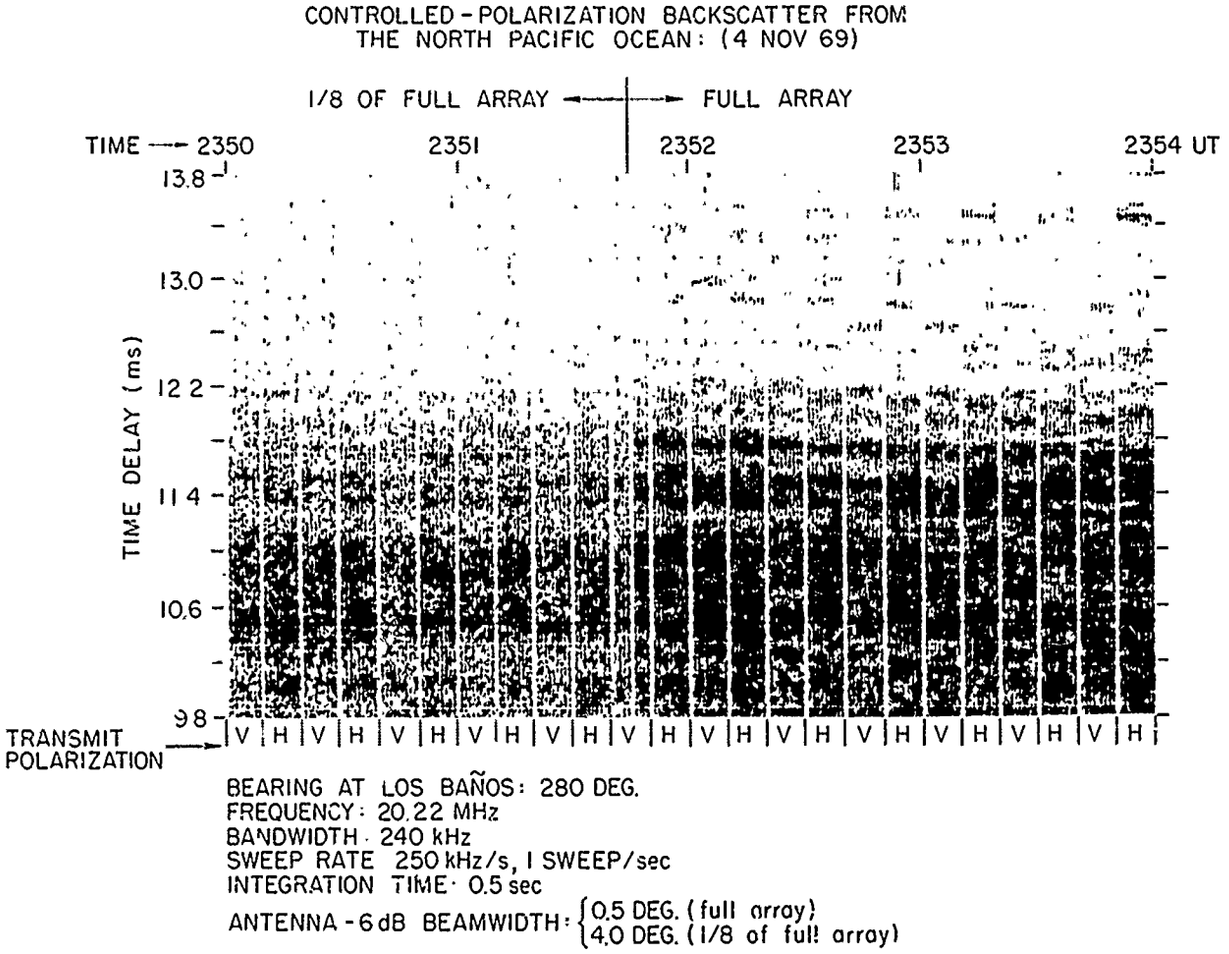

Figure 43. Same as Fig. 41, except that the receiving antenna beamwidth is 4.0 degs on the left and 0.5 deg on the right. This record shows the effect of antenna beamwidth on the ability to resolve polarization modulation.

probable that this result explains why polarization modulation has not been identified by other workers using smaller sounding antennas.

Figure 44 shows data that were taken in an attempt to display the behavior of polarization modulation with azimuth while it was being observed to vary with time delay. Thus, immediately after each frequency sweep, the receiver bearing was stepped in 1/4 deg increments. The data on the left were recorded exactly like Figs. 41 and 43, but with a bearing scan of 280° to 275-1/4°, as noted. The data on the right were taken two weeks earlier, and are included for comparison. From the previous data we expect to see polarization modulation between about 9.8 and 12.2 msec on the left two records. A careful examination of the data between these time delays reveals periodic sets of lines which slope upwards while progressing to the right. These look similar to those which appear on the data for 22 October 1969, although one cannot say for sure that the latter are due to polarization rotation. The heavy, somewhat blotchy amplitude enhancements between about 11.4 and 13.4 msec on the left are most likely caused by ionospheric-irregularity focusing. Reference to Georges and Stephenson's work [Ref. 59] supports this conclusion. It is clear that if a 4.0 deg beamwidth antenna had been used at this time, both the polarization and focusing variations would have been averaged over, which explains the data in Fig. 43.

2. Comparison With Theory

The results of Figs. 41-44 demonstrate (on the day of measurement) that the pulse lengths ($\Delta\tau$) of 16 to 4 μsec are obviously small enough to render the polarization modulation detectable over most of the data. Indeed, the amplitude peaks are spaced by 100 to 200 μsec. It is also clear that Δf and $\Delta\varphi$ for the full array are small enough. It may be true however, that Δf is too large near the skip distance (or minimum time delay) since it is known that the Faraday rotation with

probable that this result explains why polarization modulation has not been identified by other workers using smaller sounding antennas.

Figure 44 shows data that were taken in an attempt to display the behavior of polarization modulation with azimuth while it was being observed to vary with time delay. Thus, immediately after each frequency sweep, the receiver bearing was stepped in 1/4 deg increments. The data on the left were recorded exactly like Figs. 41 and 43, but with a bearing scan of 280° to 275-1/4°, as noted. The data on the right were taken two weeks earlier, and are included for comparison. From the previous data we expect to see polarization modulation between about 9.8 and 12.2 msec on the left two records. A careful examination of the data between these time delays reveals periodic sets of lines which slope upwards while progressing to the right. These look similar to those which appear on the data for 22 October 1969, although one cannot say for sure that the latter are due to polarization rotation. The heavy, somewhat blotchy amplitude enhancements between about 11.4 and 13.4 msec on the left are most likely caused by ionospheric-irregularity focusing. Reference to Georges and Stephenson's work [Ref. 59] supports this conclusion. It is clear that if a 4.0 deg beamwidth antenna had been used at this time, both the polarization and focusing variations would have been averaged over, which explains the data in Fig. 43.

2. Comparison With Theory

The results of Figs. 41-44 demonstrate (on the day of measurement) that the pulse lengths ($\Delta\tau$) of 16 to 4 μsec are obviously small enough to render the polarization modulation detectable over most of the data. Indeed, the amplitude peaks are spaced by 100 to 200 μsec. It is also clear that Δf and $\Delta\varphi$ for the full array are small enough. It may be true however, that Δf is too large near the skip distance (or minimum time delay) since it is known that the Faraday rotation with

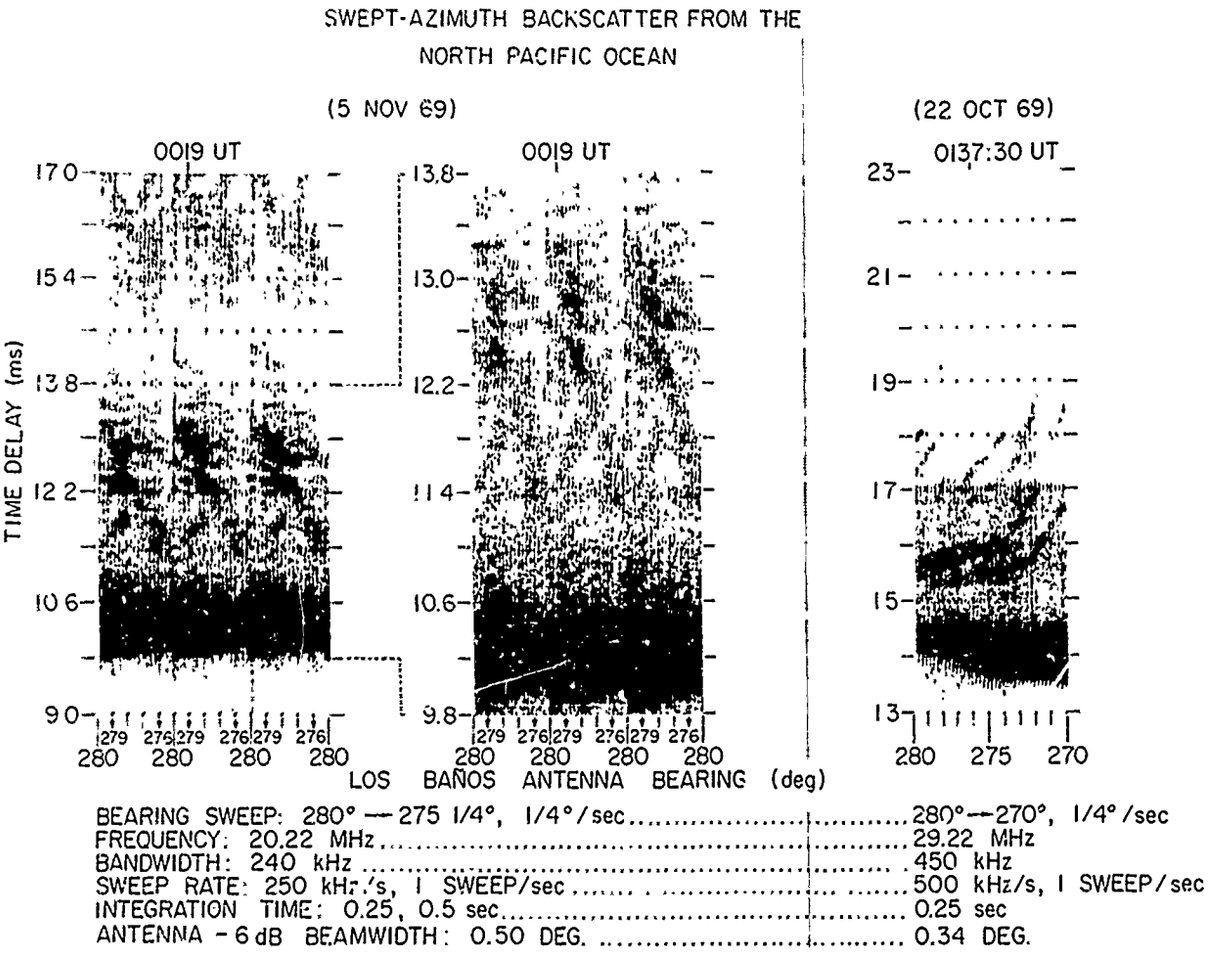

Figure 44. Data similar to Fig. 41, except that the transmit polarization was always vertical and the receiving azimuth was scanned in time. This record shows why a larger antenna beamwidth will average over the fine-scale polarization modulations, as proved in Fig. 43.

frequency rate increases near this region. This probably explains why the polarization modulation becomes blurred between 9.6 and 10.6 msec, as it also blurs near the backscatter leading edge of Figs. 38-40. Furthermore, it may also be true that a certain amount of averaging in the frequency domain occurs for the data at the higher time delays, which could modify the expected change in V_r when the polarization is switched. However, since the dynamic range of the polarization modulation is about 10 dB, it appears that such averaging is usually minimal.

For a vertical receiving antenna and scatterer, Eqs. (28) predict the change in V_{rm} for a monostatic sounder to be such as to compare $\cos^2 \Omega$ (Tx vert) to $\frac{1}{2}|\sin (2\Omega)|$ (Tx horizontal). The general results for the bistatic sounder give V_r's of $|\cos (\Omega_r + \Omega_t) + \cos (\Omega_r' - \Omega_t')|$ and $|\sin (\Omega_r + \Omega_t) + \sin (\Omega_r' - \Omega_t')|$ [Eq. (16)] for transmitter (Tx) polarizations of vertical and horizontal, respectively. One thus expects to see a shift in the maxima in backscatter amplitude and perhaps a change in the periodicity for the two transmit polarizations. It is observed in Fig. 41 that such occurs. Over very limited portions, one sees something similar to the prediction for the monostatic sounder geometry. In other portions of the data, such as around 12.6 msec, values of $\Omega_r' - \Omega_t' = \pi/4, 5\pi/4$, etc would yield V_r's to explain the half-period shifts of the backscatter enhancements. It is also true, however, that the V_r expressions for a polarization independent scatterer [Eqs. (18)] would yield the same result at these time delays, but since it fails at others, the data and theory suggest that <u>the sea is not polarization-independent</u>.

It again becomes evident that unless the specific relation between Ω_r, Ω_t, Ω_r', and Ω_t' is known for the bistatic sounder, one cannot uniquely prove the theoretical expectations for V_r. It is clear beyond reasonable doubt, however, that the expected character of V_r is reproduced by the data, and that the new type of backscatter

amplitude modulation is caused by the rotation of polarization. It is probably true that as one proceeds higher in time delay, the value of $(\Omega_r' - \Omega_t')$, as well as $(\Omega_r + \Omega_t)$, changes so that the degree of period shift in amplitude maxima (with change in polarization) varies with time delay.

C. DISCUSSION

The periodic behavior of the line families in the backscatter data clearly resembles the expected appearance of V_r in the frequency, azimuth, and time delay dimensions. The fact that the modulation changes when the transmitter polarization is switched, gives conclusive proof that polarization rotation accounts for this new type of behavior. Also, the dynamic range of the modulation was about 10 dB as expected theoretically.

The changes in the position and periodicity of the polarization modulation in the data can be explained using an appropriate V_r expression from the last chapter; however, since the sounder is bistatic, it was not uniquely possible to verify a single expression for V_r from the theory. It is clear that if the expressions for V_r are to be verified exactly, a monostatic sounder would be extremely useful. More theoretical work regarding the bistatic geometry is also needed.

Although the frequency bandwidth, Δf, may have been too large in some portions of the data in Figs. 41-44 to satisfy Eq. (41), both it and $\Delta\tau$ were small enough at other time delays to permit polarization modulation. These Δf and $\Delta\tau$ are not difficult to obtain, and many other workers have done so. It was shown that antenna beamwidth, $\Delta\varphi$, is really the major constraint on the visibility of the modulation, from which it is concluded that "polarization modulation" is not likely to be seen using an east-west backscatter path when smaller antennas are

used. For example, over the Pacific-Ocean path the use of a 4 deg -6 dB beamwidth renders the polarization modulation undetectable.

VII. CONCLUSION

It will be recalled that the purpose of the research described herein was to investigate a new type of periodic modulation on backscatter echoes from the sea. This modulation first appeared on swept-frequency backscatter data of which Figs. 17-24 are typical. The purpose has been fulfilled as follows:

A. SUMMARY OF RESULTS

A brief history of general backscatter research was given, then the topic was narrowed down to the consideration of sea backscatter alone.

In particular, it was noted that the sea possesses a "resonant" scattering behavior, whereby the sea-wave components (in the continuous sea-energy spectrum) whose crests are spaced by half the radio wavelength usually do most of the backscattering. In view of this, and because the energy in these sea waves "saturates" at moderately low wind speeds (10 - 15 knots), the sea's cross section per unit area should be much more continuous than the land's, versus range and azimuth from the sounder. On the basis of these observations, a theory was developed by others which predicts that the sea's backscatter cross section per unit area should be primarily vertically polarized at elevation angles below 30 deg. This theory agrees with previous experimental measurements at both HF and microwave frequencies, but more HF measurements of the magnitude and polarization dependence of the sea-backscatter cross section are clearly needed. Using the 2.5 km receiving array and the SFCW waveform described herein, one can achieve areas of illumination more highly resolved than ever before. Hence, it is possible to isolate and

study new features of sea backscatter. The first evidence of this came when, during routine recordings of sea backscatter during the fall and winter months, it was found that the more highly-resolved data revealed a new type of modulation--periodic in time-delay and frequency--which usually resembled thumbprints on the time-delay-frequency plots. Superficially-similar lines had been seen on backscatter data before, but these already had been explained as resulting from ionospheric focusing. The "thumbprint" lines were decidedly different from "focusing" lines, and moreover, the former were seen only in sea backscatter, while the latter are seen also over the land. Muldrew [Ref. 32] suggested that large swells at sea could produce backscatter enhancements which also appear as lines on swept-frequency data. Such lines were seen using comparatively broad-beamed antennas, and Muldrew decided that an ionospheric mechanism could not have produced them. It seems rather that the sea's typical behavior is to be more continuous in backscatter amplitude, and that the "thumbprint" type of backscatter modulation was decidedly due to an ionospheric phenomenon. The only reasonable hypothesis was that magnetoionic splitting in the ionosphere produced a polarization-rotation modulation on the received backscatter signals, and that the continuity of the sea cross section polarization dependence was responsible for making the lines visible only over the sea.

This hypothesis was interpreted by writing the expressions for the phase paths of the various ordinary (o) and extraordinary (x) modes which could travel from the transmitter to the scatterer and combine at the receiving antenna. Simple trigonometric expressions which described the way in which the rotation of polarization can modulate sea-backscatter amplitude were then derived. The expressions were first listed for the general, bistatic geometry, assuming different polarization states for the transmitter, the sea, and the receiver. Later, the expressions were simplified greatly by assuming a monostatic sounder. Then, using

an approximate computer raytracing technique and representative ionospheric models, synthetic backscatter records were constructed which showed (approximately) the expected characteristics of what is termed "polarization modulation". The predicted thumbprint lines agreed very well with those observed experimentally, which lends some credence to the mathematical theory. It is concluded further, that the inability to detect polarization modulation during the summer is due to its more sensitive dependence upon frequency, time delay, and azimuth during that season. In general, since the theoretical expressions for received voltage contain sines, cosines and constants, these expressions can be adapted to explain the continuity and periodic behavior of the thumbprint lines on the basis of polarization rotation.

Conclusive proof of the above theory was established experimentally by changing the transmitted polarization while successive backscatter records were recorded. Figure 39 shows that when the transmitter polarization is switched from "vertical" to "circular" a distinct change in the "polarization modulation" occurs. It is usually seen that for "circular" polarization the thumbprint lines are more blurred. The data of Fig. 41 represent the clearest evidence that the new type of backscatter modulation is caused by polarization rotation. The shift in the periodicity and "phase" of the enhancements were correlated with the theory. It was concluded that the sea-backscattering cross section was not polarization-independent, but rather it was linearly polarized, as predicted by its most up-to-date model (Chapter II). Because of the complexity of the theory for the bistatic sounder geometry, however, it was not possible to verify a unique expression for received voltage changes as a function of transmit polarization.

By virtue of the results shown in both Fig. 41 and Fig. 42, it was concluded that the variation in backscatter amplitude can easily be as much as 10 dB, as predicted theoretically. This also shows that the

quasi-longitudinal (QL) approximation (Chapter V) holds much of the time, for waves entering and exiting the ionosphere. This was also predicted on the basis of the model.

It was also shown that the ability to detect "polarization modulation" over the east-west Pacific-Ocean path depends on the effective antenna beamwidth of the sounder. For the Los Baños array and single LPA combination, the -6 dB beamwidth of the former is appropriate to use as the "equivalent" beamwidth. As Fig. 43 dramatically illustrates, when this equivalent beamwidth is broadened from 1/2 to 4 degrees the polarization modulation is undetectable. The azimuth-scanned fixed-frequency backscatter of Fig. 44--and its theortical counterpart, Fig. 34--explain this beamwidth dependence very well. In fact, a beamwidth of 2 deg is not likely to be sufficient to resolve polarization modulation over the east-west backscatter path. Previous backscatter sounders have achieved frequency bandwidths and pulse lengths as narrow as those described herein, but the narrow-beamwidth capability of the Los Baños receiving array has yet to be achieved elsewhere. The azimuthal-dependence of polarization rotation therefore probably explains why polarization modulation on sea-backscatter amplitude has not been positively identified in previous work.

B. APPLICATION OF RESULTS

The results just described should be applicable to future backscatter studies using high azimuthal resolution in the following ways:

(1) Once identified, polarization modulation could be controlled by (a) changing the transmitted polarization, (b) allowing time to progress (if conditions are suitable), or (c) changing the radio frequency. If desired, this modulation could be eliminated entirely by using circularly-polarized transmitting and receiving antennas.

(2) Since the character of the modulation is a function of the polarization dependence of the sea backscatter, and since this dependence could change slightly with sea-state changes--more so when the first-order sea doppler is filtered out--one might be able to detect changes in the polarization dependence of the sea-backscattering cross section per unit area. This factor should be correlated with storm activity at sea.

(3) It is clear that the measurement of changes in sea state at a distance using high resolution, must be able to account for polarization modulation--since this effect tends to alter the otherwise smoothly varying amplitude of sea backscatter with slant range, azimuth, and frequency.

(4) The fact that polarization modulation may be predicted to first order using computer raytracing, means that variations in ionospheric structure (e.g., the shape of the profile) may be studied by the way in which they affect the modulation. This information could then be used to interpret ionospheric structure from the experimental backscatter data. Furthermore, the polarization modulation line structure may be predicted for any part of the world. (It is clear, however, that more accurate computer programs should be developed.)

C. RECOMMENDATIONS FOR FUTURE WORK

(1) Determine the allowable frequency bandwidth and range resolutions for detecting polarization rotation. How does this bandwidth change as the minimum time delay over the backscatter path is approached?

(2) Record the polarization-rotation amplitude modulation on sea backscatter at night.

(3) Measure the polarization dependence of the sea's HF backscattering cross section per unit area, versus the sea state.

(4) Study the effect of sea state on polarization modulation. If possible, filter out the first-order Doppler components of the sea's backscatter.

(5) Consider what happens to the polarization-modulation lines when the polarization dependence of the sea's backscattering cross section is well defined, but not linear.

(6) Consider the behavior of polarization modulation when the o and x modes are unequally attenuated or are not circularly polarized.

(7) Investigate the effect of ionospheric irregularities on the structure of polarization-modulation lines. For example, record such data during the generation of ionospheric turbulence by a solar flare.

(8) Develop a more accurate method for predicting polarization modulation using computer raytracing.

(9) Investigate the behavior of polarization modulation when sounding along a north-south backscatter path.

APPENDICES

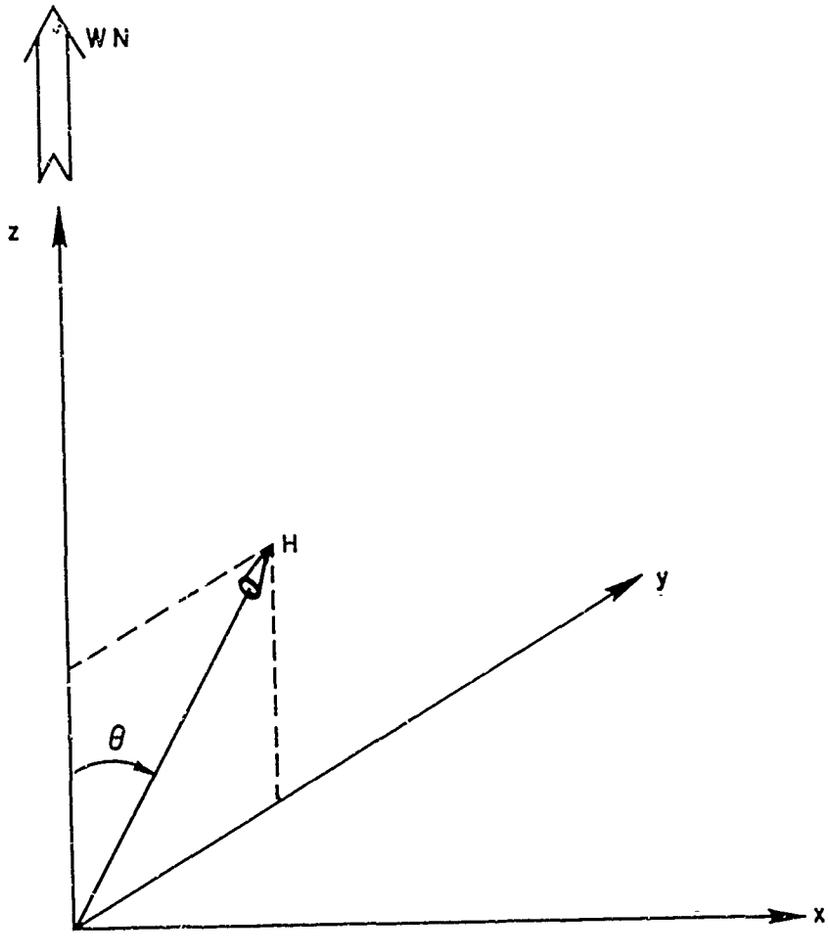

Figure 45. Coordinate system for the Appleton equations.

Appendix A

THE POLARIZATION OF THE MAGNETOIONIC COMPONENTS AND FARADAY ROTATION

In recent years, the concept of "total" or accumulated" Faraday rotation has been used to define polarization measurements on signals transmitted from satellites to the ground. For HF oblique propagation, this concept can lead to confusion. Therefore, after reviewing the basic Appleton equations [after Ratcliffe, Ref. 68], an unambiguous definition of polarization rotation will be derived herein. This groundwork is absolutely necessary for the proper development of the theories regarding "polarization modulation" on sea backscatter amplitude.

A. THE BASIC EQUATIONS FOR POLARIZATION AND REFRACTIVE INDEX

Assuming that the ionosphere is homogeneous, slowly varying, and stable, ray theory [Ref. 68] may be used, and the expressions for wave polarization R, and refractive index μ, may be written explicitly. After Ratcliffe, the coordinate system shown in Fig. 45 is employed.

The z axis is always aligned with the wave normal (WN), in the direction of phase propagation. The earth's magnetic field intensity, H, lies in the y-z plane, such that its longitudinal component lies in the z direction, and its tangential component in the y direction. From Ratcliffe, the complete expression for the polarization, R, of the characteristic waves is

$$R = \frac{E_x}{E_y} = \frac{-i}{Y_L}\left\{\frac{\frac{1}{2}Y_T^2}{1 - X - iZ} \mp \left[\frac{\frac{1}{4}Y_T^4}{(1 - X - iZ)^2} + Y_L^2\right]^{\frac{1}{2}}\right\}. \qquad (A1)$$

This expression describes two elliptical waves whose electric field components in the x and y direction, E_x and E_y respectively, have a relative amplitude and phase determined by R.

The quantity "X" is equal to ω_N^2/ω^2, where $\omega = 2\pi f$, the radio-frequency in radians/sec, and ω_N is the "plasma frequency"; ω_N^2 is equal to $(2\pi)^2\ 8.061(10)^7 N$, where N is the local electron density in electrons/m^3 Thus

$$X = \frac{80.61N(10)^{-6}}{f_M^2} \quad , \tag{A2}$$

where f_M is the frequency in MHz. It was always true that $\omega > \omega_N$ in the author's work, so that $X > 1$, and usually $X \gg 1$.

The quantity "Z" is equal to ν/ω where ν is the frequency of collision of electrons with heavy particles. Budden [Ref. 57] indicates that $\nu \leq 10^5$. Also, using formulas for ν given by Ratcliff [Ref. 68] Z is found to be less than 10^{-2} in the HF band (3-30 MHz), in the E layer, and less than 10^{-5} in the F layers. Clearly then, $Z \ll 1$. Finally, since it was usually true that $X \ll 1$, $Z \ll (1 - X)$ at HF, so that Z can be neglected.

Defining $\omega_H = \mu_o |e|H/m$ to be the "angular gyro-frequency," then $Y_L = -\cos\theta\omega_H/\omega$, and $Y_T = -\sin\theta\omega_H/\omega$, where, from Fig. 45, θ is the angle between the WN and B_o. Using the values for the μ_o, and e/m for an electron, [Ref. 56], $\omega_H = 3.52(10)^4 H(2\pi)$, so that

$$Y_L = -\cos\theta\ \frac{0.0352\ H}{f_M} \quad ,$$

$$Y_T = -\sin\theta\ \frac{0.0352\ H}{f_M} \quad . \tag{A3}$$

The refractive index, μ, of the ionosphere [Ref. 68] is given by:

$$\mu^2 = 1 - \frac{X}{(1 - iY_L R)} \quad . \tag{A4}$$

When one neglects the earth's magnetic field, $Y_L = 0$, so that μ_N (no field) is given by

$$\mu_N^2 = 1 - X \quad \text{(no field)} \quad . \tag{A5}$$

B. THE INTERPRETATION OF R AND μ

Using Eqs. (A1) and (A3), denoting R_u and R_ℓ as those when the upper and lower sign are taken in R, and noting that $R_u R_\ell = 1$, we can write

$$R_u = \frac{-i \cos\theta}{\left[\frac{Y_T^2 \sin^2\theta}{4(1 - X)^2} + \cos^2\theta\right]^{\frac{1}{2}} + \frac{|Y_T \sin\theta|}{2(1 - X)}} \quad , \tag{A6}$$

$$R_\ell = \frac{1}{R_u} \quad .$$

It is noted that $|R_u| \leq |R_\ell|$, and since $(1 - X)$ is always positive, the denominator of R_u is always positive, so that the sign of R_u is determined solely by the value of θ. Since the phase of R_u and R_ℓ is ± 90 deg, the ellipse traced by each wave will have its major axis aligned with the x or y axis, depending upon which R is greater. Accordingly, the two ellipses are perpendicular. It is also seen that $|R_u|$ determines the ellipticity (or axis ratio) of the two waves.

1. Defining the "o" and "x" Waves

Referring to Eq. (A4) we can rewrite the expression for μ as μ_u and μ_ℓ, corresponding to the upper and lower signs in R, as

$$\mu_u^2 = 1 - \frac{X}{1 + |Y_L R_u|}$$

$$\mu_\ell^2 = 1 - \frac{X}{1 - |Y_L / R_u|} \quad . \tag{A7}$$

Since it is true that $|R_u| \leq 1$, μ_ℓ deviates further from μ_N (no field) than does μ_u. Accordingly, it has become the convention to denote $R_o = R_u$ for the "ordinary" (o) wave, and $R_x = R_\ell$ for the "extraordinary" (x) wave. Likewise, $\mu_o = \mu_u$ and $\mu_x = \mu_\ell$. It is then seen from Fig. 45 that, since $|R_u| \leq 1$, $|E_x|_o \leq |E_y|_o$, hence the major axis of the "o" ellipse is on the y axis--most nearly aligned with the H field. Likewise, the "x" ellipse major axis is aligned with the x-axis, perpendicular to the field--hence acted on more so by it. Finally, since $|Y_L| \ll 1$ for the frequencies used by the author, $\mu_o \geq \mu_x$.

These two characteristic waves (o and x) will be generated when a linear wave goes into the ionosphere, and will propagate independent of one another unless mode coupling occurs. Since we can neglect collisions ($Z = 0$), and since $X \ll 1$ mode coupling can only occur if a ray strikes an irregularity in the ionosphere; this effect is assumed to be small, thus negligible.

2. The Direction of Rotation

The direction of rotation of the o and x waves are determined by the sign of R_o and R_x. After referring to Fig. 45, i $0 \geq \theta \geq 90^\circ$, so that the sign of R_o is minus, then since $R = E_x/E_y$, the o wave will rotate counterclockwise (CCW) when viewed from behind the wave (in the z direction). It then follows that the x wave will rotate clockwise (CW). When $90 \geq \theta \geq 180^\circ$, the direction of rotation is reversed.

B. THE "QL" APPROXIMATION

It is often true that a considerable simplification in the expressions for R and μ can be made by assuming that

$$(QL) \quad \frac{Y_T^4}{4Y_L^2} \ll |1 - X|^2 \quad . \tag{A8}$$

This is called the "quasi-longitudinal" (QL) approximation. Using Eqs. (A2) and (A3), assuming that $X \ll 1$, and letting $H = H_o = 25$, it is calculated that the QL approximation is valid over the following ranges of θ:

$$(QL)\ \theta \text{ within } \left\{\begin{matrix} \pm 63.5^\circ \\ \pm 80.7^\circ \\ \pm 86.8^\circ \end{matrix}\right\} \text{ from } 0^\circ \text{ or } 180^\circ \text{ at } \left\{\begin{matrix} 3 \text{ MHz} \\ 10 \text{ MHz} \\ 30 \text{ MHz} \end{matrix}\right\} \quad . \tag{A9}$$

Clearly, the QL approximation will be valid over most ray paths--except those along the magnetic equator (which were not invclved in the author's work). The polarization and direction of rotation then become

$$R_o \cong \frac{-i \cos\theta}{|\cos\theta|} \quad ,$$

(QL) (A10)

$$R_x \cong -R_o \quad ,$$

$$\text{Direction of Rotation} = \left\{ \begin{matrix} \text{CW} \\ \text{CCW} \end{matrix} \right\} \text{ if } R = \left\{ \begin{matrix} +i \\ -i \end{matrix} \right\} ,$$

and the proper sign of $R_{o,x}$ is preserved. Hence $R \approx \pm i$, and the characteristic waves are circularly polarized. Then, for the two characteristic waves, Eq. (A4) becomes

$$\mu_o^2 = 1 - \frac{X}{1 + |Y_L|} \text{ (ordinary)} \quad ,$$

(QL) (A11)

$$\mu_x^2 = 1 - \frac{X}{1 - |Y_L|} \text{ (extraordinary)} \quad .$$

These expressions and mode identifications also agree with Ratcliffe [Ref. 68].

Since $X \ll 1$, and $|Y_L| \ll 1$, it is again concluded that $\mu_o \geq \mu_x$, but that the direction of rotation of the o and x modes will change when the sign of $\cos\theta$ changes.

C. FARADAY ROTATION

When a radio wave enters the ionosphere and splits into the o and x waves, each of these components will accumulate a different phase while it propagates enroute to a receiving point or scattering region. When the time delay of the two modes is not resolved (using long pulses and/or large scattering surfaces), the addition of the energy propagated by the two paths will determine a resultant polarization. The ellipticity and orientation of this polarization is determined by the relative magnitude and phase of the o and x modes, and by $|R|$ which defines the ellipticity of the two wave components.

The relative magnitude of the two components is determined by propagation losses and the exciting polarization. For the present it is assumed that the o and x components have equal amplitude. It is also assumed that the o and x modes will come down out of ionosphere circularly polarized; or, equivalently, that the QL approximation holds at the bottom of the ionosphere.

The phase accumulated by each mode can be determined by integrating its refractive index over the actual path followed by the wave energy. When $X \ll 1$, the wave normal and direction of propagation are the same, so that [Refs. 56,57]

$$P_o = \int_{o\ path} \mu_o ds \quad ,$$

$$P_x = \int_{x\ path} \mu_x ds \quad , \tag{A12}$$

where P_o and P_x are the phase paths of the o and x modes, respectively. In principle, the o path and x path are not equal, so that the integrals are separate. Moreover, these paths can be determined by constraining the ground distance to be the same (as in point-to-point communication),

or by constraining the time delay of the modes to be equal; the latter case has application to backscatter. Thus, the phase between the o and x modes is equal to

$$\pm \frac{2\pi}{\lambda_o}\left[P_o - P_x\right] \quad , \tag{A13}$$

where λ_o is the free-space radio wavelength.

When the two equal-amplitude circular waves are added a linear resultant will be produced. The angle, Ω_i by which this resultant deviates from transmitted polarization reference is given by [Refs. 44, 56]

$$\begin{aligned} |\Omega_i| &= \frac{1}{2}|(\text{Phase difference})| \\ &= \frac{\pi}{\lambda_o}|P_o - P_x| \quad , \end{aligned} \tag{A14}$$

where the subscript "i" emphasized that this is denoted the instantaneous value of Faraday rotation. The absolute value signs are present to avoid confusion over the sign of $(P_o - P_x)$, since one must examine this sign and the sign of R_o, in order to determine whether Ω_i is a CW or CCW angle (looking in the z direction). Often, it is sufficient to know only $|\Omega_i|$, but for others, it is not. For the latter, the following rules apply:

1. If $(P_o - P_x)$ is positive, the o mode experiences a phase lag, so that $\Delta\Omega_i$ is in the direction in which x mode is rotating.
2. Likewise, if $(P_o - P_x)$ is negative, $\Delta\Omega_i$ is in the direction that the o mode is rotating.

These rules may be summed up by the following expression:

$$\Omega_i = \frac{\pi}{\lambda_o}(P_o - P_x)\left[\text{sign}\,(R_x)\right]_{EXIT} \begin{cases} > 0 \Rightarrow \text{CW} \\ < 0 \Rightarrow \text{CCW} \end{cases} \tag{A15}$$

$$= \frac{\pi}{\lambda_o}(P_o - P_x)\left[\frac{R_x}{i|R_x|}\right]_{EXIT} ,$$

where the sign of (R_x) exiting the ionosphere is given by

$$\left[R_x/i|R_x|\right]_{EXIT} .$$

This final result is completely general, and makes no assumptions about the ionosphere except that if P_o and P_x are found using Eq. (A12), then it must be true the $X \ll 1$ is satisfied. Also, if $Z = 0$, then sign (R_x) = sign $(\cos\theta)$.

In the event that the downcoming waves are not circularly polarized, it is still true that each may be broken down into a sum of a linear plus a circular wave, and that the circular components of each wave will add to produce a Faraday-rotated resultant, according to Eq. (A15). It is found, however, that the downcoming waves appear to be very nearly circular most of the time.

Appendix B

THE SIGN OF "$P_o - P_x$"

The purpose of this section is to show that the difference between o and x phase paths, $P_o - P_x$, is greater than zero when the time delay of the o and x modes is equal, and when the two modes travel through nearly identical ionospheres, in nearly the same direction.

The derivative of the phase path, P, of a characteristic mode with respect to distance along the path, s, is given by [Refs. 56, 57]

$$\frac{dP}{ds} = \mu \cos \alpha \quad , \tag{B1}$$

where $\cos \alpha$ becomes significantly different than 1 when $\mu \ll 1$. The "group path," P', is proportional to time delay, and its derivative is given by

$$\frac{dP'}{ds} = \frac{d(\omega\mu)}{d\omega} \cos \alpha \quad . \tag{B2}$$

If it can be shown that

$$\frac{dP_o}{ds} - \frac{dP'_o}{ds} > \frac{dP_x}{ds} - \frac{dP'_x}{ds} \quad , \tag{B3}$$

then it will be true that the accumulated ratio of phase path to group path will be greater for the o mode. Thus, when the time delays (group paths) of the two modes are equal, it will be true that $P_o - P_x > 0$.

Proceeding,

$$\frac{d(\omega\mu)}{d\omega} = \mu + \frac{\omega d\mu}{d\omega} \quad ; \tag{B4}$$

so we must show that

$$\frac{d\mu_x}{d\omega} > \frac{d\mu_o}{d\omega} \quad . \tag{B5}$$

The complete expression for μ, assuming that collisions are negligible ($Z = 0$), is given by [Ref. 68]:

$$\mu^2 = 1 - \frac{X}{1 - \frac{Y_T^2}{2(1 - X)} \pm \left[\frac{Y_T^4}{4(1 - X)^2} + Y_L^2\right]^{1/2}} \quad , \tag{B6}$$

where the symbols are defined elsewhere.

Let

$$D = D_1 \pm D_2 \quad ,$$

$$D_1 = 1 - \frac{Y_T^2}{2(1 - X)} \quad , \tag{B7}$$

$$D_2 = \left[\frac{Y_T^4}{4(1 - X)^2} + Y_L^2\right]^{1/2} \quad .$$

The upper (+) sign represents the "o" mode, and the lower (-) sign, the "x" mode, since X, Y_T, $Y_L < 1$. It is then found that

$$\frac{d\mu}{d\omega} = \frac{X}{2D\mu^2}\left[\frac{2D}{\omega} + \frac{dD}{d\omega}\right] \tag{B8}$$

and that

$$\frac{dD}{d\omega} = \frac{1}{\omega}\left[\frac{Y_T^2}{(1-X)^2} \mp \frac{1}{2D_2}\left(\frac{Y_T^4}{(1-X)^3} + 2Y_L^2\right)\right] \quad ; \tag{B9}$$

and finally,

$$\frac{d\mu}{d\omega} = \frac{X}{\omega\mu(D_1 \pm D_2)^2}\left\{1 + \frac{Y_T^2 X}{2(1-X)^2} \pm D_2 \mp \frac{1}{D_2}\left[\frac{Y_T^4}{4(1-X)^3} + \frac{Y_L^2}{2}\right]\right\} \quad , \tag{B10}$$

where the upper sign is taken for the "o" mode, the lower for the "X" mode.

We assume that X, Y_T, and Y_L are nearly the same for the two modes, and it is noted that $\mu_o > \mu_x$ and that $(D_1 - D_2) < (D_1 + D_2)$; thus to satisfy Eq. (B5) it is sufficient to show that

$$\frac{1}{D_1 - D_2}\{"x"\} - \frac{1}{D_1 + D_2}\{"o"\} > 0 \quad , \tag{B11}$$

where the brackets are those defined by Eq. (B10). After more algebra, Eq. (B11) becomes

$$\frac{2}{D_1^2 - D_2^2}\left[D_1(D_2 - K) + D_2(1 + L)\right] > 0 \quad ,$$

where

$$K = \frac{1}{D_2}\left[\frac{Y_T^4}{4(1-X)^3} + \frac{Y_L^2}{2}\right] \quad , \tag{B12}$$

and

$$L = \frac{Y_T^2 X}{(1-X)^2} \quad ,$$

which becomes

$$\frac{2}{D_2\left(D_1^2 - D_2^2\right)}\left[\frac{3Y_L^2}{2} - \frac{Y_L^2 Y_T^2(1 - 3X)}{4(1 - X)} + \frac{Y_T^4(1 - 2X)}{4(1 - X)^3} + \frac{Y_T^6 X}{4(1 - X)^4}\right] > 0 \quad . \text{(B13)}$$

But $D_2 > 0$, and

$$D_1^2 - D_2^2 = 1 - \frac{Y_T^2 + Y_L^2(1 - X)}{(1 - X)} \quad . \text{(B14)}$$

This expression is greater than zero for $X < (1 - Y^2)$, as assumed for HF oblique propagation. Furthermore, since Y_T^2, $Y_L^2 \ll 1$, and for $X < 0.5$, it will be true that

$$\frac{3Y_L^2}{2} \gg \frac{Y_L^2 Y_T^2(1 - 3X)}{4(1 - X)} \quad , \text{(B15)}$$

so that Eq. (B13) does hold.

Therefore, it is concluded that $P_o > P_x$, when $P_o' = P_x'$, and when the two modes travel through nearly the same ionosphere (as from an antenna to the sea). This was shown for $X < 0.5$. Since $\mu_o > \mu_x$, it will be true that $P_o > P_x$ for larger X, but to show this requires more work. For the frequencies normally used by the author, however, it was always true that $X < 0.5$.

Appendix C

THE EVALUATION OF "EQUIVALENT BEAMWIDTH"

A. PURPOSE

It is known that polarization rotation is a function of azimuth from the receiving antenna. In order to be able to detect "polarization modulation" on sea-backscatter amplitude, it was suggested in Chapter V that it is necessary that this variation with azimuth be small across the receiving antenna's main beam. The purpose of this Appendix is to evaluate the "equivalent beamwidth," $\Delta\varphi_e$, which is defined by

$$\Delta\varphi_e = \frac{1}{[G_r G_t(\max)]} \int_0^{360^\circ} G_r G_t d\varphi \quad , \tag{C1}$$

where G_r and G_t are the receiving and transmitting antenna gains as functions of the azimuth from the receiving antenna (φ). It is shown later in Chapter V that the polarization rotation with azimuth should be small compared to $\Delta\varphi_e$.

B. CALCULATION

For the Stanford system, G_r is that given for the wide aperture receiving array (Chapter III), and G_t is that for a single LPA. The computation to be described here assumes that the LPA is vertically polarized (as it was for most of the experimental data). Using Jasik's equations [Ref. 89], a known beamwidth of 125 deg, and a front-to-back ratio (F/B) of 15 dB, G_t may be expressed by

$$G_t = \begin{cases} 0.0316\ (-15\ \text{dB});\ 36^\circ \le \varphi' \le 144^\circ \\ \cos^n\left[\dfrac{\varphi' - 270^\circ}{2}\right];\ \text{elsewhere} \\ n = 4.410\ , \end{cases} \qquad \text{(C2)}$$

where φ' is the azimuth from the backscattering point to the transmitter.

A simplified sketch of the geometry is shown in Fig. 46. The field sites are separated by d_o = 185.64 km, and for the integration, the total (round-trip) range between the receiver, scatterer, and transmitter was constant at 5340 km (which is a value that happens to apply directly to another problem). The problem of finding φ' cannot be solved in closed form, since the ground range and elevation angle to the scattering point are not known for all φ. This can be solved by trial and error on the computer, but since over 2200 sets of calculations are necessary for each pattern integration, the computer costs would then be prohibitively large. Therefore, for the purpose of calculating θ and φ' it was assumed that the elevation angle was constant at 5 deg. Since this value is small, without too much error the planar geometry of Fig. 46 can be used to calculate φ' from φ. Proceeding, we can use trigonometric identities to express φ' as follows:

$$\varphi' = 2 \tan^{-1}\left[\frac{K_o \cos \alpha}{\sin \alpha}\right] - (180^\circ - 151.1^\circ) \ ,$$

where

$$K_o = \frac{5340 - d_o}{5340 + d_o} \qquad \text{(C3)}$$

and $$\alpha = \frac{151.1^\circ - \varphi}{2} \ .$$

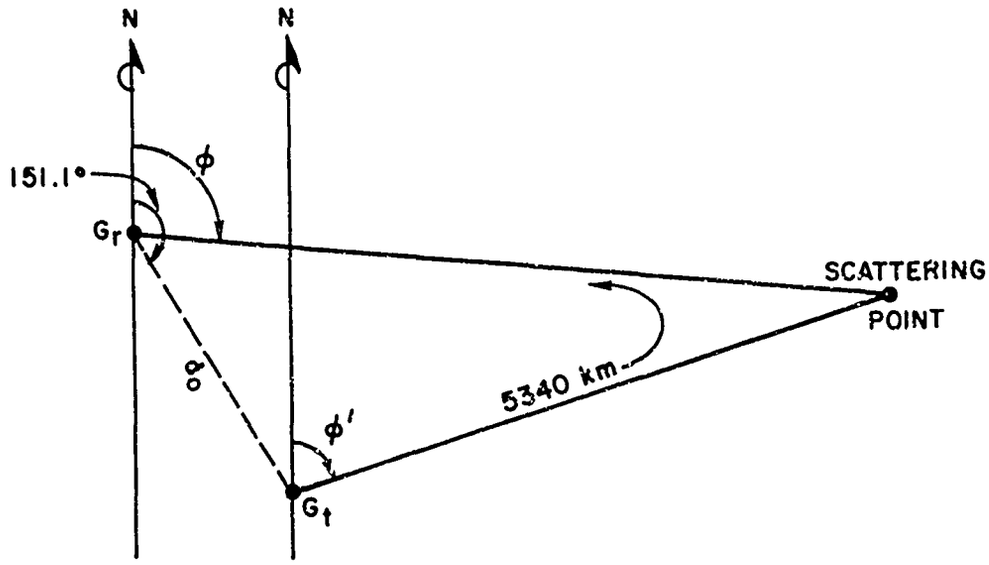

Figure 46. Simplified planar geometry used to evaluate the transmitter azimuth (φ') from the receiver azimuth (φ), in order to integrate the gain product, $G_r G_t$, versus φ.

The expressions in Eqs. (C2) and (C3), and those for G_r were programmed on a digital computer to evaluate Eq. (C1). A radio frequency of 22.35 MHz was assumed (which also applies directly to another problem, thus saving computer time). The output is plotted in Fig. 47, where I represents the accumulated value of the normalized integral of Eq. (C1) as φ increases. The azimuth scale is greatly expanded through the regions of the major beams of G_r in the forward and backward directions. The final value of I at φ = 360 deg equals $\Delta\varphi_e$. The -3 dB, the -6 dB, and the null-to-null beamwidths of G_r are shown for reference. Front-to-back ratios of 15 and 10 dB were computed for comparison and to account for the possibility of unequal ionospheric absorption between east and west. The accuracy of the computer integration procedure is ± 3 percent.

These results show that the -6 dB beamwidth of the receiving array is appropriate to use as $\Delta\varphi_e$. Furthermore, the contributions to the integral via the main lobe of G_r versus those from all other azimuths may be computed from Fig. 47 as follows: The amount outside the null-to null beamwidth is down by 13.3 dB, and outside $\Delta\varphi_e$ it is down 8.3 dB, for the 15 dB F/B. The corresponding values for the 10 dB F/B are 9.4 and 7.6 dB.

It is found by other authors [Refs. 41,86] that when the same antenna is used for both transmitting and receiving in a radar system, the -3 dB beamwidth of this antenna is appropriate to use as $\Delta\varphi_e$. Moreover, this result is independent of the radio frequency. It is interesting that this value would therefore be obtained if $G_r^2 d\varphi$ were integrated (assuming a 15 dB F/B or so), rather than $G_r G_t d\varphi$. Since G_t does not appreciably change with frequency (as assumed), it is likely that the result for $\Delta\varphi_e$ obtained here does not change with frequency--such that the -6 dB beamwidth of G_r always defines it properly. The value of the

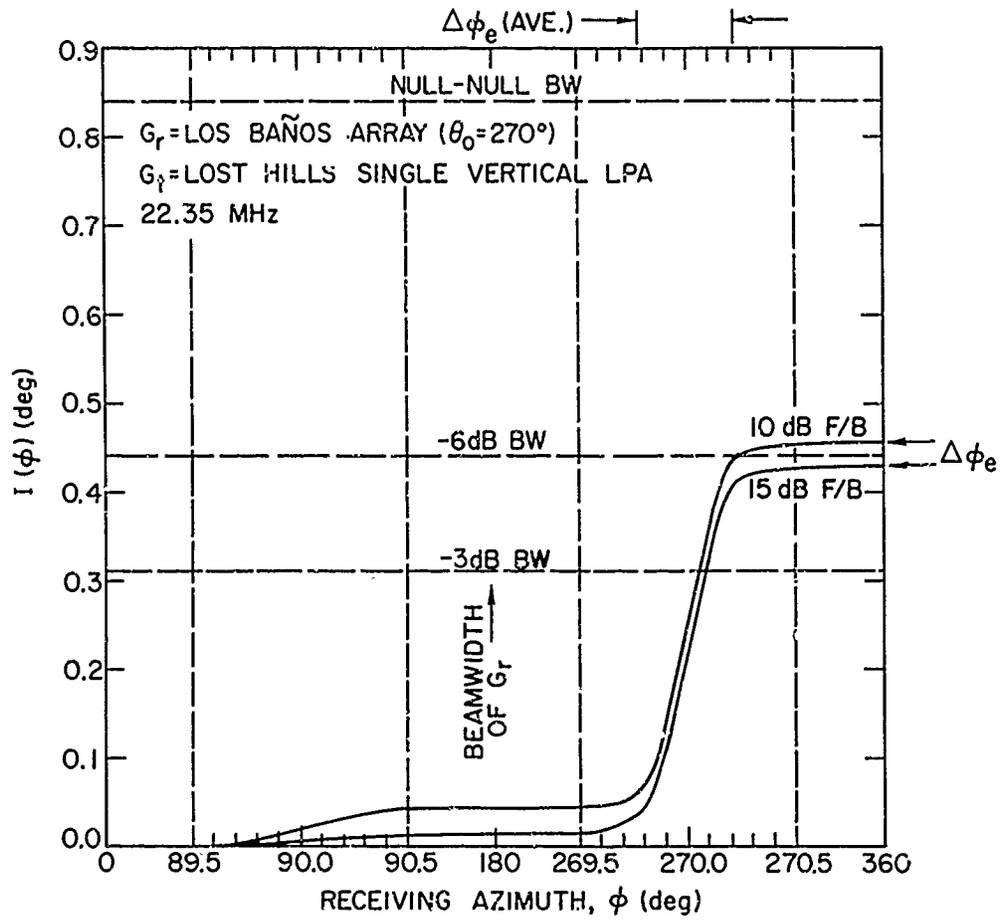

Figure 47. Plot of the accumulated value of the normalized integral (I) of $G_r G_t d\varphi$ versus receiving azimuth φ. The final value at φ = 360 deg defines the equivalent beamwidth, $\Delta\varphi_e$. Front-to-back ratios of 10 and 15 dB were assumed for the single vertical LPA defining G_t.

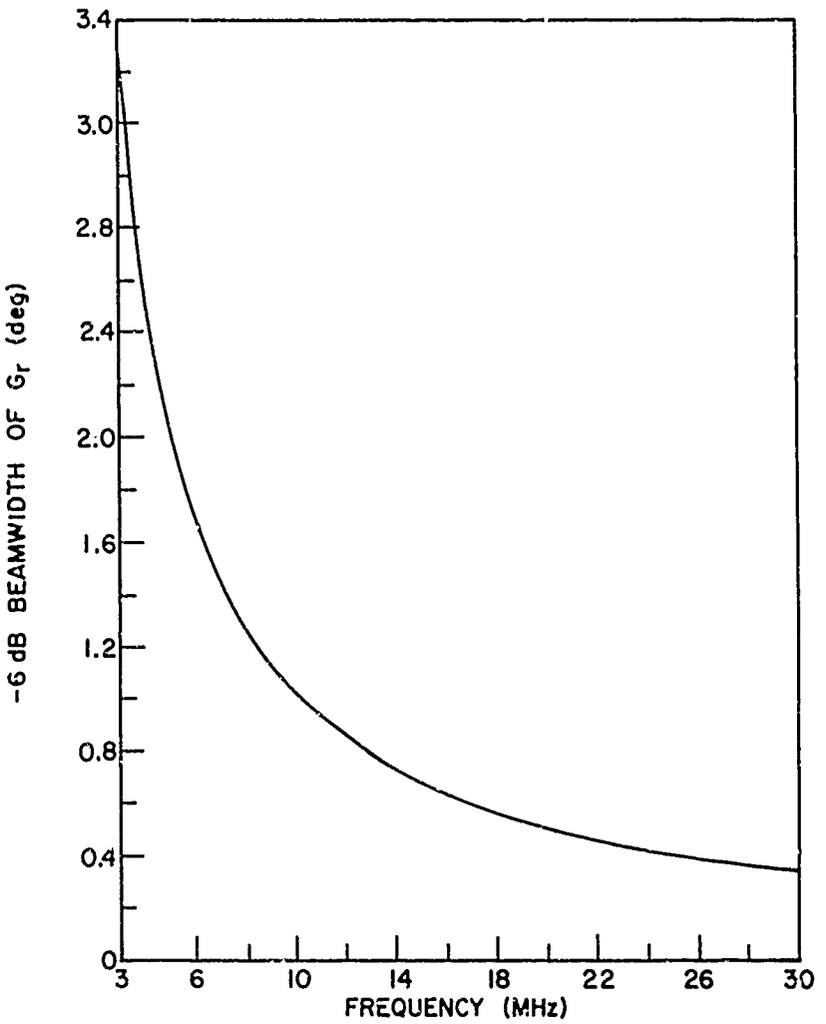

Figure 48. Plot of the -6 dB beamwidth of the Los Baños receiving array versus frequency. This beamwidth is approximately equal to $\Delta\varphi_e$.

-6 dB beamwidth will, of course, change with frequency, and this is plotted in Fig. 48 for the Los Baños receiving array. As a consequence of the above calculation and assumptions, the plot in Fig. 48 also defines the value of $\Delta\varphi_e$ with frequency.

REFERENCES

1. G. Breit and M. A. Tuve, "A Test of the Existence of the Conducting Layer," Phys. Rev., 28, Sep 1926, pp. 554-573.

2. G. W. Gardner, "Origin of the Term Ionosphere." Nature, 224, Dec 13, 1969, p. 1096.

3. T. L. Eckersley, "Short Wave Wireless Telegraphy," J. Inst. Elect. Engrs., 65, 1927, p. 600.

4. A. H. Taylor and L. C. Young, "Studies of High Frequency Radio Wave Propagation," Proc. IRE, 16, 1928, pp. 561-578.

5. A. H. Taylor and L. C. Young, "Studies of Echo Signals," Proc. IRE, 17, Sep 1929, pp. 1491-1507.

6. A. F. Wilkins and E.D.R. Shearman, "Back-Scatter Sounding: An Aid to Radio Propagation Studies," J. Brit. Instn. Radio Engrs., (London), 17, 1957, pp. 601-616.

7. A. M. Peterson, "The Mechanism of F-Layer Propagated Backscatter Echoes," J. Geo. Res., 56, Jun 1951, pp. 221-237.

8. W. Dieminger, "The Scattering of Radio Waves," Proc. Phys. Soc., B, 64, 1951, pp. 142-158.

9. W. G. Abel and L. C. Edwards, "The Source of Long-Distance Back-scatter," Proc. IRE, 39, Dec 1951, pp. 1538-1541.

10. O. G. Villard, Jr. and A. M. Peterson, "Scatter-Sounding: A Technique for Study of the Ionosphere at a Distance," IRE Trans., PGAP, 3, 1952, pp. 186-201

11. O. G. Villard, Jr. and A. M. Peterson, "Scatter-Sounding: A New Technique in Ionospheric Research," Science, 116, Aug 29, 1954, pp. 221-224.

12. C. G. McCue, "High Frequency Backscatter Observations at Salisbury, South Australia," Austral. J. Phy., 9, Dec 1956, pp. 454-470.

13. I. Ranzi and P. Dominici, "H. F. Backscatter From Land and Sea," Scientific Note 1, Centro Radioelectrico Sperimentale "G. Marconi," Rome, Italy, 1959.

14. I. Ranzi, "Radiocommunication By Backscatter," Final Tech. Rept., Centro Radioelectrico Sperimentale "G. Marconi," Rome, Italy, 1962.

15. G. Hagn, "An Investigation of the Direct Backscatter of High-Frequency Radio Waves from Land, Sea Water, and Ice Surfaces," Final Rept. II, SRI Proj. 2909, Stanford Research Institute, Menlo Park, Calif., May 1962.

16. J. G. Steele, "Backscatter of Radio Waves from the Ground," Rept. SEL-65-064 (TR No. 109), Stanford Electronics Laboratories, Stanford, Calif., Jun 1965

17. J. G. Steele, "Backscatter of 16 Mc/S Radio Waves from Land and Sea," Austral. J. Phys., 18, Aug 1965, pp. 317-327.

18. T. W. Washburn, "Scattering Prominences in Ionospherically Reflected Ground Backscatter," report in progress, Stanford University, Stanford, Calif., 1970.

19. T. W. Washburn, "Characteristics of Single Echoes in HF Ground Backscatter," Submitted to Radio Science, 1970.

20. R. P. Ingalls and M. L. Stone, "Characteristics of Sea Clutter at HF," IRE Trans, AP-5, Jan 1957, pp. 164-165.

21. J. R. Barnum, "Measurement of Sea Cross Section per Unit Area Using a Calibrated Echoing Source," Rept. SEL-70-038 (TR No. 158) (to be published), Stanford Electronics Laboratories, Stanford, Calif., 1970.

22. D. D. Crombie, "Doppler Spectrum of Sea Echo at 13.56 Mc/S," Nature, 175, Apr 1955, pp. 681-682.

23. E. P. Anderson, "Characteristics of Sea Reflections at 1.85 Mc," Final Report, June 15, 1953 to Sep 30, 1956, AFCRC-TR-56-190, Radio Propagation Laboratory, Stanford Electronics Laboratories, Stanford, Calif., 1956.

24. R. L. Dowden, "Short Range Echoes Observed on Ionospheric Recorders," J. Atm. Terr. Phy., 11, 1957, pp. 111-117.

25. I. Ranzi, "Doppler Frequency Shift of H.F. to S.H.F. Radio Waves Returned From the Sea," Tech. Note No. 6, Centro Radioelectrico Sperimentale "G. Marconi," Rome, Italy, 1961.

26. J. C. Blair et al, "H.F. Ionospheric Radar Ground-Scatter Map Showing Land-Sea Boundaries by a Spectral-Separation Technique," Elec. Letters, Feb 20, 1969.

27. L. H. Tveten, "Ionospherically Propagated Sea Scatter," Science, 157, Sep 15, 1967, pp. 1302-1304.

28. J. F. Ward, "Power Spectra from Ocean Movements Measured Remotely by Ionospheric Radio Backscatter," Nature, 223, Sep 27, 1969, pp. 1325-1330.

29. I. Ranzi, "Experiments on Backscatter of H.F. Radiowaves From Open and Coastal Sea," Scientific Note 3, Centro Radioelectrico Sperimentale "G. Marconi," Rome, Italy, 1961

30. W. C. Hoffman, "A Theoretical Model for High-Frequency Backscatter from the Sea Surface via the Ionosphere," J. Atm. Terr. Phy., 7, 1955, pp. 278-284.

31. B. Kinsman, Wind Waves, Their Generation and Propagation on the Ocean Surface, Prentice-Hall, Inc., New Jersey, 1965.

32. D. B. Muldrew, "Interference Patterns in HF Signals Backscattered From Ocean Waves," (contact author), Radio Physics Laboratory, Defense Research Telecommunications Establishment, Ottawa, Canada.

33. D.E. Barrick and W. H. Peake, "Scattering From Surfaces With Different Roughness Scales: Analysis and Interpretation," Rept. BAT-197A-10-3, Battelle Memorial Institute, Columbus Laboratories, Columbus, Ohio, Nov 1967.

34. D. E. Barrick and W. H. Peake, "A Review of Scattering From Surfaces With Different Roughness Scales," Radio Science, 3, Aug 1968, pp. 865-868.

35. W. H. Munk and W. A. Nierenberg, "HF Radar Sea Return and the Philips Saturation Constant," Nature, 224, Dec 27, 1969, p. 1285.

36. N. W. Guinard and J. C. Daley, "An Experimental Study of a Sea Clutter Model," Proc. IEEE, 58, Apr 1970, pp. 543-550.

37. J. W. Wright, "Backscatter From Capillary Waves, With Application to Sea Clutter," IEEE, Trans., AP-14, Nov 1966, pp. 749-754.

38. J. W. Wright, "A New Model for Sea Clutter," IEEE Trans., AP-16, Mar 1968, pp. 217-223.

39. R. C. Fenwick and O. G. Villard, Jr., "Continuous Recordings of the Frequency Variation of the WWV-20 Signal After Propagation Over a 4000-Km Path," J. Geo. Res., 65, Oct 1960, pp. 3249-3260.

40. R. A. Shepherd and J. B. Lomax, "Frequency Spread in Ionospheric Radio Propagation," IEEE Trans., COM-15, Apr 1967, pp. 268-275.

41. M. I. Skolnik, Introduction to Radar Systems, McGraw-Hill Book Co., Inc., New York, 1962.

42. R. B. Fenwick and G. H. Barry, "Generation of Accurate Frequency-Sweep Waveforms by Direct Synthesis," Rept. SEL-64-130 (TR No. 99), Stanford Electronics Laboratories, Stanford, Calif., Dec 1964.

43. R. B. Fenwick and G. H. Barry, Sweep-Frequency Oblique Ionospheric Sounding at Medium Frequencies," IEEE Trans., BC-12, Jun 1966, pp. 25-27.

44. M. R. Epstein, "Polarization of Ionospherically Propagated HF Radio Waves with Applications to Radio Communication," Radio Science, 4, Jan 1969, pp. 53-67.

45. M. R. Epstein, "Polarization of Ionospherically Propagated Waves," Rept. SEL-67-091 (TR No. 143), Stanford Electronics Laboratories, Stanford, Calif., Oct 1967.

46. L. E. Sweeney, Jr., "Experimental Measurements of Amplitude and Phase Distributions Across a 2.5 Km HF Array," URSI Spring Meeting, Washington, D.C., Apr 1968.

47. L. E. Sweeney, Jr., "Spatial Properties of Ionospheric Radio Propagation as Determined With Half-Degree Azimuthal Resolution," Rept. SEL-70-034 (TR No. 155), Stanford Electronics Laboratories, Stanford, Calif., Jun 1970.

48. R. B. Fenwick and J. M. Lomasney, "Test of a Monostatic FM-CW Vertical-Incidence Sounder," Rept. SEL-68-077 (TR No. 144), Stanford Electronics Laboratories, Stanford, Calif., Oct 1968.

49. T. W. Washburn, "High Resolution HF Ground Backscatter Observation," URSI Fall Meeting, Boston, Mass, Sep 1968.

50. T. A. Croft, "The Interpretation of HF Sweep-Frequency Backscatter Soundings to Deduce the Structure of Localized Ionospheric Anomalies," Rept. SEL-68-029 (TR No. 116), Stanford Electronics Laboratories, Stanford, Calif., Dec 1967.

51. T. A. Croft and T. W. Washburn, "Comparison of Simultaneous Forward and Backscatter Soudings to Verify a Proposed Focusing Mechanism of HF Sky Waves," J. Geo. Res., 74, May 1, 1969, pp. 2443-2446.

52. J. M. Lomasney et al, "Studies of Ionospheric Propagation Related to High-Frequency Radio Broadcasting," Rept. SEL-69-009 (TR No. IA-7), Stanford Electronics Laboratories, Stanford, Calif., Feb 1969.

53. Kraus, Antennas, McGraw-Hill Book Co., Inc., New York, 1950.

54. J. M. Lomasney and J. R. Barnum, "An HF Antenna for Oblique Propagation Having Approximately Circular Polarization Over Appreciable Frequency and Vertical Angle Intervals," Rept. TR-153, Stanford Electronics Laboratories, Stanford, Calif., Jun 1970.

55. J. R. Barnum, "Polarization Behavior of Orthogonal HF Log-Periodic Antennas at Low Elevation Angles," Rept. SEL-70-039 (TR No. 159) (to be published), Stanford Electronics Laboratories, Stanford, Calif., 1970.

56. K. Davies, Ionospheric Radio Propogation, NBS Mono. 80, Superintendent of Documents, U.S. Gov't. Printing Off., Washington, D.C., 1965.

57. K. G. Budden, Radio Waves in the Ionosphere, Cambridge University Press, Cambridge, England, 1961.

58. R. Silberstein, "Sweep Frequency Backscatter--Some Observations and Deductions," IRE Trans., AP-2, Apr 1954, pp. 56-63.

59. T. M. Georges and J. J. Stephenson, "HF Radar Signatures of Traveling Ionospheric Irregularities, 3D Ray-Tracing Simulation," Radio Science, 4, Aug 1969, pp. 679-696.

60. L. H. Tveten, "Ionospheric Motions Observed on High-Frequency Backscatter Soundings," (Abstract), IRE Trans., AP-4, Jan 1957, p. 150.

61. L. H. Tveten, "Ionospheric Motions Observed with High Frequency Backscatter Sounders," J. Res. Nat. Bur. Stds., 65D, Mar-Apr 1961, pp. 115-127.

62. B. Dueño, "Detection of Apparent Ionospheric Movements by Backscatter Techniques," Contract AF-19(604)-8342, U. of Puerto Rico Electrical Engineering Dept., Mayaguez, July 8, 1964.

63. R. D. Hunsucker and L. H. Tveten, "Large Traveling-Ionospheric-Disturbances Observed at Midlatitudes Utilizing the High Resolution H.F. Backscatter Technique," J. Atm. Terr. Phy., 29, 1967, pp. 909-916.

64. L. P. Bolgiano, "Some Characteristics of Multiple-Hop Sweep-Frequency Backscatter Observations Between 15 and 54 Mc/S," TR No. 17, Contract Nonr 225(33), Stanford Electronics Laboratories, Stanford, Calif., Oct 10, 1960.

65. C. R. Gilliland, "Sweep-Frequency Backscatter with Calibrated Amplitude," Rept. SEL-65-095 (TR No. 111), Stanford Electronics Laboratories, Stanford, Calif., Oct 1965.

66. T. A. Croft, "The Influence of Ionospheric Irregularities on Sweep-Frequency Backscatter," J. Atm. Terr, Phy., 30, 1968, pp. 1051-1063.

67. I. Ranzi, "Backscatter of H.F. Radio Waves From Coastal and Continental Ground Reliefs," Scientific Note 4, Centro Radioelectrico Sperimentale "G. Marconi," Rome, Italy, 1961.

68. J. A. Ratcliffe, The Magneto-ionic Theory and Its Applications to the Ionosphere, Cambridge University Press, Cambridge, England, 1962.

69. E. V. Appleton, U.R.S.I. Proc., Washington Assembly, 1927.

70. E. V. Appleton, "Wireless Studies of the Ionosphere," J. Inst. Elect. Engrs., 71, 1932, p. 642.

71. H. G. Booker, "Some General Properties of the Formulae of the Magneto-ionic Theory," Proc. Roy. Soc. A, 147, 1934, p. 352.

72. W. Snyder and R. A. Helliwell, "Universal Wave Polarization Chart for the Magneto-Ionic Theory," J. Geo. Res., 57, Mar 1952, pp. 73-84.

73. M. R. Epstein, "The Effects of Polarization Rotation and Phase Delay with Frequency on Ionospherically Propagated Signals," IEEE Trans., AP-16, Sep 1968, pp. 548-553.

74. T. L. Eckersley, "An Investigation of Short Waves," J. Inst. Elec. Engrs., 67, 1929, pp. 993-1032.

75. D. F. Martyn and A. L. Green, "The Characteristics of Downcoming Radio Waves," Proc. Roy. Soc. A., 148, 1935, pp. 104-120.

76. L. A. Hedlund and L. C. Edwards, "Polarization Fading Over an Oblique Incidence Path," IRE Trans., AP-6, Jan 1958, pp. 21-25.

77. G. A. Dulk, "Faraday Rotation Near the Transverse Region of the Ionosphere," J. Geo. Res., 68, Dec 1963, pp. 6391-6400.

78. M. R. Epstein, "Computer Prediction of the Effects of HF Oblique-Path Polarization Rotation With Frequency," Rept. SEL-67-026 (TR No. 139), Stanford Electronics Laboratories, Stanford, Calif., Feb 1967.

79. M. R. Epstein and O. G. Villard, Jr., "Received Polarization of Ionospherically Propagated Waves as a Function of Time and Frequency," Rept. SEL-68-014 (TR No. 145), Stanford Electronics Laboratories, Stanford, Calif., Jan 1968.

80. M. R. Epstein, "The Relation Between Group Path and Polarization Rotation," J. Atm. Terr. Phy., 30, 1968, pp. 1833-1836.

81. T. A. Croft, "Methods and Applications of Computer Raytracing," Rept. SEL-69-007 (TR No. 112), Stanford Electronics Laboratories, Stanford, Calif, Jan 1969.

82. T. A. Croft, "Computed Faraday Rotation During Sporadic-E Propagation," Rept. SEL-65-100 (TR No. 113), Stanford Electronics Laboratories, Stanford, Calif., Oct 1965.

83. R. M. Jones, "A Three-Dimensional Ray-Tracing Computer Program (Digest of ESSA Technical Report ITSA No. 17), " Radio Science, 3, Jan 1968, pp. 93-94.

84. T. A. Croft, "The Synthesis of Sweep-Frequency Ground Backscatter by Digital Computer," Rept. SEL-65-002 (TR No. 84), Stanford Electronics Laboratories, Stanford, Calif., Jan 1965.

85. T. A. Croft, "Computation of HF Ground Backscatter Amplitude," Radio Science, 2, Jul 1967, pp. 739-746.

86. D. E. Kerr, Propagation of Short Radio Waves, Boston Technical Publishers, Inc., Mass., 1964.

87. J. R. Barnum, "Mixed-Mode Oblique Ionograms: A Computer Ray-Tracing Interpretation," Rept. SEL-68-095 (Th No. 148), Stanford Electronics Laboratories, Stanford, Calif., Dec 1968.

88. R. F. Mlodnosky and R. A. Helliwell, "Graphic Data on the Earth's Main Magnetic Field in Space," J. Geo. Res., 67, Jun 1962, pp. 2207-2214.

89. H. Jasik, Ed., Antenna Engineering Handbook, McGraw-Hill Book Co., Inc., New York, 1961.

UNCLASSIFIED
Security Classification

DOCUMENT CONTROL DATA - R & D

(Security classification of title, body of abstract and indexing annotation must be entered when the overall report is classified)

1. ORIGINATING ACTIVITY (Corporate author)	2a. REPORT SECURITY CLASSIFICATION
Stanford Electronics Laboratories Stanford University Stanford, California 94305	Unclassified 2b. GROUP

3. REPORT TITLE

THE EFFECT OF POLARIZATION ROTATION ON THE AMPLITUDE OF IONOSPHERICALLY-PROPAGATED SEA BACKSCATTER

4. DESCRIPTIVE NOTES (Type of report and inclusive dates)

Technical Report No. 157, June 1970

5. AUTHOR(S) (First name, middle initial, last name)

J. R. Barnum

6. REPORT DATE	7a. TOTAL NO. OF PAGES	7b. NO. OF REFS
June 1970	208	89

8a. CONTRACT OR GRANT NO.	9a. ORIGINATOR'S REPORT NUMBER(S)
Nonr-225(64), NR 088 019 b. PROJECT NO. 4004 c. ARPA Order No. 196 d.	SU-SEL-70-036 TR No. 157 9b. OTHER REPORT NO(S) (Any other numbers that may be assigned this report)

10. DISTRIBUTION STATEMENT

This document has been approved for public release and sale; its distribution is unlimited.

11. SUPPLEMENTARY NOTES	12. SPONSORING MILITARY ACTIVITY
	Office of Naval Research

13. ABSTRACT

Previous experiments have shown that an ocean surface represents a strong source of high-frequency (HF) backscatter. The author has used a 2.5 km receiving antenna array--the world's largest--to study such backscatter both from the Gulf of Mexico and the Pacific Ocean. The narrow beamwidth of this antenna (1/3 deg average), together with SFCW sounding, confer unusually good azimuth and time-delay (range) resolution. The resulting detail and clarity has made possible more precise quantitative studies of sea backscatter. A particular goal of these studies is to develop a method of locating storms, or areas of unusual calm.

During routine sweep-frequency recordings, it was found that the high-resolution data revealed a new type of amplitude variation--periodic in both time-delay and radio frequency--which roughly resembled large thumbprints on the time-delay-versus-frequency plots. This was clearly a new phenomenon, seen only during the fall and winter months. It was hypothesized that magnetoionic splitting in the ionosphere produced a polarization-rotation modulation on the received backscatter signals and that the continuity of the sea cross-section polarization dependence was responsible for making the lines visible only in backscatter from the sea.

Theoretical development of this hypothesis led to simple trigonometric expressions which describe the received voltage. Using an approximate computer raytracing technique, and representative ionospheric models, synthetic backscatter records were

DD FORM 1 NOV 65 1473

UNCLASSIFIED
Security Classification

14 KEY WORDS		LINK A ROLE	LINK A WT	LINK B ROLE	LINK B WT	LINK C ROLE	LINK C WT
SEA BACKSCATTER	SWEEP FREQUENCY CW						
IONOSPHERE	OCEAN WAVES						
WIDE APERTURE	STORMS						
POLARIZATION	BACKSCATTER						
FARADAY ROTATION	ANTENNAS						
CIRCULAR POLARIZATION							

Abstract (Con't)

constructed which agree very well with the "thumbprint" line-families observed experimentally. The computer-aided predictions also showed that the inability to detect "polarization modulation" during the summer is due to the more sensitive dependence of polarization rotation upon frequency, time delay, and azimuth during that season.

Conclusive proof of the theory came when the transmitted polarization was changed while successive frequency sweeps were recorded. When the transmitter polarization is switched from vertical to approximately circular, the "thumbprint" lines in the time-delay-vs-frequency data are usually blurred. When "fixed"-frequency, amplitude-vs-time-delay data were recorded, and when the polarization at the transmitter is switched from vertical to horizontal, the shift in the positions of the enhancements in slant range correlated very well with the theory.

When the equivalent beamwidth of the 2.5 km array is broadened from 1/2 to 4 deg the polarization modulation is usually undetectable. Examination of azimuth-scanned, fixed-frequency measurements and their theoretically-synthesized counterparts explained this beamwidth dependence very well. It was found that a beamwidth as small as 2 deg is not likely to be sufficient to resolve polarization modulation on an east-west backscatter path, which probably explains why the effect was not positively identified in data taken before the use of the 2.5 km array. These conclusions do not necessarily apply to north-south backscatter paths, however.

The measurements showed that the variation in backscatter amplitude can easily be as much as 10 dB, and this also was predicted theoretically. Therefore, any measurement of changes in sea roughness versus distance made with high sounder resolution must account for "polarization modulation," since it tends to alter the otherwise smoothly-varying amplitude of the backscatter with slant range, azimuth, and frequency. It was shown, however, that the effect of this new modulation can be controlled by suitably modifying the polarization of the transmitting antenna.